QUANTIFYING MIXING INSIDE TITANIUM DIOXIDE

REACTORS THROUGH COMPUTATIONAL

FLUID DYNAMICS

By

JASON ANDREW CARLISLE
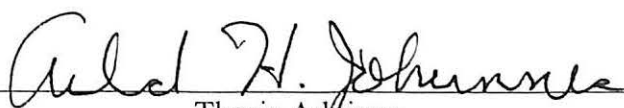
Bachelor of Science

Oklahoma State University

Stillwater, Oklahoma

2001

Submitted to the Faculty of the
Graduate College of
Oklahoma State University
in partial fulfillment of
the requirements for
the Degree of
MASTER OF SCIENCE
July 2004

QUANTIFYING MIXING INSIDE TITANIUM DIOXIDE

REACTORS THROUGH COMPUTATIONAL

FLUID DYNAMICS

Thesis Approved:

_____
Thesis Advisor

_____
Committee Member

_____
Committee Member

_____
Dean of Graduate College

PREFACE

The goal of this research was to devise a method to quantify mixing inside reactors producing titanium dioxide (TiO_2), a widely used white pigment noted for its ultra-violet light blocking properties. Computational fluid dynamics (CFD) was the method used to predict mixing occurring inside these process reactors. CFD is a mathematical method of modeling a real system using the laws of conservation to simulate phenomena occurring in a system. With information about the mixing occurring inside a reactor, improvements in efficiency and product quality can be realized by modification of the system.

I would like to express my gratitude to my graduate advisors, Dr. Gary Foutch and Dr. Arland Johannes, for the opportunity to be involved in this research. I also would like to thank Dr. Afshin Ghajar for his involvement in this project and for serving as a member of my defense committee. Without the support and experience of these three individuals, I would never have been able to stay motivated and complete this project, and I owe you my thanks.

My fellow students and research group members, Jae-Yong Kim and Sivakumar Ramaligam, are also owed my deepest thanks. Their help was invaluable whenever I was "stuck" on a problem or if I just needed to find a new perspective. I would also like to the Kerr-McGee Corporation for providing the insight and resources necessary for this endeavor.

TABLE OF CONTENTS

LIST OF FIGURES

LIST OF TABLES

NOMENCLATURE

A	Arrhenius pre-exponential factor
C	Concentration, mol/m^3
CAD	Computer-aided design
CFD	Computational fluid dynamics
E_a	Energy of activation, kJ/mol
EDM	Eddy dissipation model
EOS	Equation of state
E(t)	Exit age distribution function, s^{-1}
FRC	Finite rate chemistry
F(t)	Cumulative distribution function
GDE	General dynamics equation
h_{tot}	Specific total enthalpy, J/kg
K	Boltzmann constant, 1.3807E-23 J/K
k	Reaction rate constant, s^{-1}
k	Turbulent kinetic energy, m^2/s^2
mf	Mass fraction
MW	Molecular weight, g/mol
NASA	National Aeronautics and Space Administration

p	Pressure, Pa
R	Universal gas constant, 8.314 J/mol-K
R	Overall reaction rate, mol/m^3-s
r	Local radius, m
$R_{g,s}$	Reaction rate in gas and solid phase respectively, mol/m^3-s
RTD	Residence time distribution
s^3	Skewness, s^3
S_m	Momentum source, kg/m^2-s^2
S_c	Energy source, J/s
T	Temperature, K
t_m	Mean residence time, s
U	Vector of velocity, m/s
Y_i	Mass fraction of species i
β	Exponential temperature effect
∇	Del operator
δ	Unit tensor
ε	Maximum energy of attraction between a pair of molecules, J
ε	Turbulent dissipation rate, m^2/s^3
λ	Thermal conductivity, W/m-K
μ	Viscosity, kg/m-s
ρ	Density, kg/m^3
ρ_i	Thermodynamic density of species i, kg/m^3
σ	Variance, s^2

σ Collision diameter of a molecule, Å

Ω_μ Function for prediction of gases viscosity at low density

CHAPTER I

INTRODUCTION

Titanium Dioxide

Titanium dioxide (TiO_2) is one the most widely used inorganic powders in the world today. The white pigment market is essentially served by TiO_2 pigments with virtually no other competition. Used in a wide variety of applications, more than 3.5 million tons of TiO_2 pigment is consumed by the world's industries each year (Braun 1997). Applications for TiO_2 pigment include use in paints, paper, plastics, cosmetics, catalyst support, and many other products.

The popularity of TiO_2 (sometimes called titania) pigment, stems from superior chemical, physical, and optical properties. One of TiO_2 most important characteristics is chemical stability and non-reactivity in most applications. This chemical inactivity is most important in the paints and plastics industries where product degradation is a major factor.

Commercially, two crystalline forms of TiO_2 are used, rutile and anatase, which are both extremely hard. Rutile is the more dense crystal phase and has the higher refractive index of 2.74, while anatase has a refractive index of 2.54 (Jain et al. 1997). The difference in these physical properties can lead to a light scattering advantage of 20% for rutile. Rutile is also the stable phase for the crystal lattice but requires temperatures

higher than 500 °C for conversion from anatase. Because rutile has more favorable

properties, it has replaced anatase in virtually all but paper applications (Braun 1997).

Manufacture of titania is typically performed in an aerosol reactor where the

particle size is easily controlled. Particle size is important since pigment must be small

enough to "hide" and also because the light scattering characteristics of TiO_2 are most

effective in the 0.15 to 0.25 μm range (Akhtar et al. 1991). (The term hide is used in the

pigment industry and means that the pigment can be added to paint etc. and not be

discernable from the product as a whole.) Production of TiO_2 has been performed by

other methods, however, such as aqueous phase chemistry.

Production of TiO_2

Commercial production of TiO_2 has historically been performed by two different

processes: the so called "chloride" and "sulfate" processes. The sulfate process has been

used since the early 1930's and involves aqueous phase batch chemistry. This process is

a less efficient manufacturing method than the newer chloride process, however, and

requires more intensive labor and waste disposal costs (Powell 1968). The newer

chloride process is based on a continuous aerosol reaction scheme. In an aerosol

reaction, powders are formed by a gas phase reaction with the product gases coalescing

through a variety of mechanisms to form solid particles. The advantages of this type of

reactor are small product particles, typically 10^{-9}-10^{-6} meters in diameter, and narrow

particle size distributions. Another advantage for this reaction scheme is that both of

these product characteristics can usually be adjusted by modifying the operating

conditions.

In the chloride process, titanium tetrachloride ($TiCl_4$) reacts with oxygen (O_2) to produce TiO_2 and chlorine gas (Cl_2). The overall chemical equation for this reaction is as follows:

$$TiCl_4(g) + O_2(g) \rightarrow TiO_2(s) + 2Cl_2(g) \qquad (1\text{-}1)$$
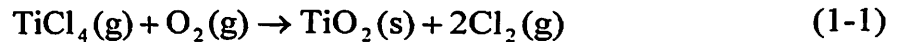
As presented in Equation 1-1, the overall reaction is mildly exothermic having a standard heat of combustion of -181.6 kJ/mol; however, the initial steps of the reaction involve $TiCL_4(g)$ converting to $TiO_2(g)$ which is endothermic and only evolves heat after forming the solid phase $TiO_2(s)$. Because of this phenomenon, many reactor patents introduce feed preheating or the addition of a heat source, such as a hydrocarbon fuel, to promote the reaction. After the reaction zone, there is typically a quench zone where particle growth/agglomeration can be further manipulated. Finally, the product particles are milled to break apart particle clusters.

The major problem associated with the chloride process is oxide scaling near the $TiCl_4$ inlet regions (Ross 2001). This scaling eventually leads to inlet plugging and requires the shutdown and cleaning of the reactor or the addition of a scouring agent, which can introduce new problems. There are, however, many patents that address this issue and claim to have reduced or eliminated the scaling problem. Several examples can be seen in US Patents 2,670,272; 3,328,126; and 3,351,427.

Objectives

The objective of this research is to identify possible methods to quantify mixing and turbulence in TiO_2 aerosol reactors. By quantifying these parameters it will be possible to design and alter reactor configurations to reduce regions of backflow or

stagnation and increase gas phase mixing. The effect of these design changes has the possibility of increasing reactor efficiency, decreasing scaling problems and, thus, increasing profitability of the reactor.

Computational fluid dynamics (CFD) is the method that will be used to quantify mixing and turbulence in this research. CFD is a method of modeling physical systems by using mass, momentum, energy, and chemical species balance equations to mathematically simulate real phenomena inside the system. CFD accomplishes this by subdividing a system into a series of nodes or volumes that describe the geometry and by solving the modeling equations differentially at each node or volume. The simulation generates realistic information, if properly modeled, about the temperature, pressure, velocity, and composition at each node or volume. This information can then be used to evaluate a reactor configuration or operating conditions. The commercial software package used in all CFD simulations for this research is CFX 5.5.1.

CHAPTER II

LITERATURE REVIEW

Introduction

A review of literature that is pertinent to the production of TiO_2 and to methods of describing mixing is presented in this chapter. The first section provides a brief summary on the production of TiO_2 by the chloride process. Afterwards, a section detailing kinetic rate models and suggested particle growth mechanisms is presented. Finally, a brief review of methods historically used to describe mixing in non-ideal reactors is presented.

Titanium Dioxide Production

DuPont first introduced the "chloride process" on an industrial scale in the 1950's. The chloride process has many advantages over the older sulfate process for production of TiO_2 including: easier waste disposal, less energy consumption, better quality (rutile) product, and a more narrow particle size distribution (Braun 1997). The overall process can be generalized in the following six steps:

1. Processing of the raw titanium so that the ore may be chlorinated to produce feed stock.

2. Chlorination of the ore which produces titanium and iron chlorides, this step is usually done in a shaft furnace (Powell 1968).

5

3. Separation of the solid and gaseous iron chlorides and other chlorination gases from the $TiCl_4$ produced.

4. Distillation of the $TiCl_4$ to further remove any unwanted impurities such as silicon and vanadium compounds.

5. Oxidation of $TiCl_4$ at high temperature to produce a largely rutile product in a controlled flame reactor.

6. Separation of product particles for grinding from gas products and recycling of chlorine gas for step 2.

Kinetics and Particle Growth

Production of TiO_2 by the chloride process is not completely understood. This lack of understanding is due in large part to the rapid chemical kinetics and particle growth mechanism (Pratsinis and Spicer, 1998). Many studies on the kinetics and growth mechanism have been performed in order to develop more accurate models. The following discussion presents several models that have been suggested to describe the reaction pathway.

The overall chemical reaction of $TiCl_4$ with O_2 can be generalized by the following irreversible reaction:

$$TiCl_4(g) + O_2(g) \rightarrow TiO_2(s) + 2Cl_2(g) \qquad (2\text{-}1)$$
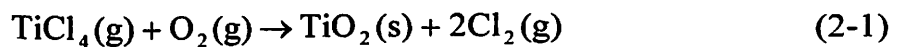
Oxidation of $TiCl_4$ occurs in the gas phase (forming small titania nuclei) and on the solid surface of condensed TiO_2 particles simultaneously, leading Pratsinis and Spicer (1998) to propose a reaction rate that relied on both pathways. The resulting overall reaction rate can be stated as:

$$\frac{dC}{dt} = -R = -(R_g + R_s) \qquad (2\text{-}2)$$

where C is the vapor phase concentration of TiCl$_4$, R is the overall reaction rate, and R$_{g,s}$ are the gas phase and the surface oxidation reaction rates, respectively. By modeling the gas phase and surface oxidation reactions using the overall reaction rate, the following first-order, general rate equation can be used to describe the reaction rate:

$$R = kC \qquad (2\text{-}3)$$

where k is the temperature dependant reaction rate constant defined by the Arrhenius expression.

Several values for the pre-exponential constant (A) and energy of activation (E$_a$) are present in the literature. These values have been determined with a variety of experimental apparati and operating conditions. Table 2-1 lists three references where the Arrhenius constants where determined experimentally. In all experiments no exponential temperature effect (β) was observed and the reaction rate was found to be first order with respect to TiCl$_4$ and zero order with respect to oxygen (at ratios of O$_2$/TiCl$_4$ less than 10:1).

TABLE 2-1: Literature Values for TiCl$_4$ Oxidation Arrhenius Constants.
Arrhenius Equation : k=AT$^\beta$exp[-E$_a$/(RT)]

Reference	A*10^{-4} (s^{-1})	E$_a$ (kJ/mol)	β	Temperature Range (K)
Pratsinis et al. (1990)	8.26	88.8	0	973-1273
Kobata et al. (1991)	25	102	0	1123-1473
Lee (2000)	511	124	0	916-1492

The mechanism for TiO$_2$ particle growth in the chloride process has widely been disputed (Pratsinis and Spicer, 1998). At the center of this dispute is whether the

particles grow by surface reaction or by gas phase reaction and coagulation. Several different experimental setups and studies have suggested that both mechanisms are the controlling factor for TiO_2 particle growth, leading the experimenters to dissenting opinions on the growth mechanism.

Akhtar et al. (1991) concluded that the gas phase reaction and coagulation mechanism controlled the particle concentration, average size, and polydispersity of TiO_2 particles. Particle size distribution was measured using three control variables: reactor temperature, reactant concentration, and residence time. These values varied between 1,200 and 1,723 K, inlet concentrations of 9.34E-06 to 1.56E-05 mol liter^{-1} of $TiCl_4$, and 0.8 to 1.6 seconds. Oxygen used in these experiments was between 5-10 times stoichiometric excess. When Akhtar et al. compared the experimental results to those obtained by theoretical prediction from the solution of the aerosol general dynamics equation (GDE) using a sectional technique, qualitative agreement was observed, and with a coagulation enhancement factor, excellent quantitative agreement was observed. These results are in agreement with the findings of Jain et al. (1996) who studied the role of surface reaction during TiO_2 synthesis using theoretical means. Jain et al. modeled three reactor cases, two at laboratory scale and one at industrial scale, using the GDE and a log-normal model. From results obtained with the reactor models, Jain et al. concluded that surface reaction is not an important growth mechanism for either the laboratory or industrial scale setups and went on to suggest two dimensionless quantities that characterize the importance of surface reaction in particle synthesis by gas to particle conversion.

Jang and Jeong (1995) studied the effects of reactant feed temperature, reactor temperature, and reactant feed concentrations on particle growth. Using reactor conditions where temperature and inlet concentration ranged from 900-1100 °C and 0.05 to 1.00 mol % $TiCl_4$, respectively, they concluded that reactants entering the reactor at temperatures lower than the reaction temperature and that higher $TiCl_4$ concentrations tended to increase particle size and distribution by surface reaction. These findings agree with Morooka et al. (1989) conclusions on the mechanism of growth. Using two reactors in series with various operating modes, Morooka et al. concluded that particle growth occurred because of heterogeneous deposition of TiO_2 followed by fusion. This fusion was initiated at 1,000 °C if unreacted $TiCl_4$ was present and at 1,200 °C if no $TiCl_4$ was available.

In a paper specifically aimed at the competition of gas phase and surface reaction of $TiCl_4$, Pratsinis and Spicer (1998) developed a model for titania aerosol dynamics that accounted for both growth mechanisms. Predictions from the model were compared with experimental results and previous interpretations of the growth mechanism. The model predicted the observed experimental results and Pratsinis and Spicer were able to reconcile the conflicting views. Furthermore, Pratsinis and Spicer concluded that the initial mole fraction of $TiCl_4$ was the controlling factor for determining the level of pure gas phase or surface reaction oxidation.

Methods to Quantify Mixing in Non-ideal Reactors

Knowledge of the velocity distribution inside a reactor is needed to accurately predict the behavior of a reactor. Before the advent of computational fluid dynamic

(CFD) as a design tool, obtaining the velocity distribution for a reactor was impractical due to the complexity and enormous time requirements for a solution. Danckwerts (1953) defined a less complex method to analyze reactor performance, known as the residence time distribution (RTD). This concept provides information about how long the individual molecules stay in a reactor and thus gives clues about the level of mixing. However, this method does not provide information on exactly where the molecules resided in the reactor and so point to point variations can not be inferred (Levenspiel 1962).

Fluid elements inside a reactor can take many different paths that may require the same or different lengths of time to exit the vessel. Danckwerts defined the residence time distribution, also know as the exit age distribution E(t), as the distribution of the time these elements have resided in the reactor measured at the exit. This age distribution information can be directly obtained from a stimulus-response experiment called a tracer test. A tracer test is performed by injecting a non-reactive substance with physical properties similar to the fluid of interest at a vessels entrance and then measuring the tracers outlet concentration as a function of time. The two most popular methods of introducing the tracer are a pulse input, an instantaneous injection of a know quantity, and a step input, instantaneous change to a constant known injection rate. Examples of concentration curves as a function of time for both tracer input methods are illustrated at the top of the next page in Figure 2-1.

The residence time distribution is defined as a normalized distribution for convenience. The E(t) curve is defined by:

$$\int_0^\infty E(t)dt = 1 \qquad (2\text{-}4)$$
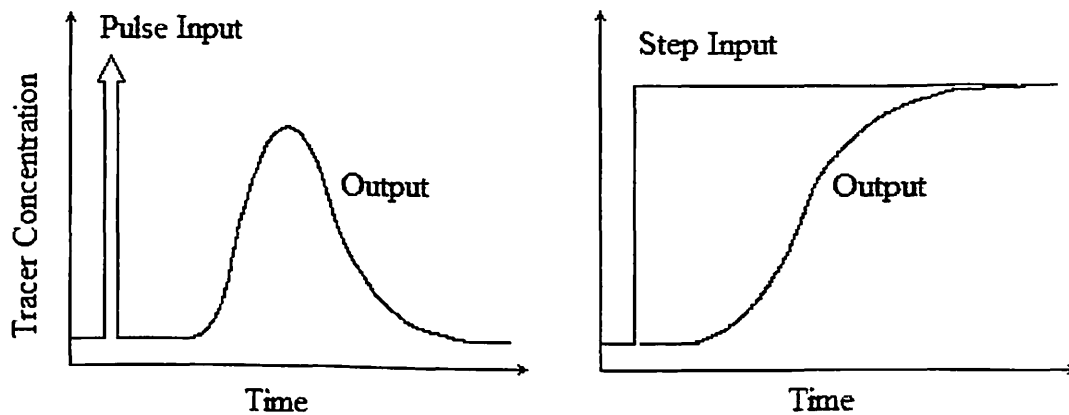
FIGURE 2-1. Tracer concentration curves for a pulse input (left) and for a step input (right).

Using this function it is possible to calculate the fraction of tracer that has resided in a vessel for a period of time less than or greater than an arbitrary value t. Since the RTD is a normalized distribution, this fraction will always fall between zero and one and was defined by Danckwerts as the cumulative distribution function F(t). This distribution function is stated as:

$$\int_0^t E(t)dt = F(t) \tag{2-5}$$

The cumulative distribution curve is most useful for determining the amount of time necessary for a desired fraction of material to exit the reactor and for determining the fraction of material residing in the reactor between two times of interest.

The residence time distribution can be quantitatively defined by its moments. In order to completely characterize a distribution all moments are needed; however, when comparing RTDs it is a common to use just the first three moments (Fogler 1999). The first moment of the E(t) curve gives the mean value of a variable and for the RTD this

11

provides the mean residence time any molecule spends in a vessel. The mean residence time (t_m) is defined as:

$$t_m = \int_0^\infty t\, E(t)\, dt \qquad\qquad (2\text{-}6)$$

The second moment is taken about the mean and is known as the variance. The square root of the variance gives the standard deviation (σ) about the mean which is a useful statistical measure. The variance is calculated by:

$$\sigma^2 = \int_0^\infty (t - t_m)^2\, E(t)\, dt \qquad\qquad (2\text{-}7)$$

The third moment is also taken about the mean and is know as the skewness (s^3). The skewness gives a measure of how much and in which direction the distribution is skewed about the mean. The skewness is calculated by:

$$s^3 = \frac{1}{\sigma^{3/2}} \int_0^\infty (t - t_m)^3\, E(t)\, dt \qquad\qquad (2\text{-}8)$$

When calculating the value for skewness, a negative value indicates a distribution is skewed left while the opposite is true for a positive value.

In order to calculate values for the moments from experimental data or simulated information, the E(t) curve must be generated from the concentration at the exit of the reactor as a function of time. Once the E(t) curve is generated, Equations 2-6, 7, and 8 may be numerically integrated to solve for the moments. Appendix B provides more detailed information on numerical integration of these equations.

CHAPTER III

METHODS AND ANALYSIS

Introduction

This chapter focuses on the methods used to analyze TiO_2 reactors. In this section a brief description of computational fluid dynamics (CFD) is given as well as the basic equations solved in a simulation. Afterwards a description of the reactors simulated in this research and the methods and assumptions used to model these reactors is presented.

The methods used to describe and quantify mixing for this analysis involved the use of computational fluid dynamics (CFD). Computational fluid dynamics is a modeling tool that mathematically describes a system using equations for the transport of mass, momentum, and energy. These equations are solved numerically during a "simulation" using a geometry representing the system of interest. During a simulation, the geometry is broken up into a series of nodes or volume elements and then the equations of interest are solved for each node or volume element. Once a solution is found at each node or element, profiles of temperature, pressure, and velocity etc. can be viewed over the geometry or variables such as conversion for reactions and many more variables of interest can be calculated for use in design or description purposes.

The software used in this research is the commercially available CFD package CFX 5.5.1. This software package included three separate programs: CFX-Build, CFX-5

Solver Manager, and CFX-Post. CFX-Build was used to generate and mesh the geometry, and then the solver manager was used to obtain solutions to the equations of transport. Once solutions were obtained, CFX-Post was used to export data from the simulation and provide graphical representation of the solution. All simulations where performed using a HP Pavilion 750n with an Intel® Pentium® 4, 1.60 GHz processor and 512 MB of RAM.

General Modeling Equations

As previously stated, the equations of transport must be solved to produce a solution to a CFD simulation. The equations of transport are derived from the laws of conservation of energy, mass, and momentum. Depending on the type of simulation performed, one or more of the conservation equations must be solved to find a solution.

The instantaneous form of the conservation of mass (or continuity equation) is written as:

$$\frac{\partial \rho}{\partial t} + \nabla \bullet (\rho U) = 0 \qquad (3\text{-}1)$$

where ρ is the fluid density, t is the time, and U is the vector of velocity. For simulations with multiple species present, the density used in the continuity equation is the overall fluid density and is computed from the thermodynamic density of each component by:

$$\frac{1}{\rho} = \sum_{i=A,B...}^{N} \frac{Y_i}{\langle \rho_i \rangle} \qquad (3\text{-}2)$$

where Y_i is the mass fraction of a component and ρ_i is the thermodynamic density of a component calculated from the appropriate equation of state (EOS).

The instantaneous momentum and energy equations written in terms of transport properties are, respectively:

$$\frac{\partial \rho U}{\partial t} + \nabla \bullet (\rho U \otimes U) = \nabla \bullet \left(-p\delta + \mu \left(\nabla U + (\nabla U)^T\right)\right) + S_m \qquad (3\text{-}3)$$

$$\frac{\partial \rho h_{tot}}{\partial t} - \frac{\partial p}{\partial t} + \nabla \bullet (\rho U h_{tot}) = \nabla \bullet (\lambda \nabla T) + S_E \qquad (3\text{-}4)$$

where p is the static pressure, μ is the fluid viscosity, λ is the thermal conductivity, T is the temperature, h_{tot} is the specific total enthalpy, and $S_{m,e}$ is a momentum or energy source.

To obtain solutions to the general modeling equation listed in this section, CFX Solver Manager uses numerical differentiation and integration techniques. Generalized numerical methods are presented in Appendix B. The exact methods using in the Solver Manager follow similar techniques but are solved in a proprietary manner.

Description of Reactors

The reactors chosen for simulation in this research were the Montecatini Edison reactor, the Kronos reactor, and the simplified Kerr-McGee reactor. The Montecatini Edison reactor was chosen for claims made about backmixing and residence time in the reaction chamber. The Kronos reactor was selected because it is typical of industrial scale reactors and to see if claims made in the patent may be the result of mixing patterns occurring in the reactor. Finally, the simplified Kerr-McGee reactor was selected due to interest in the mixing occurring inside the reactor and interest in ways to generally improve mixing in the reactor.

Montecatini Edison Reactor Patent # 3,725,526

This patent claims both to provide a large recycling of solid product downstream from the $TiCl_4$ inlets and to draw $TiCl_4$ upstream into the oxygen rich zone. The patent asserts that the operating conditions and mixing occurring in the reactor lead to a smaller number of TiO_2 particles with larger dimensions owing to the surface growth mechanism rather than gas phase reaction and nucleation only. The reactor configuration and operating condition supplied in the patent place the reactor in the turbulent flow regime.

The Montecatini Edison reactor is of a fairly simple design and is characterized by Figure 3-1 (next page). In this setup, oxygen is fed into the reactor at locator 1 (37 mm diameter) and is given a swirling helical motion. This gas is originally at 700-900 °C and is mixed with carbon monoxide and combusted to produce oxidizing gas that is approximately 1,800-2,300 °C, while still containing a sufficient amount of O_2 to convert $TiCl_4$ to TiO_2. This oxidizing gas then passes through a divergent frusto-conical duct and is contacted downstream with hot (400-600 °C) $TiCl_4$ being fed through annular slot 3 (2 mm width) at an angle 30°. The mixed species continue down the cylindrical reaction chamber (100 mm diameter) to be cooled and processed later.

Kronos Reactor Patent # 5,196,181

Most of the claims in the Kronos reactor patent focus on the preheating section of the reactor. In particular, this patent claims that the geometry and operating conditions supplied help to create a protective oxygen film on the surface of the refractory lined preheating section. It is reported that this film increases the life span of the refractory material from 300 hrs to more than 9,000 hrs. This patent does not, however, make any
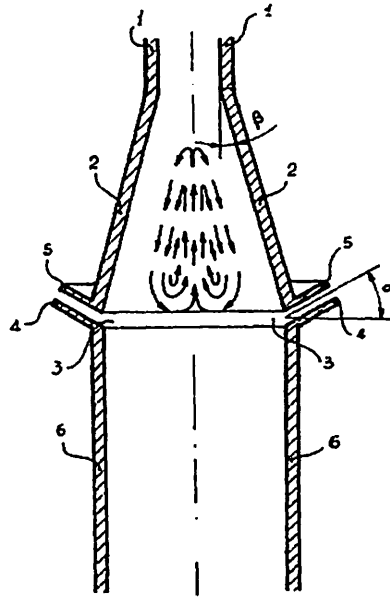
FIGURE 3-1. Montecatini Edison Reactor diagram from U.S. patent #3,725,526.

claims about how the geometry and operating conditions effect mixing and what effects mixing might have on the operation of the reactor. The operating conditions supplied by the patent place this reactor in the turbulent flow regime.

The Kronos reactor is typical of other industrial reactors described in patent literature. Figure 3-2 (next page) represents the reactor preheating section as described by the patent. Oxygen at a temperature of 950 °C is fed to the reactor in four semi-circular inlets at locators 16-19 (60 mm radius). The oxygen is then further heated to approximately 2600 °C by the combustion of toluene being fed into the reactor at locator 14. This oxidizing gas travels axially downstream until reacting with hot (450 °C) $TiCl_4$ being fed at locators 28 and 29 (60X60 mm square ducts). Separation of TiO_2 is later performed in a bag filter plant.

17
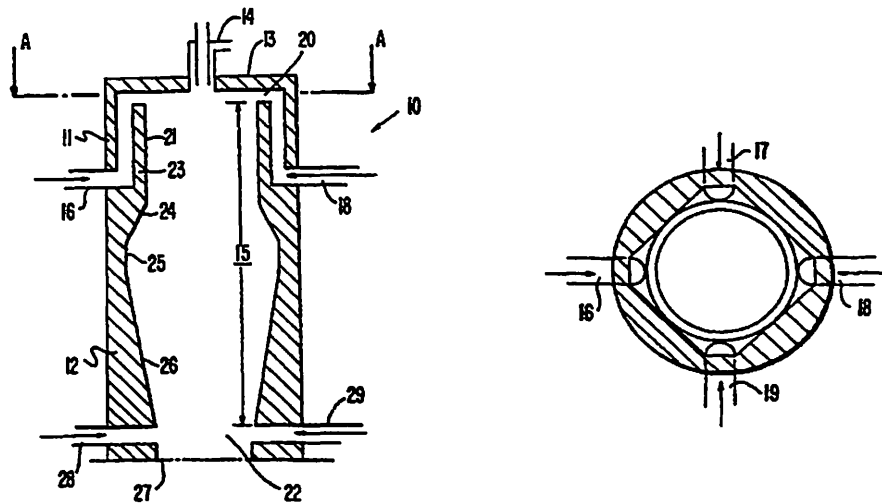
FIGURE 3-2. Kronos Reactor diagram from U.S. patent #5,196,181; side view (left) and top view (right).

Simplified Kerr-McGee Reactor

A simplified model of the Kerr-McGee chloride reactor was studied in this research. There are no claims about mixing or operating conditions available for this reactor. Assumptions and boundary conditions that placed the reactors operation in the turbulent regime were used in this work. The geometry is of a simple design with a tubular reaction chamber being fed O_2 and a hydrocarbon fuel at the entrance and a $TiCl_4$ distribution spool feeding the reactant downstream.

Modeling of TiO_2 Reactors

In order to simulate a reactor using CFX 5.5.1, several steps that define the reactor model are required. These steps are geometry creation, domain specification, boundary condition specification, initialization, mesh generation, and solver setup. By

18

altering the models geometry or boundary and initial conditions, the effect such a change will have on a reactor can be approximated and studied.

Geometry Modeling

Geometry creation is the first step required when setting up a simulation. During geometry creation a computer-aided design (CAD) type file is generated that represents the physical geometry and dimensions of the reactor to be modeled. The geometry can be generated in a separate file using software, such as Pro Engineer, that is capable of exporting the file to CFX Build in a supported file format, or the geometry can be created using the CFX Build geometry generation tools. Figures 3.3-5 show wire-frame and solid surface representation for the geometries simulated in this research. For all geometries studied in this research, the CFX Build geometry generation tools were used.

The geometry for the Montecatini Edison reactor, Figure 3-3 (next page), was shortened due to memory constraints. The original patented reaction zone is shortened from 1,400 mm to 250 mm. In the figure locator one is the O_2 and combustion gas feed, locator two is the $TiCl_4$ feed, and locator three is the exit from the shortened reaction zone.
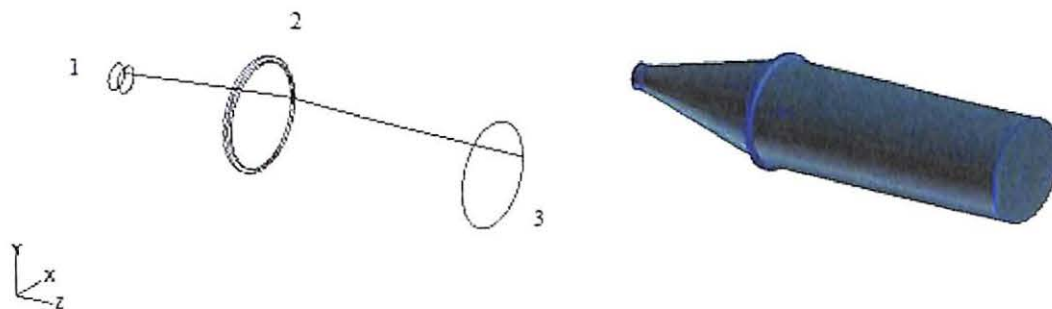
FIGURE 3-3. Wire-frame (left) and solid surface (right) simulation geometry for the Montecatini Edison patent #3,725,526.

For the Kronos reactor, the geometry was assumed to have a symmetric flow profile and was modeled using a quarter-section instead of the full geometry. This assumption helped to decrease calculation time and allowed for a smaller mesh to be used which increased both resolution and accuracy. Also assumed was the geometry had four square TiCl$_4$ inlets and a reaction tube that was divergent. From Figure 3-4, locator one is an O$_2$ inlet, locator two is a TiCL$_4$ inlet, locator three is the outlet, and locator four is the inlet for combustion gases.
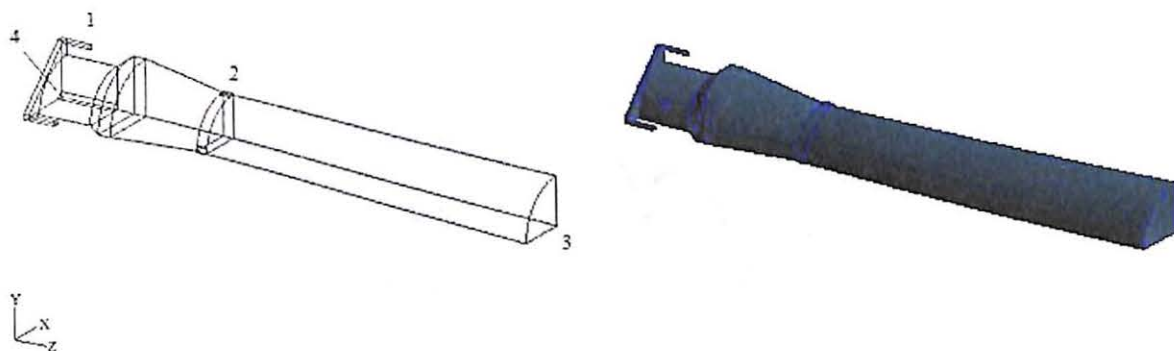
FIGURE 3-4. Wire-frame (left) and solid surface (right) simulation geometry for the Kronos patent #5,196,181.

The final reactor configuration studied in this research is a simplified model of the Kerr-McGee reactor. Figure 3-5 (next page) shows the reactor geometry used for simulation. From the figure, locator one is the O$_2$ inlet, locator two is the combustion gas inlet, locator three is the TiCl$_4$ inlet, and locator four is the outlet. As with the Kronos geometry, a divergent reaction chamber was assumed.
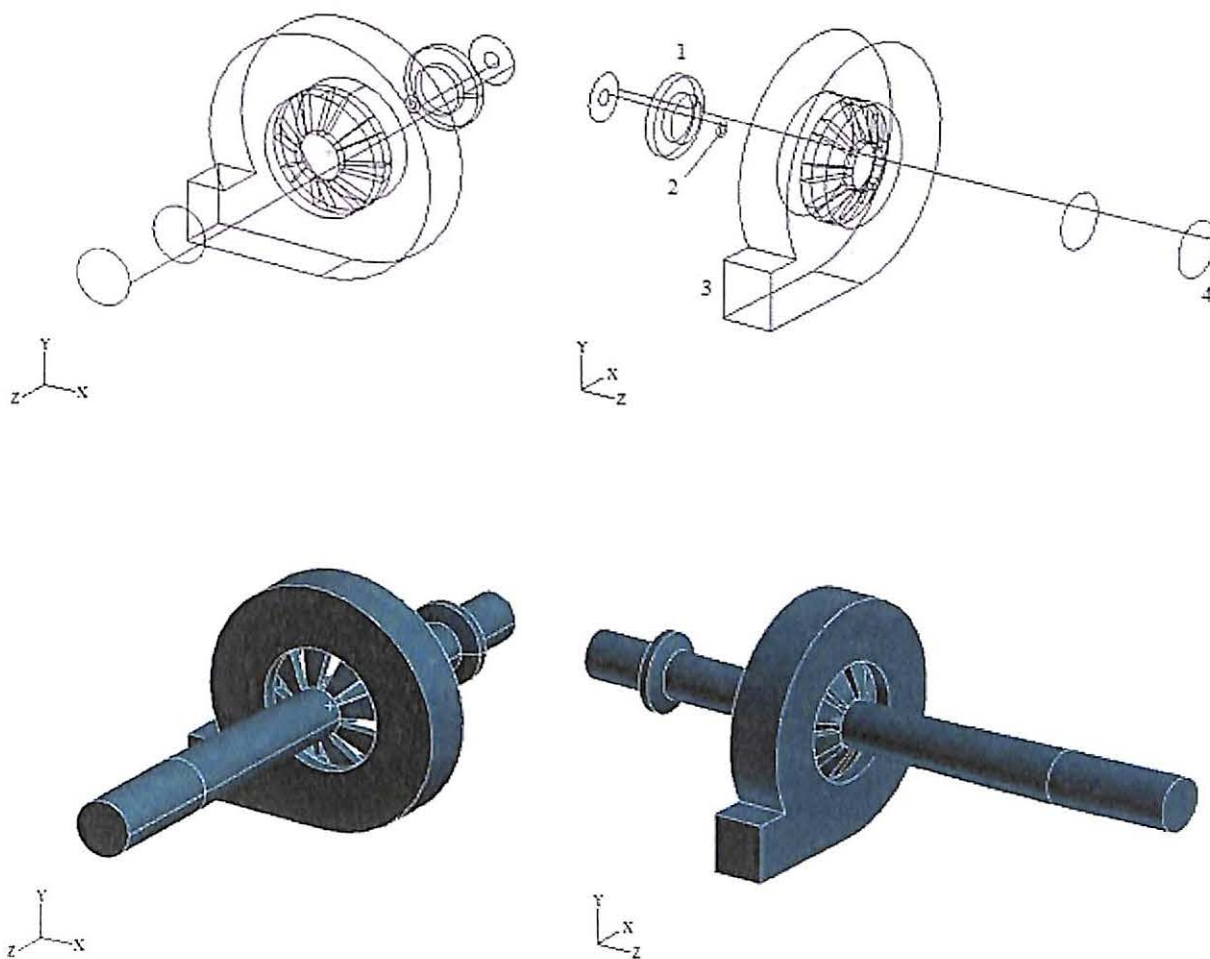
FIGURE 3-5. Wire-frame (top) and solid surface (bottom) simulation geometry for the simplified Kerr-McGee geometry.

Defining Domain

Once the geometry has been set up, it is necessary to define the domain of the simulation. The domain defines all physical properties and models to be used during the simulation of a reactor. Defining the domain of a simulation can be broken into three main components: domain setup, fluid and component details, and physical models.

The domain setup provides the backbone from which the simulation is based. During the domain setup, several crucial simulation parameters are set. The first parameter is the reference coordinate system used to describe the geometry. There are three coordinate systems available in CFX 5.5.1: Cartesian (x,y,z), Cylindrical (r,θ,z), and Spherical (r,θ,φ). For all simulation in this research the default Cartesian coordinate system was used. The second parameter in domain setup is the reference pressure, which provides a basis for all calculations involving pressure. The third parameter set in domain setup defines the type of simulation to be performed. The two types of simulations are transient, which is time dependant, and steady state. A final parameter is used when multiple phases are present and need to be modeled. For this research the solid phase TiO_2 particles are modeled as part of the gas phase due to the complexity required to simulate a gas-to-solid reaction and the lack of particle tracking models in CFX-5.

After the domain setup is complete, details about the components involved in the simulation are provided. During this step, the species present in the simulation are defined and values for each species physical properties are input. Table 3-1 on the next page provides the physical properties used for the simulations in this research. Not shown in table are the heat capacities which are calculated from regressed physical data and entered into CFX-5 using the NASA specific heat equations and format, which are presented in Appendix A. Also, an equation of state (EOS) relating density and specific heat to pressure, temperature, and/or additional variables is set. All simulations in this research use the ideal gas law to calculate density due to the low pressures and relatively high temperatures used in this work.

TABLE 3-1: Physical Properties.

Compound	Chemical Formula	MW (g/gmol)	Viscosity[a] $*10^8$ (kg/m-s)	Thermal Cond.$*10^3$ (W/m-K)	Reference Enthalpy (kJ/mol)	Reference Entropy (J/mol K)
Carbon Dioxide	CO_2	44.01	$30.0*T^{0.715}$	14.5	-393.52	213.79
Chlorine	Cl_2	70.91	$30.0*T^{0.708}$	3.4	0.00	223.08
Nitrogen	N_2	28.01	$40.0*T^{0.656}$	25.9	0.00	192.56
Oxygen	O_2	31.99	$50.0*T^{0.661}$	26.6	0.00	205.07
Propane	C_3H_8	44.10	811.0	17.3	-103.90	269.92
Titanium Dioxide (Rutile)	TiO_2	79.90	$2.0*T^{0.985}$	48.0	-944.75	50.29
Titanium Tetrachloride	$TiCl_4$	189.68	$10.0*T^{0.770}$	17.0	-763.20	354.84
Water	H_2O	18.02	940.0	19.3	-241.83	188.84

[a]The equations for viscosity are calculated as a function of temperature from a regressed power-law equation using Chapman-Enskog theory (except for propane and water which were held constant). See Appendix A

The final step to define a domain requires the selection of physical models to describe phenomena occurring inside the reactor. These physical models describe phenomena such as the flow regime, heat transfer, reaction rates, thermal radiation, and diffusivity. When selecting a model for the flow regime, it is important to determine whether the fluid flow is laminar or turbulent since turbulent fluctuations can greatly increase transport. Several turbulence models are available in CFX 5.5.1 based on the eddy viscosity and Reynolds stress transport concepts. For all simulations the turbulence model used is the RNG k-ε model due to its wide applicability over the entire turbulent range and its robustness (CFX 5 Online Documentation). A heat transfer model predicts the temperature through the fluid in a simulation. The total energy model is used for all simulations to model heat transfer by conduction, convection, and turbulent mixing. The total energy model also accounts for kinetic energy effects, which become significant when the Mach number exceeds 0.2. There are three default reaction rate models included in CFX 5.5.1: the finite rate chemistry model (FRC), the eddy-dissipation model

(EDM), and a combined EDM/FRC model. The combined EDM/FRC model, which is used in all simulations for this work, predicts a reaction rate from both models and applies the lesser rate. Several radiation models are available in CFX Build but where not used in this research due to computational and time constraints. The final step during model selection is determining how diffusivity is calculated. Use of multicomponent binary diffusivities is the most theoretically correct way to calculate diffusivity; however, Aggus (2000) found that the use of binary diffusivities lead to oscillating non-convergence and Ross (2001) found that an increase or decrease of 50% in mixture diffusivity had little effect on the results. For these reasons the molecular diffusivity used in all simulations is that seen by the bulk.

Boundary Conditions

The boundary conditions of a simulation supply information about what occurs at the surface of the geometry. This includes information on heat transfer from the system as well as flow into or out of the system. The tables below give the inputs used in each simulation. For all simulations it was assumed that the reactors were insulated so the reactor walls were modeled as adiabatic and that the default intensity and autocompute value in CFX accurately describe inlet turbulence values.

Boundary conditions for the Montecatini Edison reactor are given on the next page in Table 3-2. For the oxygen and combustion gases inlet, it was assumed that carbon monoxide and O_2 were pre-combusted producing a stream with a composition of 65% O_2 (by weight) with the remainder being CO_2. This inlet stream also has a swirling velocity and is modeled using the x, y, and z component given in Table 3-2, where r is

the local radius and R is the radius of the inlet. For all other boundary conditions flow is normal to the surface.

TABLE 3-2: Boundary Conditions for Montecatini Edison Reactor

Boundary Name	Boundary Type	Value	Temperature	X	Y	Z
Oxygen/Combustion Gases	Inlet	0.01474 kg/s	1900 °C	1.2*(r/R)	-1.2*(r/R)	1
Titanium Tetrachloride	Inlet	0.05 kg/s	500 °C	N/A	N/A	N/A
Exit	Outlet	101.325 kPa	N/A	N/A	N/A	N/A

The boundary conditions for the Kronos reactor are listed in Table 3-3. As with the Montecatini Edison reactor, the toluene combustion feed is assumed to have combusted before entering the reactor producing a stream of 81% CO_2 and 19% water (by weight). This assumption was made for simplicity due to the complexity of toluene combustion kinetics. It should also be noted that the value listed for the $TiCl_4$ feed in Table 3-3 is a total feed rate which is assumed to be distributed evenly over four inlets.

TABLE 3-3: Boundary Conditions for Kronos Reactor

Boundary Name	Boundary Type	Value	# of Inlets	Temperature
Oxygen	Inlet	101 m/s	4	950 °C
Titanium Tetrachloride	Inlet	3.15 kg/s	4	450 °C
Combustion Gases	Inlet	0.171 kg/s	1	2600 °C
Exit	Outlet	290.0 kPa	N/A	N/A

Boundary conditions used in the simulation of the simplified Kerr-McGee reactor are listed on the next page in Table 3-4. Unlike previous simulations, the combustion of propane and $TiCl_4$ are both modeled in the Kerr-McGee reactor with propane combustion being modeled using the eddy-dissipation model. Also, for the combustion of propane a limiting mixing rate was set to maintain a peak reaction temperature of approximately

25

3,300 °C. Finally, the exit stream for this reactor is modeled as an opening instead of an outlet to help aid in convergence.

TABLE 3-4: Boundary Conditions for Kerr-McGee Reactor

Boundary Name	Boundary Type	Value	Temperature
Oxygen	Inlet	0.4208 kg/s	955 °C
Titanium Tetrachloride	Inlet	1.669 kg/s	400 °C
Propane	Inlet	0.0138 kg/s	25 °C
Nitrogen	Inlet	0.003 kg/s	25 °C
Exit	Opening	140.0 kPa	1800 °C

Initialization

The initialization process of a simulation provides a numerical basis from which calculations proceed. With bad initial values for the calculations to proceed from, convergence can be greatly slowed or make a solution unachievable and in certain cases produce incorrect solutions. For all simulations the auto-initiate function was used except for component specification. For these initial conditions a value of five weight percent was set for all species involved in the simulation except O_2 which comprised the remainder of the faction. Also, in several instances it was advantageous to calculate a cold flow solution (no reactions occurring) to generate initial conditions for a simulation with reaction occurring.

Mesh Generation

Mesh generation is the process which spatially discretization of a CFD model occurs (CFX-5 Online Documentation) and is perhaps the most important step when setting up a simulation. Typically the smaller and more refined a mesh is the more accurate the results will be; however, with a smaller mesh more computer power and time

is required for a solution which leads to a trade off between the desired accuracy level and the time or "cost" of a simulation.

In this research the meshing procedure is based on CFX-Build's default triangular/tetrahedral method. For all simulations, the mesh size was set as close as possible to the background length scale which is based off of 1% of the overall maximum model dimension. This was done due to computational limitations. In regions of interest or in regions with large gradients, mesh controls where used to refine the size of the mesh.

Solver Setup

The solver setup of a simulation defines values used by CFX-5 Solver Manager to calculate results. Several important values set in this section include: number of timesteps, duration of a timestep, target residuals, the advection scheme, mesh adaptation, and transient file output information. Selection of these parameters can influence both the output and performance of the solver.

Information about the number and duration of timesteps are the first input parameters. The number of timesteps tells the solver how many iterations to calculate before terminating a run unless the target residuals are met beforehand. Duration of a timestep is the length of time simulated during a single timestep. For all simulations the typical number of timesteps used was two thousand and the duration was calculated by the automatic timestep or by a local timestep factor of three.

The target residuals and advection scheme help to set the level of accuracy of a simulation. The target residuals are calculated from the deference of solution variables

from one timestep to the next. When this criterion is set and all variable residuals are below this set level, a simulation is considered converged and is terminated even if there are still timesteps left to calculate. The level of convergence set for all simulations was 10^{-4} for the maximum residual of a variable. The advection scheme increases the accuracy of a simulation by increasing the accuracy of differentiation. Two levels of differentiation are available in CFX 5.5.1, first order and high resolution (second order). For all simulations in this work first order differentiation was used to calculate initial results for use in the high resolution simulation.

The final information needed in the solver control is about transient output files and mesh adaptation. Transient output files are used when a transient simulation is performed. These data tell the solver how often and what solution data to write to the output file. Mesh adaptation is used to refine the mesh in areas with high gradients to increase accuracy and aid in convergence. During adaptation larger elements are broken into smaller elements in areas of the highest gradients for a selected variable or variables. For this research, variables were chosen by the convergence rate with the slowest converging variables being select as an adaptation parameter such as TiO_2 mass fraction (TiO_2.mf).

TABLE 3-5: Mesh Adaptation Information for Simulation Reactors

Reactor	Nodes before	Nodes after	Variables used for adaptation
Montecatini Edison Reactor	100943	117878	Cl_2.mf, O_2.mf, and $TiCl_4$.mf
Kronos Reactor	89708	118950	Velocity
Kerr-McGee Reactor	87988	113125	O_2.mf, TiO_2.mf, and Temperature

Once the reactor model has been completely setup, a definition file is written for the model containing all the information provided during setup. This definition file can then be simulated using CFX-5 Solver Manager where the general modeling equations

for mass, momentum, and energy transport are numerically integrated using the information provided in the definition file. Once target residuals are reached during the solution phase of the simulation, the Solver Manager writes an output file containing values for all the variables solved in each volume element in the geometry. This information can then be viewed using CFX Post.

CHAPTER IV

RESULTS

Introduction

This chapter focuses on the results obtained from simulation of the three reactors discussed in Chapter 3. The information obtained from the simulations is analyzed to determine the level mixing present in each of the reactors. Three separate simulations were performed for each reactor to gather the information needed to quantify the different types of mixing present in the reactors. The first simulation performed was a transient simulation to gather residence time distribution (RTD) information. Second, a simulation modeling multiple tracers for species of interest was performed. Finally, a simulation predicting the age of fluid at any point in the reactor was performed.

The first simulation in this research, which is used to determine the RTD of the reactors, provides a macroscopic view of mixing in the reactor. This macroscopic view helps to describe the different levels of mixing as related to the residence time that are available to a molecule of $TiCl_4$ (Weinstein and Adler 1967). In this work, the method used to find the RTD involved first solving the reactor for a solution when operating under normal conditions then using this solution as an initial starting point for a step tracer simulation as described in Chapter 2. Figure 4-1 (next page) illustrates how the tracer moves through the reactor in a slice plane taken at several different timesteps.

30
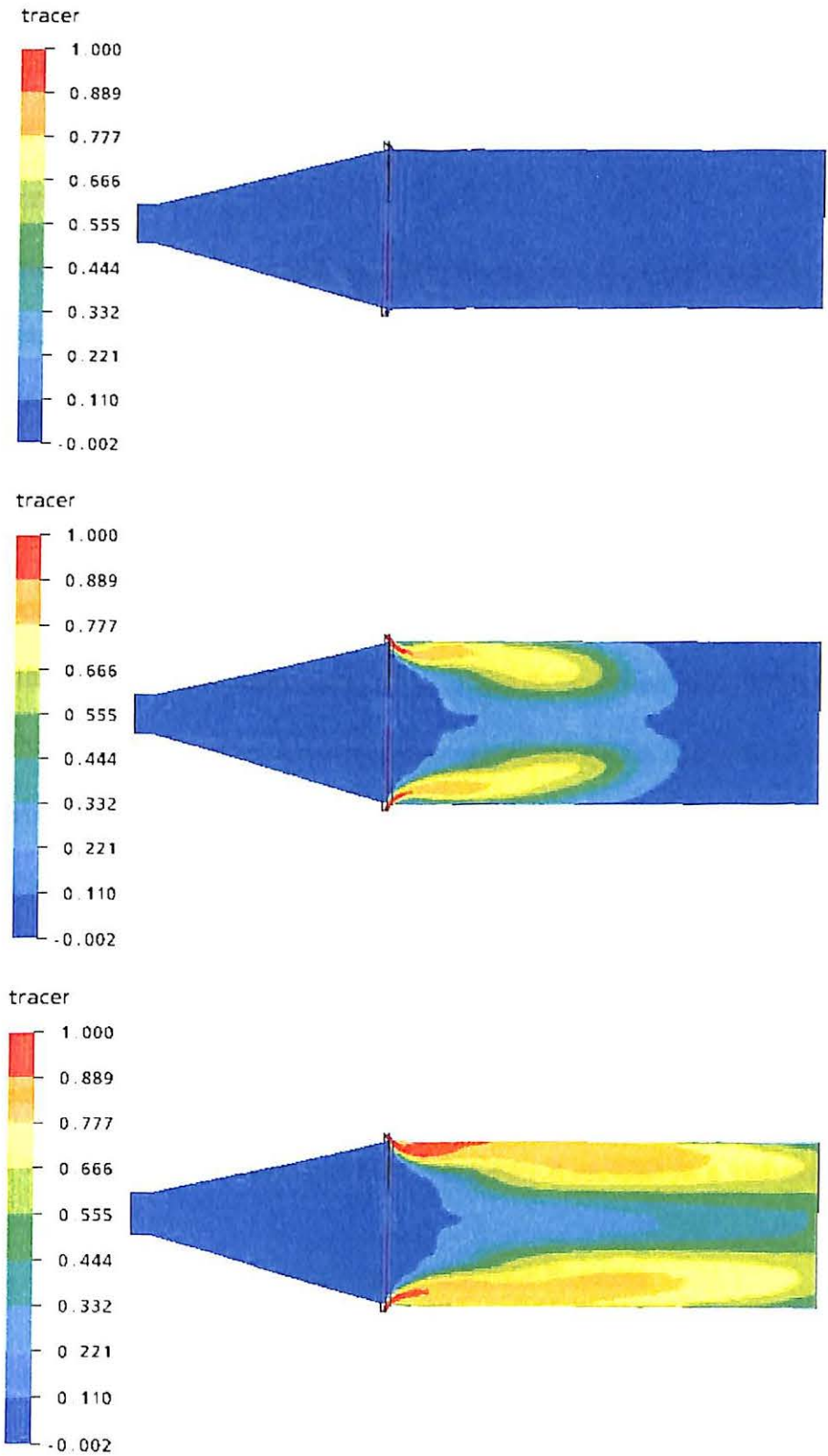
FIGURE 4-1. Example of tracer movement during a transient simulation of Montecatini Edison reactor at three timesteps: 0.0 s, 0.0075 s, and 0.0175 s (top to bottom).

Normally when calculating the RTD, the concentration of tracer at the exit is the monitored variable; however, in this work there are multiple inlets to the reactors leading to dilution of the tracer and therefore the mass flowrate of tracer at the exit is the monitored variable.

The second simulation in this research used tracer flow patterns for both O_2 and $TiCl_4$ to determine the level species mixing and interaction inside the reactor. With information on the species mixing, locations of poor mixing can be identified and corrected. This simulation was performed by adding a tracer to each of the O_2 and $TiCl_4$ inlets and running until a steady state solution was obtained then comparing tracer levels at various locations in the geometries.

The third simulation performed in this research involved calculating the "age" of the fluid in the reactor. For this work the term age refers to the amount of time fluid of interest has resided inside the reactor. By calculating the age of the fluid this can give a measure of the amount of recirculation at a given point. With knowledge on areas of high recirculation, or regions where the age is higher than surround areas, modification can be made to increase efficiency. The method used to calculate the age of the fluid involved creating a subdomain with a source term where age was a transported additional variable and was added to a volume of fluid whenever it resided in a volume element.

RTD Analysis of Selected Reactor

The ability of the residence time distribution information to describe the macroscopic mixing occurring in the three selected reactors is presented. When possible

comparisons to claims made in a patent are provided. Also comparisons between the different reactors are presented.

Montecatini Edison Reactor

Simulating a tracer step input for the Montecatini Edison reactor and normalizing the outlet tracer flowrate by the tracer feed-rate gives the cumulative distribution function, F(t). From the F(t) curve more than 80% of the tracer resides in the reactor less than 20 ms and approximately 95% resides in the reactor less than 35 ms. For the tracer to completely exit the reactor, 71 ms is requires and implies a small percentage of the tracer is recirculating for much longer than the rest of the tracer. This information also implies that there is a large amount of non-ideal mixing occurring in the reactor.
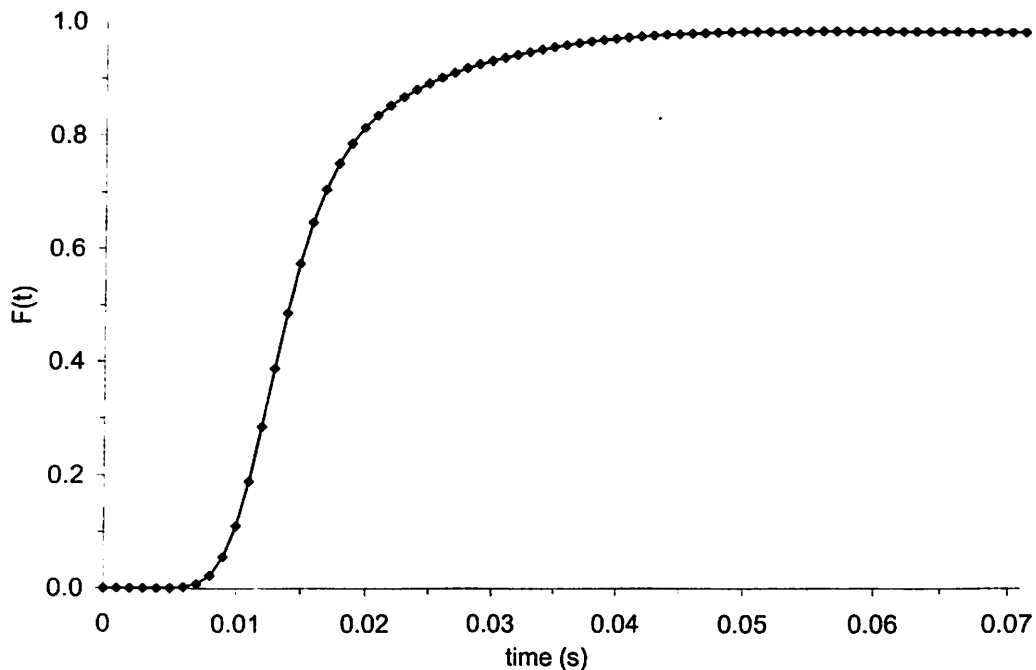
FIGURE 4-2. Cumulative distribution function for the Montecatini Edison reactor.
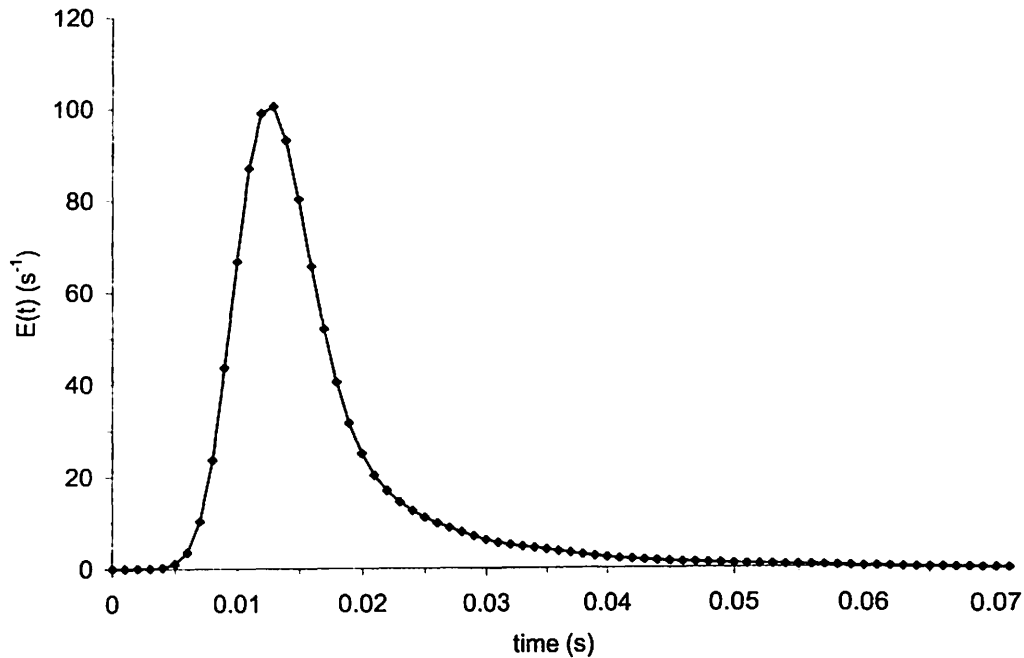
FIGURE 4-3. Exit age distribution function for the Montecatini Edison reactor.

The exit age distribution, E(t), was calculated by differentiation of the F(t) curve. Again, the long tail on the curve indicates that there is non-ideal mixing occurring in the reactor, and the curves peak indicates that the large majority of tracer resides in the reactor between 5-30 ms.

From the E(t) curve, the first three moments of the RTD are calculated. Solving Equation 2-6, the mean residence time for this reactor was found to be 16.3 ms. In the Montecatini Edison patent, the residence time in the reaction chamber is claimed to be 90 ms; however, the simulated reaction chamber is 250 mm while the patent reaction chamber is 1400 mm. (This length was shorted due to computational limitations.) By using the average downstream velocity at the reactor exit of 21.6 m/s, the tracer would require a minimum of 53.2 ms of additional time to travel the 1,150 mm difference in the reaction chambers. Adding this additional time to the mean residence time the 'adjusted' mean residence time is 69.5 milliseconds. There is still a difference of 23% in the

34

reported value and the adjusted value, but the adjusted value would mostly likely be higher due to momentum and friction losses that would be experienced in the longer reaction chamber. With the mean residence time and Equation 2-7, the variance is calculated to be 60.8 ms^2. This leads to a standard deviation for the distribution of 7.8 ms, which is quite large since it is almost half of the mean residence time. The skewness is calculated from the variance and Equation 2-8 and gives a value of 1,122 ms^3 meaning that the distribution is moderately skewed to the right of the mean.

Kronos Reactor

For the Kronos patent very little information was given on mixing occurring inside the reactor. Therefore, information gained during simulation is presented but not compared to any physical data. The F(t) curve for the Kronos reactor is very similar to the Montecatini Edison reactor curve in the overall curves shape, but the Kronos reactor has a much large capacity and thus a longer residence time. The F(t) curve (next page) shows that approximately 80% of the tracer leaves the reactor in the first 0.15 s and that 95% of the tracer has exited by 0.2 s. The last 5% of the tracer requires an additional 0.5 s to exit the reactor, which indicates that a small percentage of the tracer is caught in a region of strong recirculation.

The E(t) curve (next page) is generated from the cumulative distribution function. This exit age curve is very similar to the Montecatini Edison E(t) curve except in the order of magnitude. The main difference in these curves is the severity of the slope for the Kronos reactor both before and after the peak. This implies that the flow in the Kronos reactor is closer to that of an ideal reactor than for the Montecatini Edison reactor.
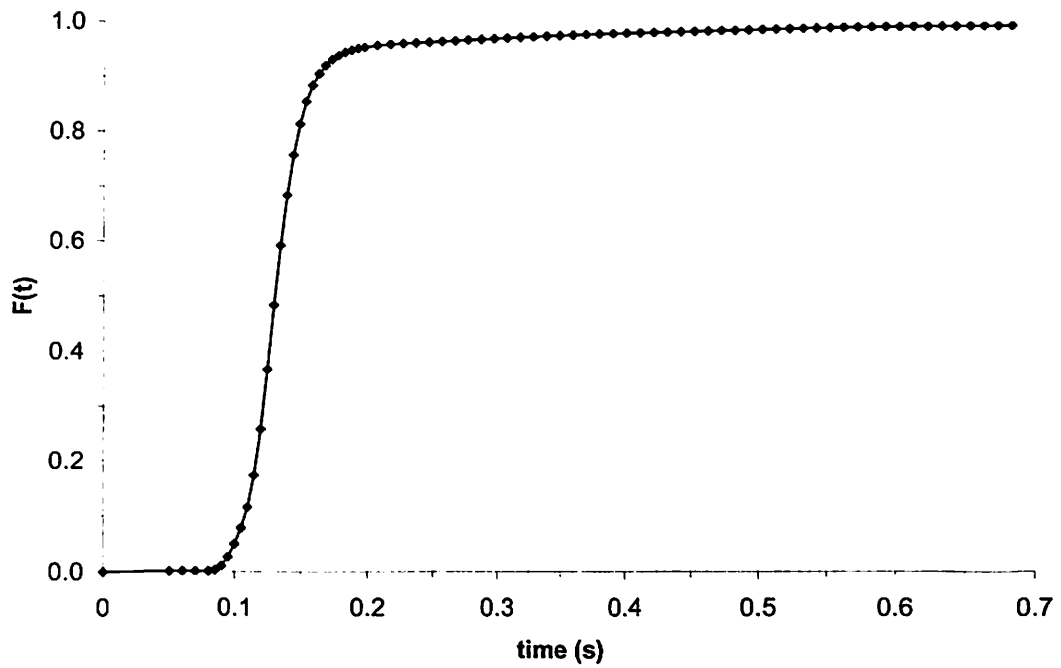
FIGURE 4-4. Cumulative distribution function for the Kronos reactor.
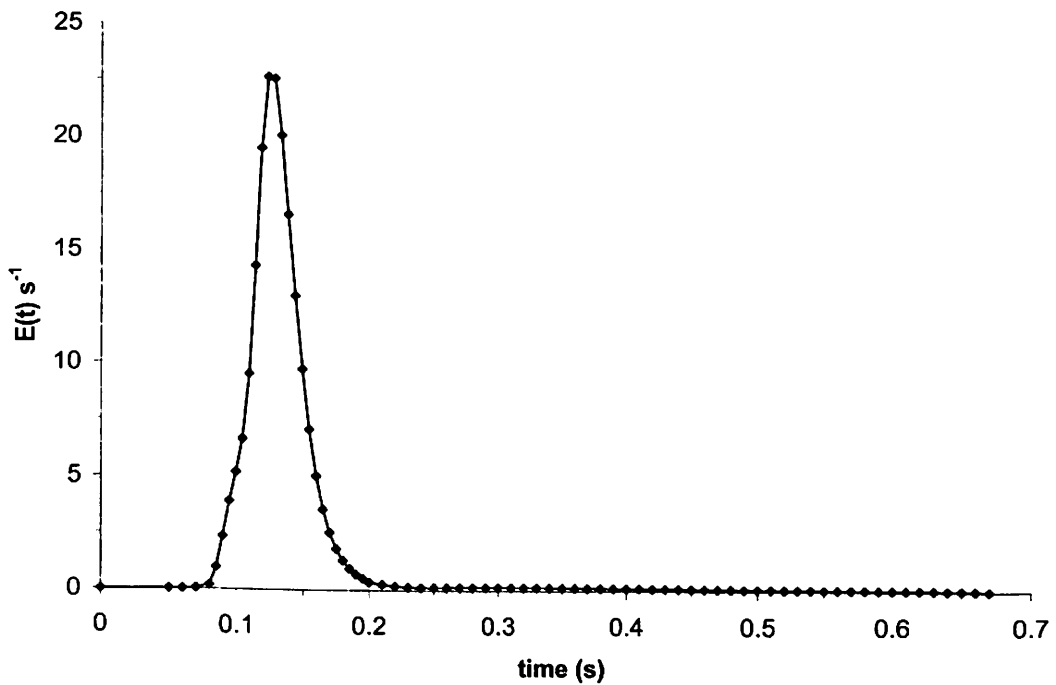
FIGURE 4-5. Exit age distribution function for the Kronos reactor.

Using the E(t) curve for the Kronos reactor, the first three moments of the RTD were calculated. First, the mean residence time for the Kronos reactor is 0.142 s, which is almost nine times the mean residence time for the Montecatini Edison reactor. Next, the variance is 0.00385 s^2 giving a standard deviation of 0.062 s which is again nearly half the mean residence time. Finally, the distribution has a skewness of 0.076 s^3 meaning the distribution is skewed right of the mean residence time.

Simplified Kerr-McGee Reactor

Information about the level of mixing inside the simplified Kerr-McGee reactor is unavailable and therefore simulation information is not compared to physical data. The cumulative distribution function for the simplified Kerr-McGee reactor is presented in Figure 4-6. The F(t) curve (next page) begins to rise and ends at approximately the same times as the Kronos reactor; however, the simplified Kerr-McGee reactor has a much smoother and more S-shaped curve with a shorter tail at the end implying that there is more non-ideal mixing occurring in this reactor compared to the Kronos reactor. In this reactor setup 80% of the tracer resides in the reactor less than 0.28 s and 95% resides less than 0.41 s. This means the final 5% of tracer leaves the reactor during the final 0.30 s giving a shorter tail region than the Kronos reactor.

The exit age distribution for the simplified Kerr-McGee reactor varies greatly from the Montecatini Edison and Kronos reactors E(t) curves. The E(t) curves for the first two reactors were large spikes that rose and dropped sharply with long tails on the end. For this reactor, the E(t) curve is nearly bi-modal and is much wider than the previous curves. E(t) curves of this type typically mean a reactor has compartmentalized
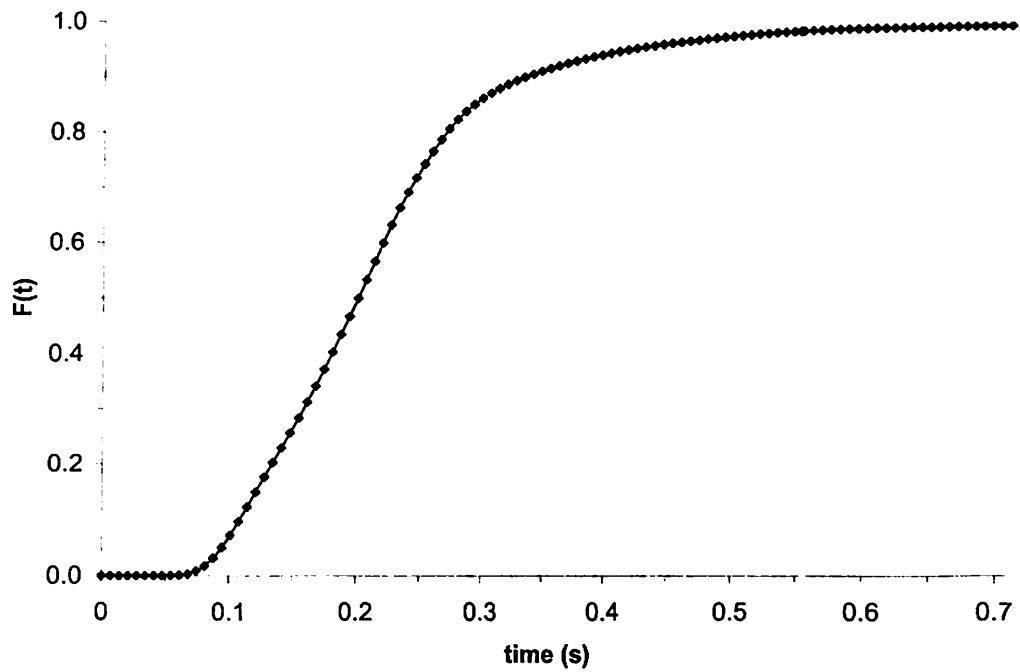
FIGURE 4-6. Cumulative distribution function for the simplified Kerr McGee reactor.
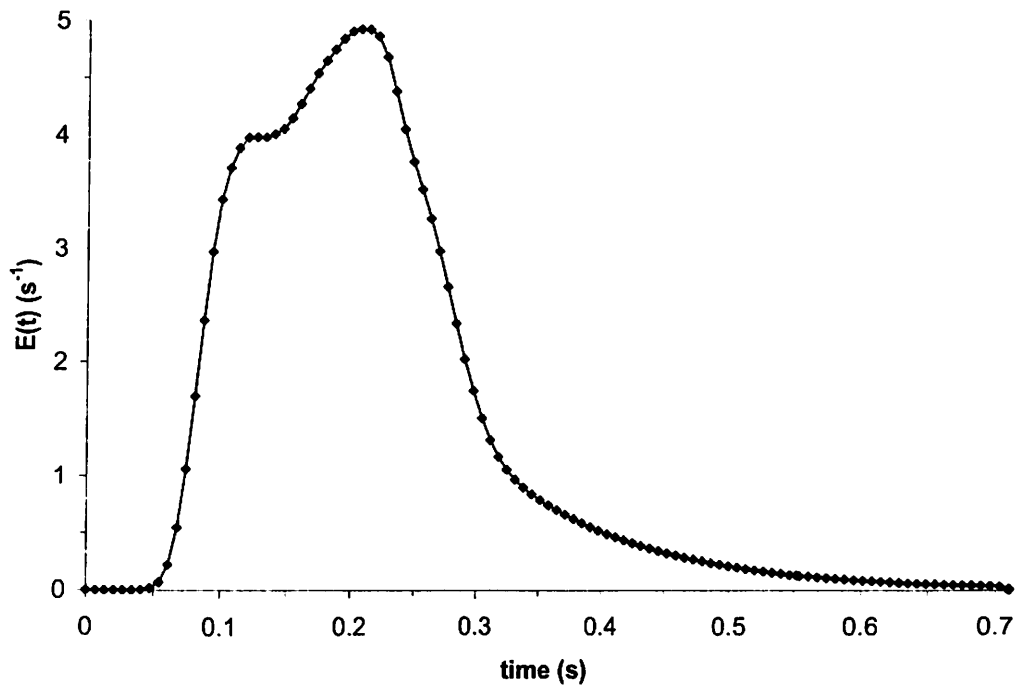
FIGURE 4-7. Exit age distribution function for the simplified Kerr-McGee reactor.

mixing occurring. In the simplified Kerr-McGee reactor this is mostly likely due to recirculation in the distribution spool and mixing in the main reaction chamber.

For the simplified Kerr-McGee reactor, the first three moments of the tracer distribution are: 0.216 s for the mean residence time, 0.0096 s^2 for the variance, and 0.043 s^3 for the skewness. From the variance the standard deviation is 0.098 s and is comparable with the deviations of the other reactors when measured against the reactors mean residence time. (All standard deviations are approximately 45% of the mean residence time.) Also, the distribution for the simplified Kerr-McGee reactor is skewed right of the mean but not as much as the previous reactors. Table 4-1 provides a synopsis of the moments for the three reactors.

TABLE 4-1: Moments of RTD for the Simulated Reactors

Reactor	Mean Residence Time (t_m)	Variance (σ^2)	Skewness (s^3)
Montecatini Edison	16.3 ms	60.77 ms^2	1121.96 ms^3
Kronos	0.142 s	0.00385 s^2	0.076 s^3
Simplified Kerr-McGee	0.216 s	0.0096 s^2	0.043 s^3

Analysis of Tracer Flow Patterns

Tracer flow patterns for O_2 and $TiCl_4$ in the simulated reactors are presented in this section to quantify species mixing in the simulated geometries. This information provides insight into the micro-mixing occurring at any specific point in the reactors and will also help to identify regions where mixing is poor. The tracer flow patterns are compared with the simulated species profile to show how depletion from reaction alters the profiles.

Montecatini Edison Reactor

In the Montecatini Edison reactor design, the oxidizing gas is fed into the system with a swirling helical motion. According to the patent, this setup provides an up-drawing of $TiCl_4$ into the O_2 rich zone and it is claimed that this setup helps to promote nucleation of TiO_2 particles which produces a smaller number of particles with larger dimensions.

The results of a $TiCl_4$ tracer analysis performed at steady-state are presented in Figure 4-8. A two-dimensional slice pane taken along the length of the reactor is shown in the figure where areas colored red represent a tracer concentration of 5% by mass or higher. As the figure shows, there is a small amount of tracer being drawn into the front region of the reactor which supports the claim made in the patent that $TiCl_4$ is being drawn into the O_2 rich zone of the reactor.
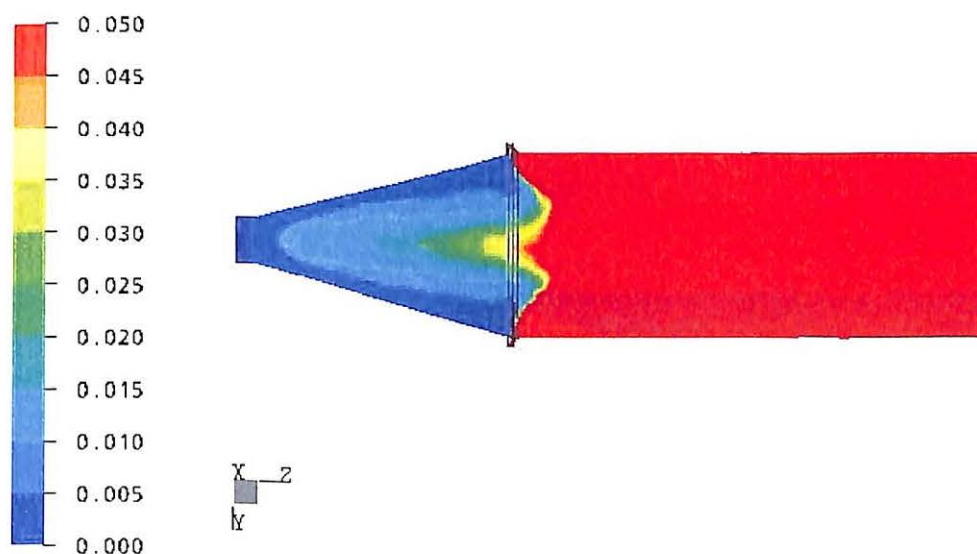
FIGURE 4-8. Contours showing the up-drawing of $TiCl_4$ tracer into the O_2 rich region for the Montecatini Edison reactor.

Figures 4-9 and 10 illustrate the TiCl₄ and O₂ tracer contours over the entire concentration range. In these figures the concentration profiles represent how the respective species would flow through the system if not being consumed in the reaction. As expected the TiCl₄ tracer concentration is highest near the walls of the reaction chamber while the O₂ tracer is channeled more into the center of the chamber.
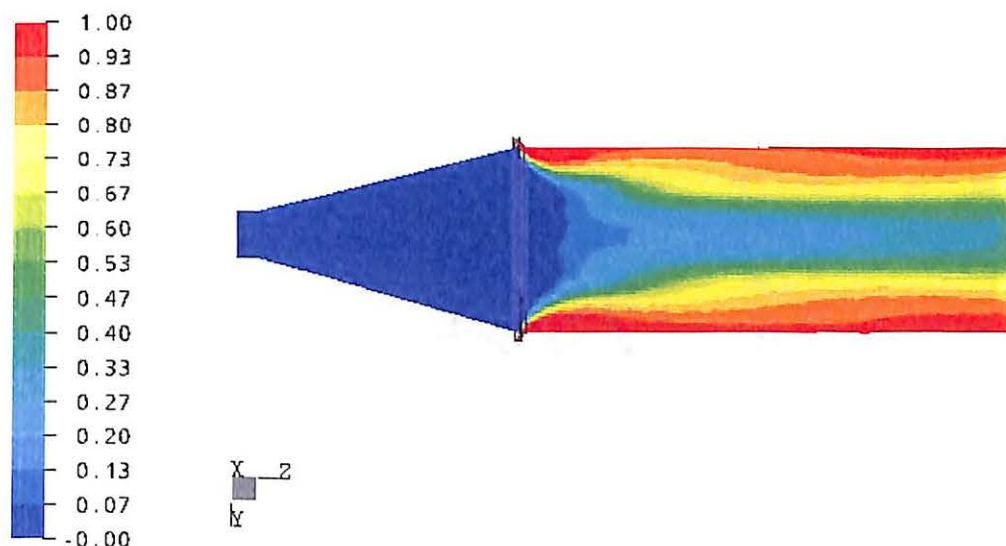
FIGURE 4-9. Tracer contours for $TiCl_4$ concentration in the Montecatini Edison reactor.
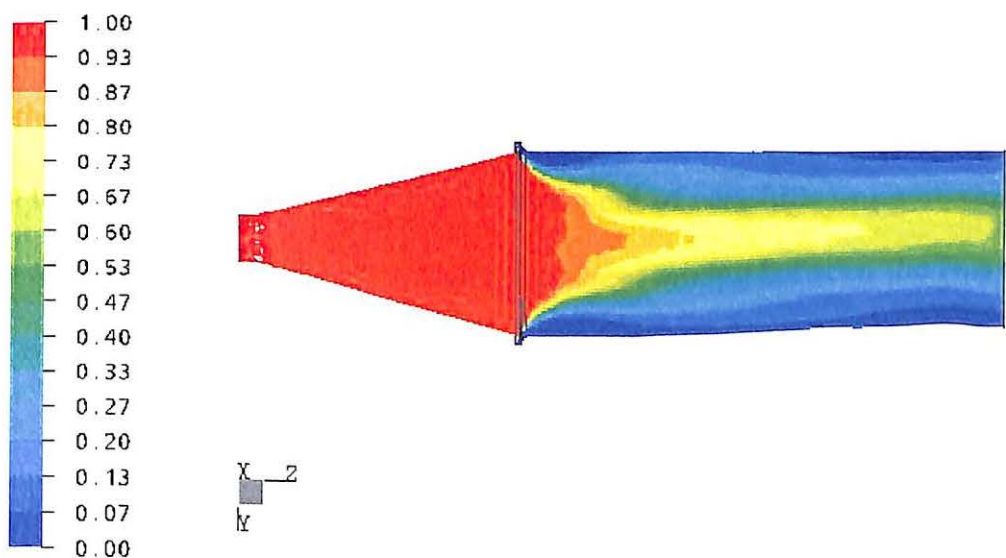
FIGURE 4-10. Tracer contours for O_2 concentration in the Montecatini Edison reactor.

To determine the level of species mixing in the reactor, an additional analysis was performed by overlaying the two figures shown on the previous page. The figure generated in this analysis graphically shows regions of good species mixing (near 1:1) and also regions of very poor species interaction.
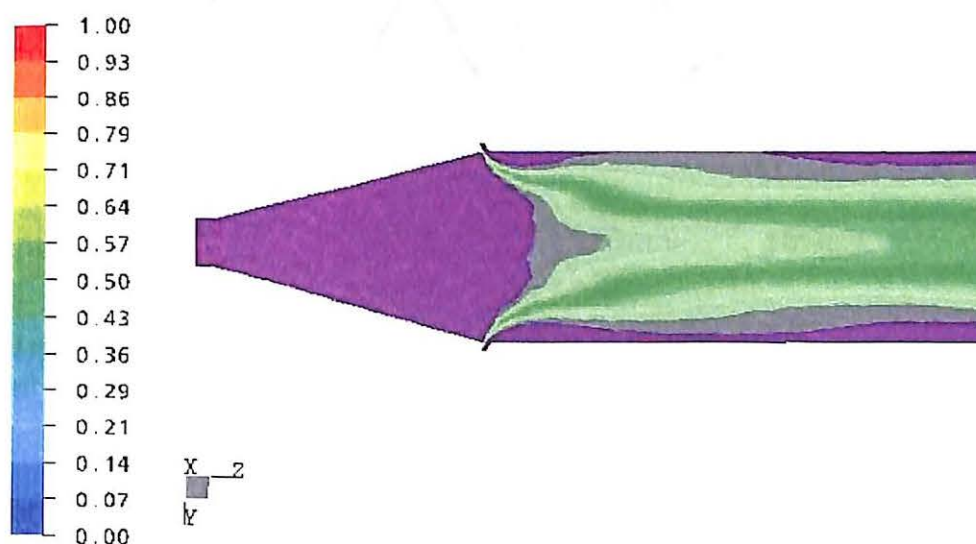
FIGURE 4-11. Contour profile showing the interaction between $TiCl_4$ and O_2 tracers in the Montecatini Edison reactor.

From Figure 4-11, when the concentration of one species is near 100% (red) in a region the other is near 0% (blue), so when the two are overlaid the resulting color scheme is purple. Therefore, purple indicates regions of very little or no mixing between the two reacting species. The green regions represent mixing between the two species at or near a 1:1 ratio. The more vivid the color of green the better the species mixing ratio is in that region.

A similar comparison can be made by overlaying the contours for $TiCl_4$ and O_2 molar fractions. The same color schemes are observed where areas of good species mixing occur in the green regions and areas of poor species mixing occur in the purple

regions; however, since $TiCl_4$ and O_2 are being exhausted in the reaction, regions of blue are now seen and represent areas where both species are near zero concentration.
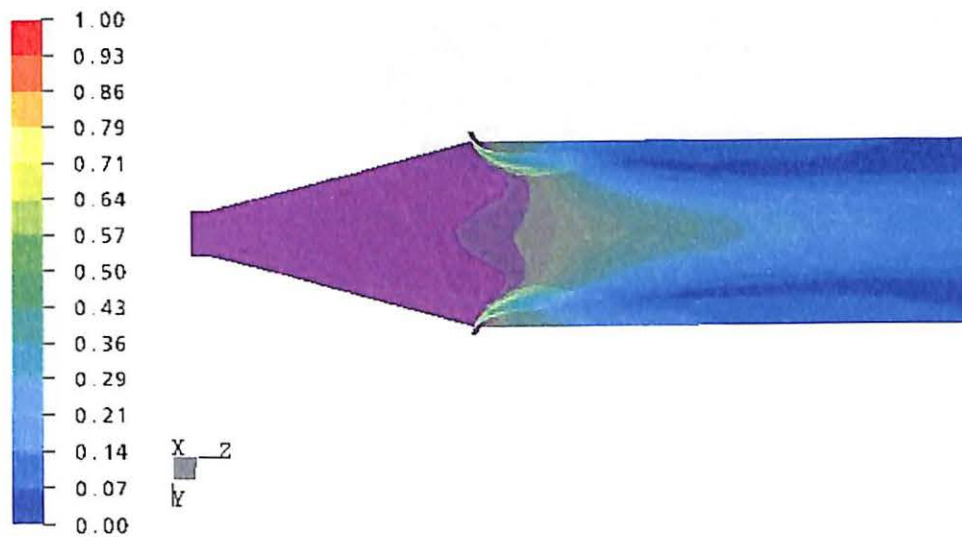
FIGURE 4-12. Contour profile showing the interaction between $TiCl_4$ and O_2 molar fractions in the Montecatini Edison reactor.

From Figure 4-12 it seems that the area of highest species mixing occurs near the front edge of the $TiCl_4$ inlet and extend slightly towards the center of the reactor and downstream while very little mixing occurs in the reactors center. This is the expected result and coincides with the contours showing the region of the highest reaction rate as seen in Figure 4-13 (next page).
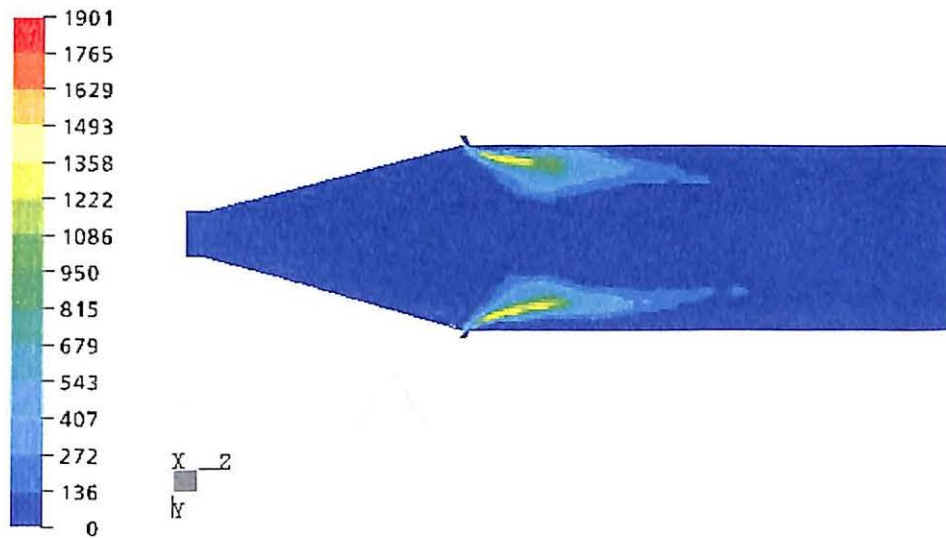
FIGURE 4-13. Reaction rate contours for the Montecatini Edison Reactor. (units for the reaction rate are in mol m^{-3} s^{-1})

Kronos Reactor

The Kronos reactor setup is typical of industrial scale TiO$_2$ reactors. At the beginning of the reactor, oxygen is added and pre-heated by combustion of a hydrocarbon. Afterwards, TiCl$_4$ is introduced and oxidized in a tubular reaction chamber. One feature of this reactor is atypical, however, and is the focus for a majority of the patent. This feature is the shape of the pre-heating chamber and was specifically designed to protect the walls of the reactor from excessive temperatures. Simulation of this reactor configuration show that the design of the preheat chamber greatly effects the mixing of TiCl$_4$ and O$_2$.

The results of the tracer analysis can be seen in the following figures. Flow profiles for the TiCl$_4$ and O$_2$ tracers on a symmetry plane are given in Figures 4-14 and 15. From Figure 4-14, the design of the pre-heat chamber causes backflow of the TiCl$_4$ tracer and recirculation in the expanded region just before the TiCl$_4$ feed. This result is

44

unwanted since mixing of the reactants will cause the formation of TiO_2 near the $TiCl_4$ inlet and on the walls of the reactor prior to the inlet, which can lead to scaling.
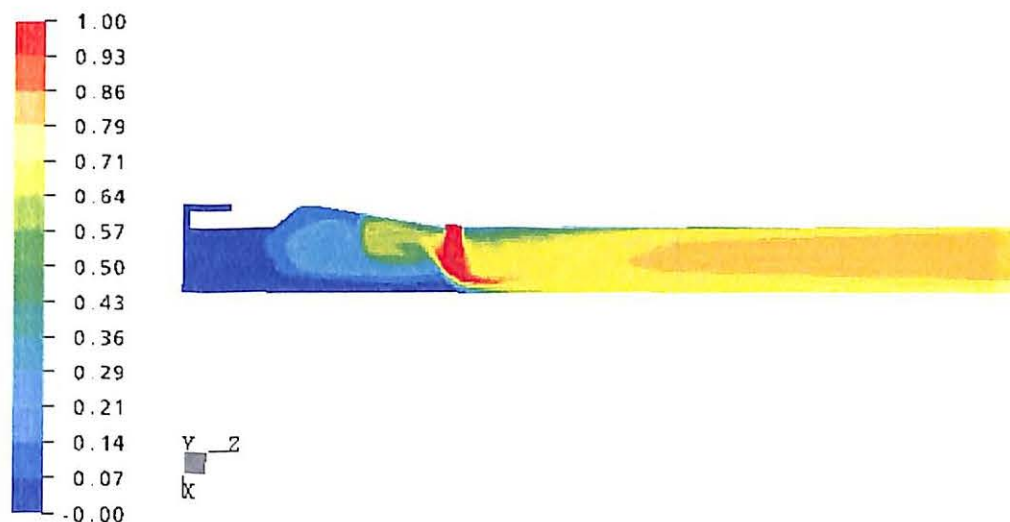
FIGURE 4-14. Tracer contours for $TiCl_4$ concentration in the Kronos reactor.
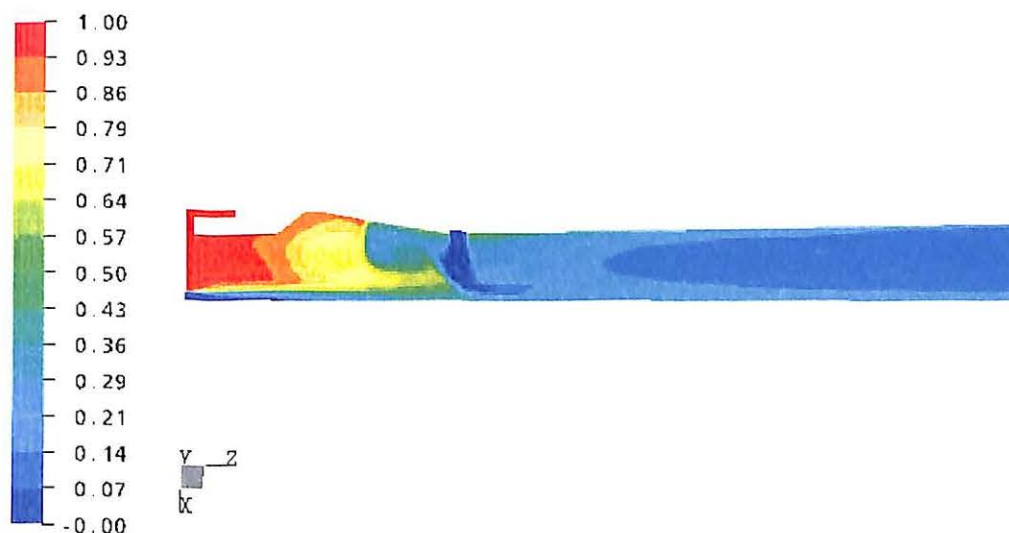
FIGURE 4-15. Tracer contours for O_2 concentration in the Kronos reactor.

Overlaying the tracer and molar fraction curves, as with the Montecatini Edison reactor, illustrates the level of mixing in the area of recirculation. Again, areas of purple indicate little or no mixing while areas of green indicate good mixing. From Figure 4-16,

the areas with the best mixing are the region of recirculation before the $TiCl_4$ inlet and directly after the $TiCl_4$ feed.
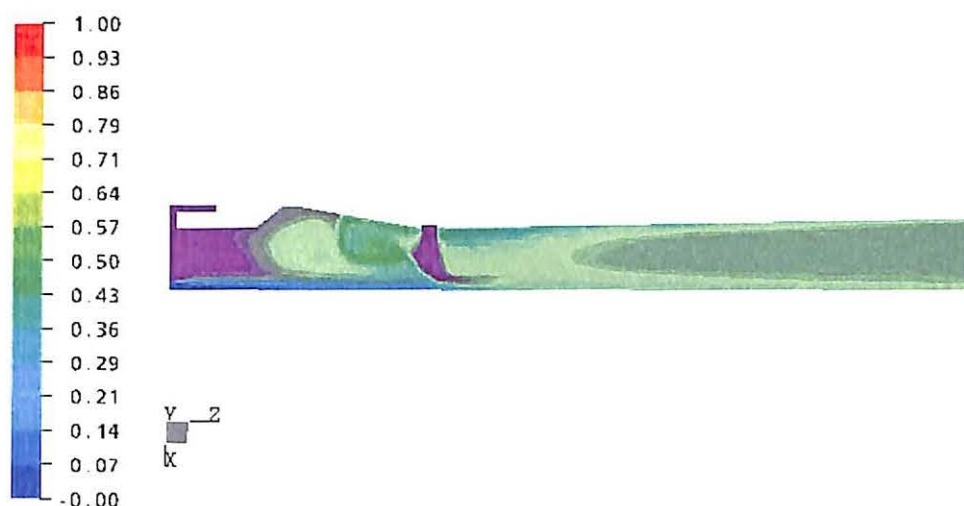
FIGURE 4-16. Contour profile showing the interaction between $TiCl_4$ and O_2 tracers in the Kronos reactor.

Figure 4-17 shows the affect that the reaction of the two species has on the mole fraction contours. The large area of blue before the $TiCl_4$ inlets indicates the rapid oxidation of $TiCl_4$ near the wall in that region. This outcome is unwanted since it leads to inlet plugging and scaling.
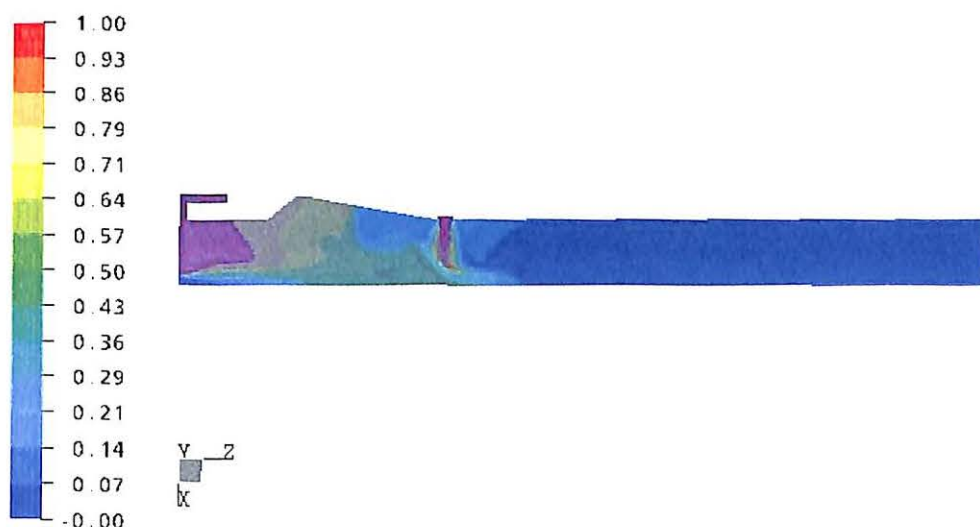
FIGURE 4-17. Contour profile showing the interaction between $TiCl_4$ and O_2 molar fractions in the Kronos reactor.

Simplified Kerr-McGee Reactor

The simplified Kerr McGee reactor is similar to the Kronos reactor setup. The reaction occurs in an expanding reaction chamber with O_2 being fed at the front of the reactor and combustion gases being added to increase the temperature. The simplified Kerr-McGee geometry has an additional $TiCl_4$ distribution system modeled with eight inlet nozzles into the main reaction chamber while the distribution system is not modeled in the Kronos reactor.

The results of a steady state tracer analysis for the Kerr-McGee reactor are shown below. The first two figures show the $TiCl_4$ and O_2 tracer contours along a two-dimensional slice plane taken down the length of the reactor. One of the most noticeable differences from the two previous reactors is the lack of $TiCl_4$ tracer backflow or recirculation in the preheating portion of the reactor. This is an important feature meaning the simplified Kerr-McGee reactor is less susceptible to scaling problems before the $TiCl_4$ inlet feed.
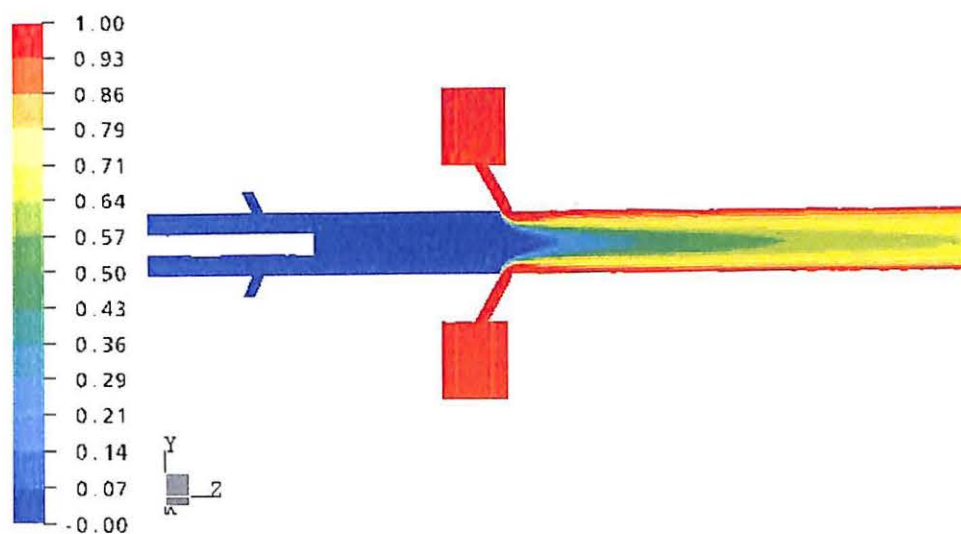
FIGURE 4-18. Tracer contours for $TiCl_4$ concentration in the simplified Kerr-McGee Reactor.
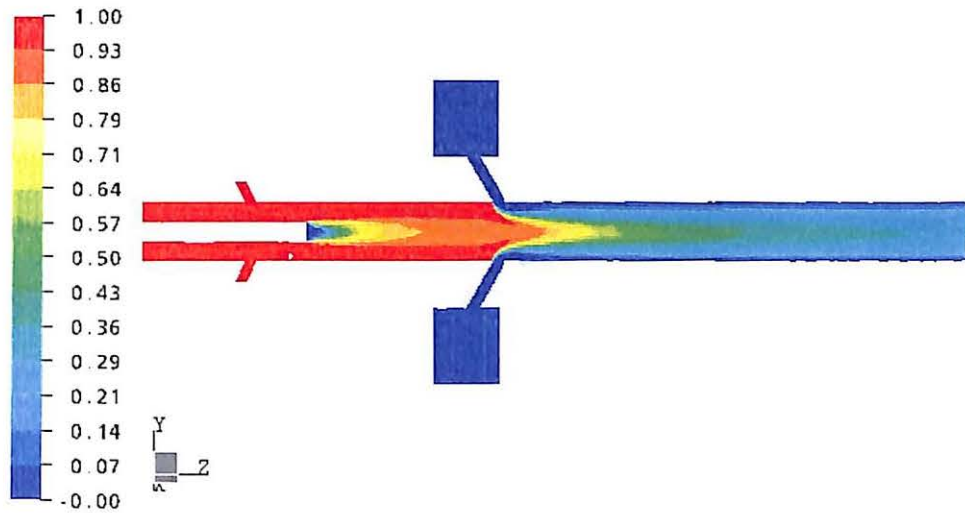
FIGURE 4-19. Tracer contours for O_2 concentration in the simplified Kerr-McGee Reactor.

As in the previous simulations, Figure 4-20 shows regions of good and poor species mixing by overlaying the two tracer contours, Figures 4-18 and 19. As expected, the best mixing between the O_2 and $TiCl_4$ tracers occurs in the center region of the reaction chamber. Figure 4-20 also shows that there is little to no mixing occurring after the $TiCl_4$ inlet or along the wall down the length of the reactor.
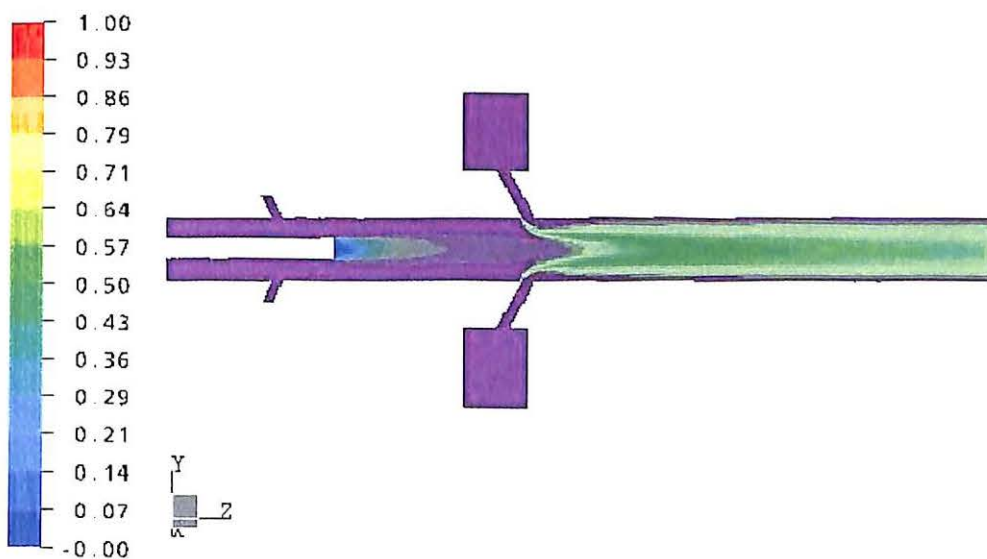
FIGURE 4-20. Contour profile showing the interaction between $TiCl_4$ and O_2 tracers in the simplified Kerr-McGee reactor.

This observation is compared to a species interaction profile taken along a slice plane between two of the eight TiCl$_4$ inlets, Figure 4-21. From this figure, there is a good deal of species interaction near the wall between the TiCl$_4$ inlets but not along the wall further downstream. This interact begins slightly after the front of the inlets and travels inward toward the center of the reaction chamber as it moves downstream with a small amount of TiCl$_4$ and O$_2$ tracer remaining near the wall. A close-up of this region, which includes the locations of the inlets, can be seen in Figure 4-22.
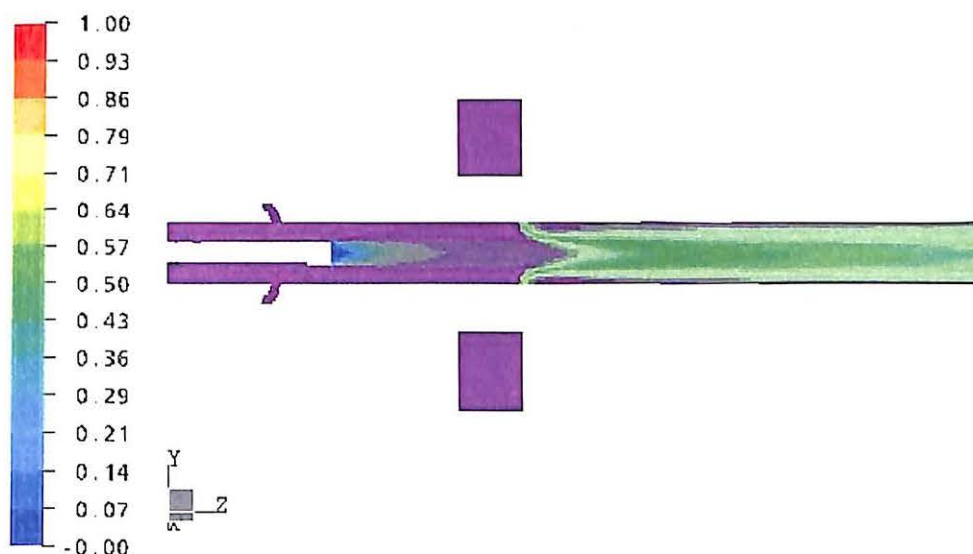
FIGURE 4-21. Contour profile showing the interaction between TiCl$_4$ and O$_2$ tracers between the TiCl$_4$ inlets in the simplified Kerr-McGee reactor.
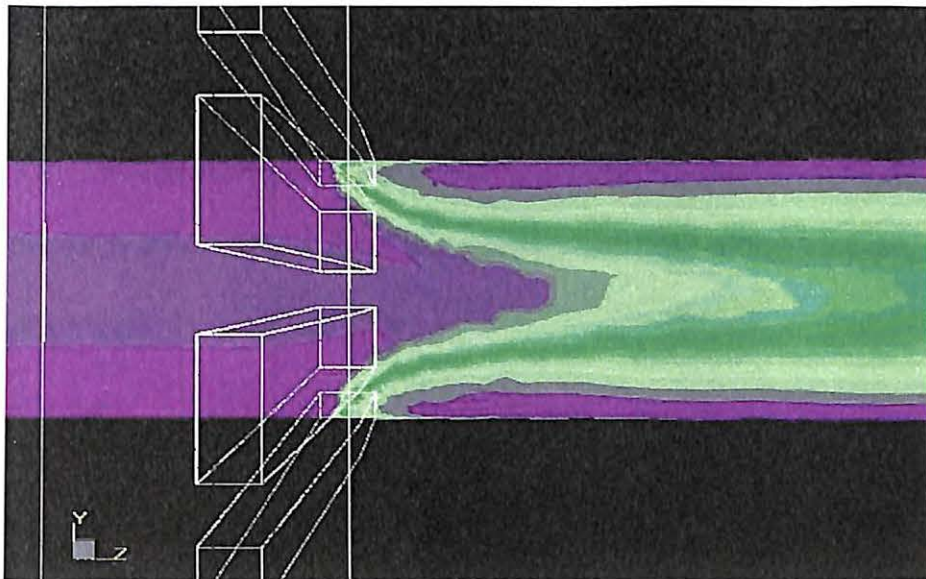
FIGURE 4-22. Close-up of contour profile showing the interaction between TiCl₄ and O₂ tracers between the TiCl₄ inlets in the simplified Kerr-McGee reactor.

Analysis of Fluid Age

The age of the fluid inside the studied reactors are presented in this section to quantify the level of backmixing and recirculation present in the simulated geometries. This information can be used to locate specific regions in a reactor where recirculation is occurring and also quantify the extent of the recirculation.

Montecatini Edison Reactor

The results of the age simulation analysis performed at steady-state for the Montecatini Edison reactor are presented below. The two-dimensional slice pane taken along the length of the reactor is the same as in the tracer study. The figure show two main locations where recirculation is occurring. The first region is in the O_2 rich region before the TiCl₄ inlet. The average fluid age in this region of recirculation is

approximately 18 ms. This value is slightly higher than the 16.3 ms mean residence time for TiCl$_4$ in the reactor, but the age in the simulation is for all fluids in the reactor including O$_2$. The second region of recirculation is more difficult to see and is located just after the TiCl$_4$ inlet. A close up of this region is provided in Figure 4-24.
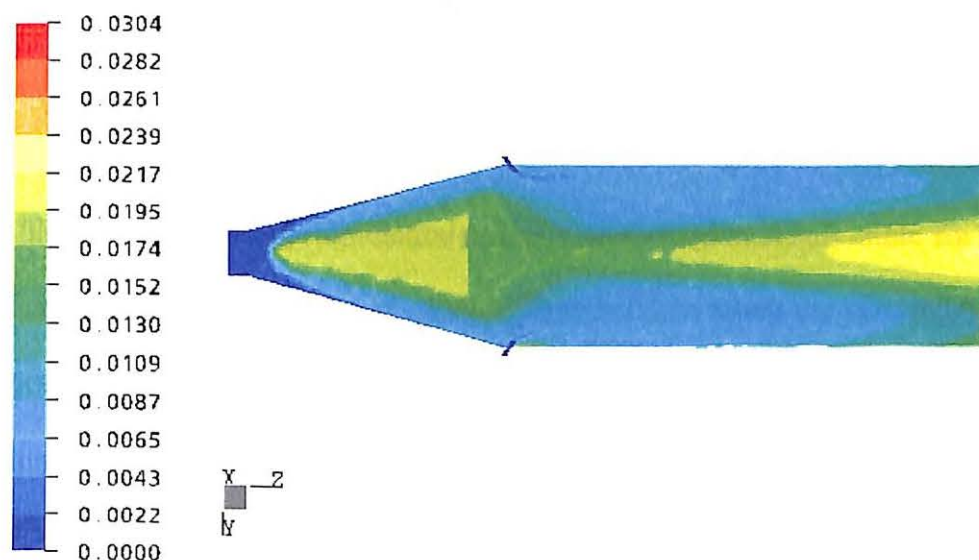
FIGURE 4-23. Fluid age contours for the Montecatini Edison reactor. (units are in seconds)
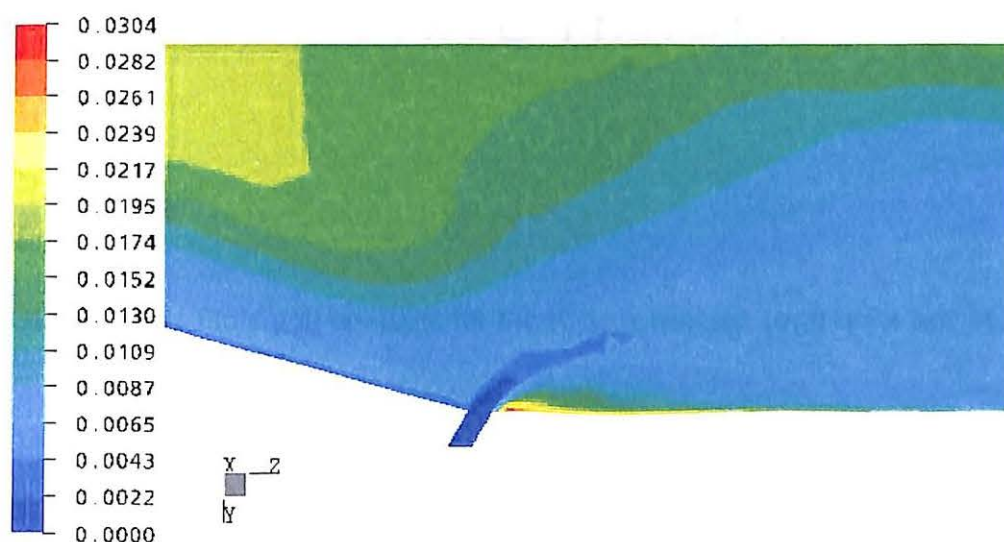
FIGURE 4-24. Fluid age contours at the TiCl$_4$ inlet for the Montecatini Edison reactor. (age units are in seconds)

The area of recirculation after the inlet is only a small region but in this region the extent of the recirculation is between 20-30 ms which is much higher that any other location in the reactor. This is of import since Figure 4-12 showed that there is a small amount of mixing between the two reactants in this region and any recirculation there may lead to deposition of TiO_2, thus reducing reactor efficiency.

Kronos Reactor

The results of the age simulation analysis performed at steady-state for the Kronos reactor are presented in this section. A slice plane is taken along the symmetry plane as in previous sections. Figure 4-25 illustrates how the fluid ages as it moves along this slice plane.
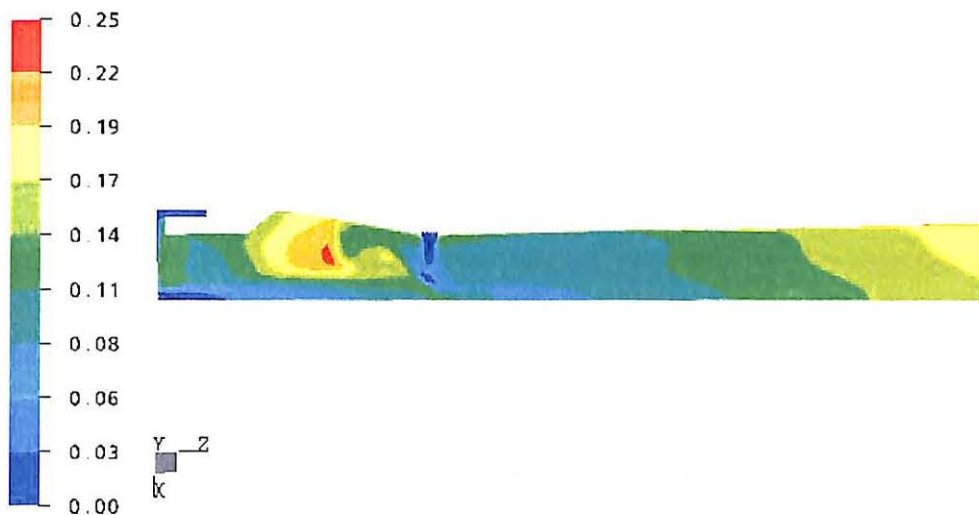
FIGURE 4-25. Fluid age contours for the Kronos reactor. (age units are in seconds)

From Figure 4-25, several interesting features about the way the fluid moves though the reactor can be seen. The first noticeable feature is the region of recirculation in the expanded portion of the reactor before the $TiCl_4$ inlets. This region shows strong

recirculation going back to the front end of the reactor with the fluid age approaching 0.25 s. This is almost 80% higher than the mean residence time for this reactor and is mostly likely the cause of the long tail on the Kronos reactors E(t) curve. The next interesting feature is the area just after the $TiCl_4$ inlet. From the results of the Montecatini Edison reactor, a small region of recirculation would be expected; however, in this region the fluid age is nearly the same age of the surrounding fluid (excepting the age at the actual inlet). This is mostly like due to the separate inlets used in this reactor compared to one continuous inlet in the Montecatini Edison reactor.

A second age contour taken half-way between the two symmetry planes (and $TiCl_4$ inlets) shows similar results to Figure 4-25. The main noticeable differences are that the level of recirculation in the region before the $TiCl_4$ inlets is greater and that the downstream fluid aging is more uniform. The uniform fluid aging downstream implies that there are fewer disturbances in the fluid flow between the $TiCl_4$ inlets.
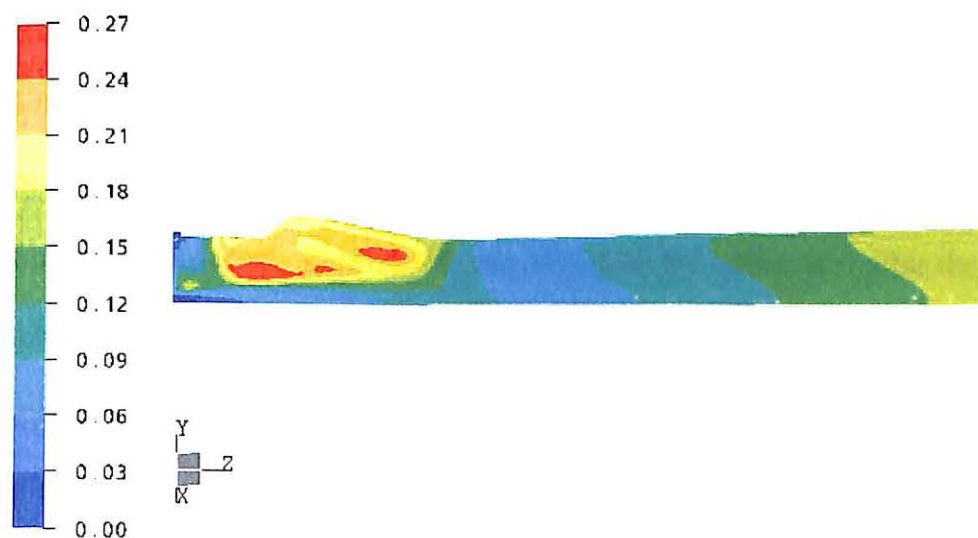
FIGURE 4-26. Fluid age contours between $TiCl_4$ inlets for the Kronos reactor. (age units are in seconds)

Simplified Kerr-McGee Reactor

The results of the age simulation analysis performed at steady-state for the simplified Kerr-McGee reactor are presented in this section. The slice plane is the same used in the previous tracer simulation section. From Figure 4-27, the major problem associated with using this technique can be seen. When two regions of fluid that have been separated for a moderate amount time meet, a discontinuity results and causes the age to be rapidly altered in that region.
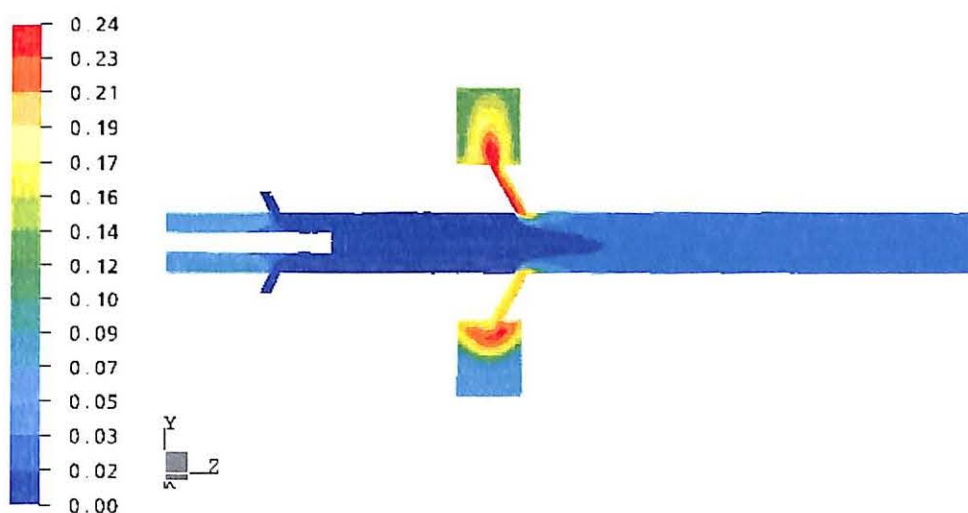
FIGURE 4-27. Fluid age contours for the simplified Kerr-McGee reactor. (age units are in seconds)

This problem is illustrated where the fluid entering the reaction chamber from the $TiCl_4$ distribution spool occurs. From this figure, the age in the region just after the inlet spool drastically drops and averaged with younger fluid from the preheat section. Figure 4-28 (next page) provides a more refined contour plot of the age in this region.
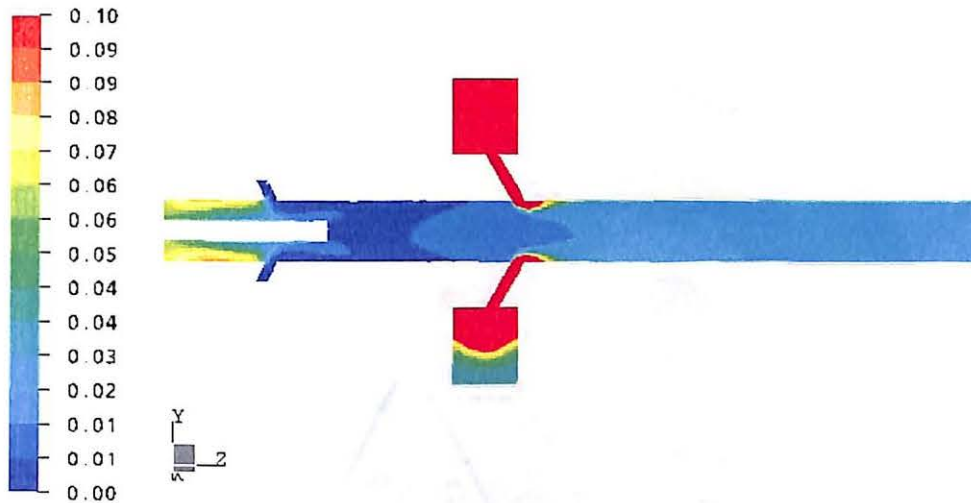
FIGURE 4-28. Refined fluid age contours for the simplified Kerr-McGee reactor. (age units are in seconds)

In order to see the age distribution in the spool, a slice plane was made perpendicular to the previous slice plane in the TiCl₄ distributor. In this view the strength of this method at predicting the fluid age can be seen since the spool is one contiguous region of the reactor.

From Figure 4-29 (next page), several interesting and unexpected observations can be made. One of the most interesting observations is the age of the fluid when it enters the nozzles. The nozzles with the "youngest" fluid entering them are the first two encountered upon entering the spool as might be expected; however, the fluid entering the last nozzle seen as the fluid circles around the spool is almost the same age. Another interesting feature is the age of the fluid as moves though the spool forming a ring around the spool. This implies that some of the fluid may circles around the spool several times before finally entering the nozzles.
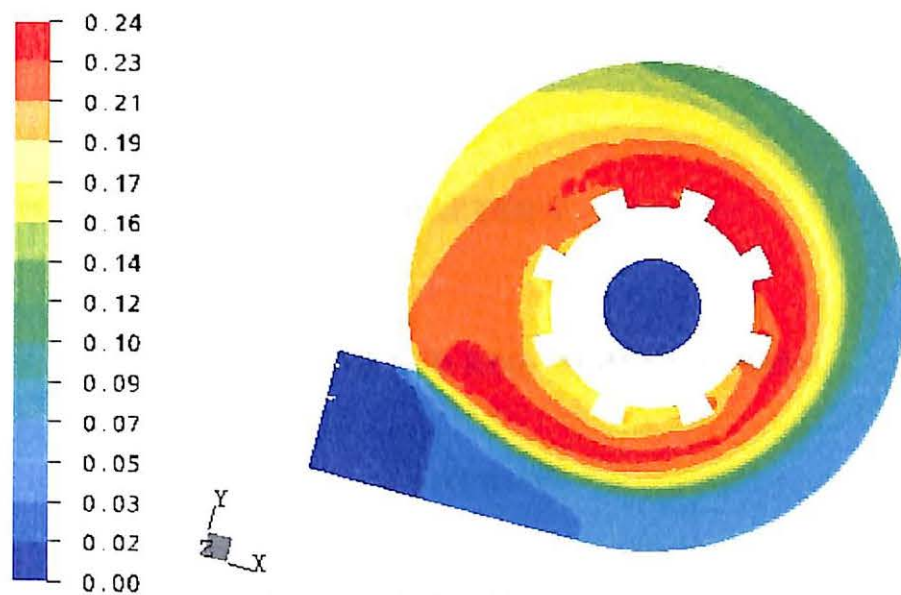
FIGURE 4-29. Fluid age contours for the simplified Kerr-McGee reactor in TiCl$_4$ distributor. (age units are in seconds)

CHAPTER V

CONCLUSIONS AND RECOMMENDATIONS

Conclusions

Three methods of quantifying mixing inside a reactor producing TiO_2 where evaluated using CFD. Specifically, the three methods were aimed at quantifying the level of macro-mixing, species interaction, and extent of recirculation. For this work, three different reactors where analyzed using these methods. The Montecatini Edison and Kronos reactors were both patented reactors and provided operating conditions and some information about the mixing or production of TiO_2. The third reactor, simplified Kerr-McGee, was modeled off assumptions and a simplified geometry of Kerr-McGee's chloride reactor.

Residence Time Distribution Analysis

The RTD was used to describe the level of macro-mixing available to the molecules of $TiCl_4$ in each of the three reactors. The exit age curves for all three reactors showed long tails at the end and were left skewed. This means that there is non-ideal mixing present in each reactor and specifically implies the presence of backmixing or recirculation. Also, in each reactor there is no evidence that bypassing is occurring. Of

the three reactors, only the Montecatini Edison reactor provided information on the residence time of TiCl$_4$. A comparison of the value in the patent and the value generated during simulation showed marked difference. This difference can be explained by the shortened reaction chamber studied in simulation, however. Table 5-1 provides a summary of the first three moments for each reactor.

TABLE 5-1: Moments of RTD for the Simulated Reactors

Reactor	Mean Residence Time (t_m)	Variance (σ^2)	Skewness (s^3)
Montecatini Edison	16.3 ms	60.77 ms^2	1121.96 ms^3
Kronos	0.142 s	0.00385 s^2	0.076 s^3
Simplified Kerr-McGee	0.216 s	0.0096 s^2	0.043 s^3

The residence time distribution information is also a very useful tool for qualifying results from a simulation. A tracer study can be performed on a real reactor and compared to the results obtained through simulation. While agreement between the two studies does not guarantee the simulation model is accurate, a certain measure of reassurance in the model can obtained.

Tracer Flow Pattern Analysis

Tracer flow patterns for the reacting species where used to quantify the level of component mixing in the reactors. The tracer flow profiles illustrated how each species would flow through the system if no reaction were present to consume them. The curves for each species can be overlapped to generate a new profile showing regions where component mixing is very poor and very good. This new profile could accurately predict the regions where the reaction rate is the highest or regions where the reaction will occur readily if the proper conditions are available (i.e. temperature).

Information on the level of component mixing is very useful information for optimizing and designing equipment. With this information, changes can be made to a reactor in order to increase or decrease the component mixing depending on the desired effect.

Fluid Age Analysis

Modeling the age of the fluid inside the reactors was the method used to locate and determine the extent of recirculation and backmixing in this research. Using this method it is possible to show that each reactor had regions of recirculating flow. Some of these regions had minor recirculation while others had strong regions of recirculation that effected the fluid movement and RTD as a whole. When modeling the simplified Kerr-McGee reactor, the strength and weakness of this method of quantifying mixing are seen. The fluid age in the $TiCl_4$ distributor provided excellent insight into the fluid flow patterns and recirculating flows present; however, when the fluid entered the reaction chamber and met new fluid of a much young age, the fluid was not able to show the level of recirculation very effectively.

As a modeling tool, this method can be very effective. The most promising feature of this method is the ability to quantify the extent of recirculation. This is important because some regions of a system may always have some recirculation and small changes in operating conditions and design may affect the amount of time fluid spends in this area without changing the size or shape of the recirculating region.

Recommendations

The methods of quantify mixing using CFD presented in this paper can all be useful. Calculation of the residence time information is particularly useful for this work since the residence time of a TiO_2 particle directly affects the size of the particle. Residence time distribution information should be used with correlated data from previous work for the production of TiO_2 and if possible with actual residence time data. Tracer profiles for multiple species are useful for visualization of regions with good mixing but should not be relied upon as a stand alone test. Also, this method should only be used in reactors where the species of interest compose the large majority of inlet flow. The final method for quantifying mixing is the most promising, even though this method has problems modeling geometries where fluid of different ages mix together. This method would work well for systems where hold-up time is important or where biological effects such as bacteria growth may be a concern.

BIBLIOGRAPHY

Aggus, B., "Analysis of Reactors for the Production of Titanium Dioxide through Computational Fluid Dynamics," M.S. Thesis, Department of Chemical Engineering, Oklahoma State University, Stillwater, Oklahoma (2001).

Akhtar, M.K., Y. Xiong, and S.E. Pratsinis, "Vapor Synthesis of Titania Powder by Titanium Tetrachloride Oxidation," *AIChE Journal* 37, 1561-1570 (1991).

Bałdyga, J. and J.R. Bourne, Turbulent Mixing and Chemical Reactions, John Wiley and Sons, Chichester, England (1999).

Bird, R.B., W.E. Stewart, E.N. Lightfoot, Transport Phenomena, John Wiley and Sons, New York, New York (1960).

Bischoff, K.B. and E.A. McCracken, "Tracer Tests in Flow Systems," *Industrial and Engineering Chemistry* 7, 18-31 (1966).

Braun, J.H., "Titanium Dioxide – A Review," *Journal of Coating Technology* 69, 59-72 (1997).

CFX 5.5.1, ANSYS Incorporated, Canonsburg, Pennsylvania (2002).

CFX 5, "CFX 5 Help Online User Guide," ANSYS Incorporated, Canonsburg, Pennsylvania (2002).

Chase M.W. Jr., C.A. Davies, J.R. Davies, Jr., D.J. Fulrip, R.A. McDonald, and A.N. Syverud, "JANAF Themochemical Tables," *Journal of Phyiscal and Chemical Reference Data* 14, Supplemental no. 1 (1985).

Danckwerts, P.V., "Continous Flow Systems : Distribution of Residence Times," *Chemical Engineering Science* 2, 1-13 (1953).

Fogler, H.S., Elements of Chemical Reaction Engineering, Third Edition, Prentice Hall PTR, Upper Saddle River, New Jersey (1999).

Hartmann, A., "Process for the Production of Titanium Dioxide," U.S. Patent, US5196181 (1993).

Jain. S., T.T. Kodas, M.K. Wu, and P. Preston, "Role of Surface Reaction in Aerosol Synthesis of Titanium Dioxide," *Journal of Aerosol Science* 28, 133-146 (1997).

Jang, H.D. and J. Jeong, "The Effect of Temperature on Particle Size in the Gas-Phase Production of TiO₂," *Aerosol Science and Technology* 23, 553-560 (1995).

Jang, H.D. and S.K. Kim, "Controlled Synthesis of Titanium Dioxide Nanoparticles in a Modified Diffusion Flame Reactor," *Material Research Bulletin* 36, 627-637 (2001).

Kobata, A., K. Kusakabe, and S. Morooka, "Growth and Transformation of TiO₂ Crystallites in Aerosol Reactor," *AIChE Journal* 37, 347-359 (1991).

Lee, D.C., "Study of TiCl₄ Oxidation Kinectics," M.S. Thesis, Department of Chemical Engineering, Case Western Reserve University, Cleveland, Ohio (2000).

Levenspiel, O. Chemical Reaction Engineering, Second Edition, John Wiley and Sons, New York, New York (1962).

Morooka, S., T. Yasutake, A. Kobata, K. Ikemizu, and Y. Kato, "A Mechanism for the Production of Ultrafine Particles of TiO₂ by a Gas-Phase Reaction," *International Chemical Engineering* 29, 119-126 (1989).

Nutting, R.D. and E.I. du Pont de Nemours and Company, "Metal Oxide Production," U.S. Patent, US2670272 (1954).

Pethö, A. and R.D. Noble, Residence Time Distribution Theory in Chemical Engineering, Verlag Chemie, Weinheim, Germany (1982).

Pieri, G., A. Ducato, L.J. Held, and G. Bedetti, "Process for Producing Pigment Quality Titanium Dioxide," U.S. Patent, US3725526 (1973).

Powell, R., Chemical Process Review Number 18 – Titanium Dioxide and Titanium Tetrachloride, Noyes Publications, Ridge Park, New Jersey (1968).

Pratsinis, S.E., H. Bai, and P. Biswas, "Kinetics of Titanium(IV) Chloride Oxidation," *Journal of American Ceramics Society* 73, 2125-2162 (1990).

Pratsinis, S.E. and P.T. Spicer, "Competition between Gas Phase and Surface Oxidation of TiCl₄ During Synthesis of TiO₂ Particles," *Chemical Engineering Science* 53, 1861-1868 (1998).

Riggs, J.B., An Introduction to Numerical Methods for Chemical Engineers, Second Edition, Texas Tech University Press, Lubbock, Texas (1994).

Ross, M., "Analysis of Chloride Process Reactors for the Reduction of Oxide Scale Though Computational Fluid Dynamics," M.S. Thesis, Department of Chemical Engineering, Oklahoma State University, Stillwater, Oklahoma (2001).

Stefano, V.N.D., J.F. Skrivan, G.Butler, and American Cyanamid Company, " Pigment Via Plasma Jet-Improved Preheater Configuration," U.S. Patent, US3328126 (1967).

Weinstein, H. and R.J. Adler, "Micromixing Effects in Continuous Chemical Reactors," *Chemical Engineering Science* 22, 65-75 (1967).

Wendell, C.B., C.L.R. Carpenter, M.J. Carpenter, and Cabot Corporation, "Vapor Phase Process for Producing Metal Oxides," U.S. Patent, US3351427 (1967).

Zwietering, T.N., "The Degree of Mixing in Continuous Flow Systems," *Chemical Engineering Science* 11, 1-15 (1959).

APPENDIX A

CALCULATION OF PHYISCAL PROPERTIES

The physical properties used to solve the modeling equations for all simulations are summarized in Table 3-1. Properties with constant values where obtained from the Nation Institute of Standards and Technology (NIST) database and publications. For this work, the viscosity and specific heat capacity where calculated as functions of temperature. The viscosity of each species was calculated using Chapman-Enskog theory, and the specific heat capacity was calculated using the NASA specific heat equation, which uses a polynomial equation with parameters regressed from experimental data.

Chapman-Enskog theory uses kinetic theory for monatomic gases at low density to estimate viscosity (μ) and has been found to be reliable for polyatomic gases as well (Bird et al. 1960). Written as a function of temperature, the viscosity can be calculated using:

$$\mu = 2.6693 \times 10^{-5} \frac{\sqrt{MT}}{\sigma^2 \Omega_\mu} \tag{A-1}$$

where M is the molecular weight of a molecule, T is the temperature of the molecule, σ is the collision diameter of the molecule, and Ω_μ is a slowly varying function of temperature and the maximum energy of attraction between a pair of molecules divided

by the Boltzmann constant (ϵ/K). Table A-1 lists the values of σ and ϵ used to calculate the viscosity for each species.

TABLE A-1: Parameters Used to Estimate Viscosity Via Chapman-Enskog Method

Compound	σ (Å)	ϵ/K (K)	T_c (K)	P_c (atm)	T_m (K)	V_m (cm^3/mol)
Carbon Dioxide	3.996	190.0	-	-	-	-
Chlorine	4.115	357.0	-	-	-	-
Nitrogen	3.681	91.5	-	-	-	-
Oxygen	3.433	113.0	-	-	-	-
Titanium Dioxide (Rutile)[a]	3.344	4057.0	-	-	2113	20.487
Titanium Tetrachloride[a]	5.863	491.3	638.0	45.99	-	-

[a]Values for the critical temperature, pressure, and melting point information are referenced from Aggus (2000).

Values of σ and ϵ were unavailable for TiCl$_4$ and TiO$_2$; however, they may be estimated from the critical point and melting point by the following correlations (Bird et al. 1960):

$$\epsilon/K = 0.77T_c \qquad \sigma = 2.44\left(\frac{T_c}{P_c}\right)^{1/3} \qquad \text{(A-2,3)}$$

$$\epsilon/K = 1.92T_m \qquad \sigma = 1.222v_m^{1/3} \qquad \text{(A-4,5)}$$

The NASA specific heat equation is based off a polynomial equation which calculates the specific heat as a function of temperature. Equation A-6 provides the equation used to calculate the specific heat:

$$C_p^o/R = a_1 + a_2T + a_3T^2 + a_4T^3 + a_5T^4 \qquad \text{(A-6)}$$

where C_p^o is the specific heat capacity of an ideal gas, R is the universal gas constant, and a_{1-5} are parameter regressed from experimental work for each specific compound. Parameters for each species are presented in Table A-2. Unless otherwise stated the parameters listed are the default values from the CFX Build database.

TABLE A-2: NASA Heat Capacity Parameters[a]

Heat Capacity Equation : $C_p^{\circ}/R = a_1 + a_2T + a_3T^2 + a_4T^3 + a_5T^4$

Compound	Chemical Formula	a_1	a_2	a_3	a_4	a_5	Coefficient Range (K)
Carbon Dioxide	CO_2	4.453623E+00	3.140169E-03	-1.278411E-06	2.393997E-10	-1.669033E-14	300-1000
		2.275725E+00	9.922072E-03	-1.040911E-05	6.866870E-07	-2.117280E-12	1000-5000
Chlorine[b]	Cl_2	4.747275E+00	-4.885817E-04	2.684449E-07	-2.434761E-11	-1.036831E-15	200-1000
		2.736381E+00	7.835257E-03	-1.451050E-05	1.257308E-08	-4.132471E-12	1000-6000
Nitrogen	N_2	2.926640E+00	1.487977E-03	-5.684761E-07	1.009704E-10	-6.753351E-15	300-1000
		3.298677E+00	1.408240E-03	-3.963222E-06	5.641515E-09	-2.444855E-12	1000-5000
Oxygen	O_2	3.697578E+00	6.135197E-04	-1.258842E-07	1.775281E-11	-1.136435E-15	300-1000
		3.212936E+00	1.127486E-03	-5.756150E-07	1.313877E-09	-8.768550E-13	1000-5000
Propane	C_3H_8	7.525217E+00	1.889034E-02	-6.283924E-06	9.179373E-10	-4.812410E-14	300-1000
		8.969208E-01	2.668986E-02	5.431425E-06	-2.126001E-08	9.243330E-12	1000-5000
Titanium Dioxide[b] (Rutile)	TiO_2	6.848915E+00	4.246346E-03	-3.008898E-06	1.060252E-09	-1.437960E-13	300-1000
		-1.611752E-01	3.796666E-02	-6.515475E-05	5.255214E-08	-1.620005E-11	1000-2130
Titanium Tetrachloride[b]	$TiCl_4$	1.238603E+01	7.093132E-04	-3.174608E-07	6.260396E-11	-4.533704E-15	300-1000
		6.949676E+00	2.604966E-02	-4.652030E-05	3.838483E-08	-1.202792E-11	1000-5000
Water	H_2O	2.672146E+00	3.056293E-03	-8.730260E-07	1.200996E-10	-6.391618E-15	300-1000
		3.386842E+00	3.474982E-03	-6.354696E-06	6.968581E-09	-2.506588E-12	1000-5000

[a] Specific heat calculation follows "old" NASA format and equation as discussed by Sanford Gordon and Bonnie J. McBride, "Computer Program for Calculation of Complex Chemical Equilibrium Composition and Applications: I. Analysis", NASA Reference Publication 1311, October 1994.

[b] Coefficients obtained from the Explosion Dynamics Laboratory for the Graduate Aeronautical Laboratories at the California Institute of Technology, Pasadena CA website: http://www.galcit.caltech.edu/EDL/public/thermo/nasadat.

APPENDIX B

NUMERICAL TECHNIQUES

The numerical techniques referred to in this section apply only to calculations performed by hand. These calculations include differentiation of the reactor outlet tracer concentration for the purpose of determining residence time distribution (RTD) information and numerical integration of the first three moments of the RTD. Numerical techniques used by CFX 5 Solver Manager are proprietary and not included in this work.

In order to calculate the moments of the RTD, it is first necessary to generate the E(t) curve. For a step tracer input the E(t) curve is found by (Fogler 1999):

$$E(t) = \frac{d}{dt}\left[\frac{C(t)}{C_o}\right]$$ (B-1)

where C(t) is the concentration of tracer at the exit with respect to time and C_o is the inlet tracer concentration. Since the outlet concentration from the reactor is given in discrete intervals (length of the simulation timestep), the concentration information much be numerically differentiated to obtain the E(t) curve. The following finite difference approximation was used:

$$C'(t_i) = \frac{C(t_{i+1}) - C(t_{i-1})}{2\Delta t}$$ (B-2)

where $C'(t_i)$ is the derivative of C at time t_i. This method of differentiation is know as central differencing and is second order accurate.

With the E(t) curve it is possible to calculate the first three moments of the RTD. This is done by numerically integrating Equations 2-6, 7, and 8. The method used to integrate these equations follows the trapezoidal rule and once applied these equations gives the follow results:

$$t_m = \int_0^\infty tE(t)dt \cong \sum_{i=1}^n \frac{t_i E(t_i) + t_{i-1} E(t_{i-1})}{2}(t_i - t_{i-1}) \qquad (B-3)$$

$$\sigma^2 = \int_0^\infty (t - t_m)^2 E(t)dt \cong \sum_{i=1}^n \frac{(t_i - t_m)^2 E(t_i) + (t_{i-1} - t_m)^2 E(t_{i-1})}{2}(t_i - t_{i-1}) \qquad (B-4)$$

$$s^3 = \frac{1}{\sigma^{3/2}}\int_0^\infty (t - t_m)^3 E(t)dt \cong \frac{1}{\sigma^{3/2}}\sum_{i=1}^n \frac{(t_i - t_m)^3 E(t_i) + (t_{i-1} - t_m)^3 E(t_{i-1})}{2}(t_i - t_{i-1}) \qquad (B-5)$$

where n is the total number of integration steps and i=1 corresponds to the beginning point of the simulation.

Residence time information obtained from simulation is provided in the spreads sheets on the next three pages. Also included are the incremental differentiation and integration intervals used for solving the above equations.

reactor simulation data					mean time calc		standard deviation calc			skewness calc	
t	m(t)	F(t)	E(t) (s⁻¹)	intergrate	t*E(t)	integrate	t-t_m	(t-t_m)²*E(t)	integrate	(t-t_m)³*E(t)	integrate
Time (s)	Tracer exit (kg/s)	Tracer exit/Tracer input	RTD function	E(t)		t*E(t)			(t-t_m)²*E(t)		(t-t_m)³*E(t)
0.000	0.000000	0.000000	0.000	0.000000	0.000000	0	-0.0162947	0	0	0	0
0.001	0.000000	0.000000	0.000	0.000003	0.000000	5.32E-09	-0.0152947	0	5.435E-10	0	-7.77E-12
0.002	0.000000	0.000000	0.005	0.000026	0.000011	7.659E-08	-0.0142947	1.087E-06	4.743E-09	-1.55E-08	-6.36E-11
0.003	0.000001	0.000011	0.048	0.000157	0.000143	6.041E-07	-0.0132947	8.398E-06	2.433E-08	-1.12E-07	-3.03E-10
0.004	0.000005	0.000095	0.266	0.000672	0.001066	3.227E-06	-0.0122947	4.027E-05	8.889E-08	-4.95E-07	-1.02E-09
0.005	0.000027	0.000543	1.078	0.002331	0.005389	1.345E-05	-0.0112947	0.0001375	2.587E-07	-1.55E-06	-2.73E-09
0.006	0.000113	0.002251	3.585	0.006932	0.021507	4.673E-05	-0.0102947	0.0003799	6.34E-07	-3.91E-06	-6.08E-09
0.007	0.000386	0.007712	10.280	0.016988	0.071961	0.0001308	-0.0092947	0.0008881	1.259E-06	-8.25E-06	-1.09E-08
0.008	0.001141	0.022811	23.697	0.033710	0.189573	0.0002915	-0.0082947	0.0016304	1.978E-06	-1.35E-05	-1.52E-08
0.009	0.002755	0.055106	43.723	0.055263	0.393508	0.0005308	-0.0072947	0.0023266	2.487E-06	-1.7E-05	-1.68E-08
0.010	0.005513	0.110257	66.804	0.076922	0.668036	0.0008127	-0.0062947	0.002647	2.544E-06	-1.67E-05	-1.48E-08
0.011	0.009436	0.188713	87.039	0.093022	0.957433	0.0010727	-0.0052947	0.00244	2.133E-06	-1.29E-05	-1.04E-08
0.012	0.014217	0.284336	99.006	0.099751	1.188066	0.0012473	-0.0042947	0.0018261	1.458E-06	-7.84E-06	-5.72E-09
0.013	0.019336	0.386724	100.496	0.096788	1.306448	0.0013048	-0.0032947	0.0010909	7.905E-07	-3.59E-06	-2.36E-09
0.014	0.024266	0.485328	93.080	0.086703	1.303120	0.001254	-0.0022947	0.0004901	3.124E-07	-1.12E-06	-6.5E-10
0.015	0.028644	0.572884	80.325	0.073041	1.204875	0.0011285	-0.0012947	0.0001346	7.018E-08	-1.74E-07	-8.8E-11
0.016	0.032299	0.645978	65.756	0.058898	1.052096	0.0009684	-0.0002947	5.711E-06	1.58E-08	-1.68E-09	8.288E-12
0.017	0.035220	0.704396	52.039	0.046308	0.884663	0.0008075	0.0007053	2.589E-05	7.194E-08	1.83E-08	1.097E-10
0.018	0.037503	0.750056	40.576	0.036110	0.730368	0.0006658	0.0017053	0.000118	1.748E-07	2.01E-07	4.139E-10
0.019	0.039277	0.785548	31.644	0.028346	0.601236	0.0005511	0.0027053	0.0002316	2.877E-07	6.27E-07	9.503E-10
0.020	0.040667	0.813344	25.047	0.022684	0.500940	0.0004638	0.0037053	0.0003439	3.969E-07	1.27E-06	1.696E-09
0.021	0.041782	0.835642	20.320	0.018629	0.426720	0.0003997	0.0047053	0.0004499	5.006E-07	2.12E-06	2.631E-09
0.022	0.042699	0.853984	16.938	0.015717	0.372636	0.000353	0.0057053	0.0005513	6.015E-07	3.15E-06	3.758E-09
0.023	0.043476	0.869518	14.496	0.013573	0.333408	0.0003185	0.0067053	0.0006518	7.014E-07	4.37E-06	5.078E-09
0.024	0.044149	0.882976	12.669	0.011904	0.303576	0.0002913	0.0077053	0.000717	7.983E-07	5.79E-06	6.574E-09
0.025	0.044741	0.894816	11.158	0.010539	0.278950	0.0002684	0.0087053	0.0008456	8.899E-07	7.36E-06	8.214E-09
0.026	0.045265	0.905292	9.919	0.009393	0.257894	0.0002487	0.0097053	0.0009343	9.752E-07	9.07E-06	9.973E-09
0.027	0.045733	0.914654	8.867	0.008388	0.239409	0.0002304	0.0107053	0.0010162	1.05E-06	1.09E-05	1.178E-08
0.028	0.046151	0.923026	7.909	0.007460	0.221452	0.0002124	0.0117053	0.0010836	1.108E-06	1.27E-05	1.353E-08
0.029	0.046524	0.930472	7.010	0.006614	0.203290	0.0001949	0.0127053	0.0011316	1.15E-06	1.44E-05	1.519E-08
0.030	0.046852	0.937046	6.217	0.005891	0.186510	0.0001795	0.0137053	0.0011678	1.186E-06	1.6E-05	1.685E-08
0.031	0.047145	0.942906	5.565	0.005316	0.172515	0.0001673	0.0147053	0.0012034	1.227E-06	1.77E-05	1.866E-08
0.032	0.047409	0.948176	5.067	0.004883	0.162144	0.0001586	0.0157053	0.0012498	1.281E-06	1.96E-05	2.077E-08
0.033	0.047652	0.953040	4.699	0.004542	0.155067	0.0001521	0.0167053	0.0013113	1.343E-06	2.19E-05	2.312E-08
0.034	0.047879	0.957574	4.384	0.004217	0.149056	0.0001454	0.0177053	0.0013743	1.396E-06	2.43E-05	2.542E-08
0.035	0.048090	0.961808	4.050	0.003866	0.141750	0.0001372	0.0187053	0.001417	1.424E-06	2.65E-05	2.734E-08
0.036	0.048284	0.965674	3.683	0.003492	0.132588	0.0001274	0.0197053	0.0014301	1.423E-06	2.82E-05	2.875E-08
0.037	0.048459	0.969174	3.302	0.003115	0.122174	0.0001167	0.0207053	0.0014156	1.398E-06	2.93E-05	2.963E-08
0.038	0.048614	0.972278	2.928	0.002765	0.111264	0.0001064	0.0217053	0.0013794	1.361E-06	2.99E-05	3.021E-08
0.039	0.048752	0.975030	2.603	0.002465	0.101517	9.73E-05	0.0227053	0.0013419	1.325E-06	3.05E-05	3.073E-08
0.040	0.048874	0.977484	2.327	0.002210	0.093080	8.943E-05	0.0237053	0.0013076	1.292E-06	3.1E-05	3.127E-08
0.041	0.048984	0.979684	2.092	0.001993	0.085772	8.266E-05	0.0247053	0.0012769	1.264E-06	3.15E-05	3.186E-08
0.042	0.049083	0.981668	1.894	0.001807	0.079548	7.673E-05	0.0257053	0.0012515	1.239E-06	3.22E-05	3.245E-08
0.043	0.049174	0.983472	1.719	0.001640	0.073917	7.132E-05	0.0267053	0.0012259	1.212E-06	3.27E-05	3.298E-08
0.044	0.049255	0.985106	1.562	0.001496	0.068728	6.656E-05	0.0277053	0.001199	1.189E-06	3.32E-05	3.353E-08
0.045	0.049330	0.986596	1.431	0.001371	0.064395	6.235E-05	0.0287053	0.0011771	1.168E-06	3.38E-05	3.411E-08
0.046	0.049398	0.987968	1.311	0.001251	0.060306	5.812E-05	0.0297053	0.0011568	1.139E-06	3.44E-05	3.441E-08
0.047	0.049461	0.989218	1.190	0.001134	0.055930	5.384E-05	0.0307053	0.001122	1.103E-06	3.44E-05	3.44E-08
0.048	0.049517	0.990348	1.078	0.001027	0.051744	4.976E-05	0.0317053	0.0010836	1.063E-06	3.44E-05	3.423E-08
0.049	0.049569	0.991374	0.975	0.000927	0.047775	4.589E-05	0.0327053	0.0010429	1.021E-06	3.41E-05	3.39E-08
0.050	0.049615	0.992298	0.880	0.000838	0.044000	4.23E-05	0.0337053	0.0009997	9.792E-07	3.37E-05	3.348E-08
0.051	0.049657	0.993134	0.796	0.000759	0.040596	3.91E-05	0.0347053	0.0009587	9.402E-07	3.33E-05	3.309E-08
0.052	0.049695	0.993890	0.723	0.000690	0.037596	3.621E-05	0.0357053	0.0009217	9.034E-07	3.29E-05	3.27E-08
0.053	0.049729	0.994580	0.657	0.000626	0.034821	3.348E-05	0.0367053	0.0008852	8.655E-07	3.25E-05	3.219E-08
0.054	0.049760	0.995204	0.595	0.000567	0.032130	3.089E-05	0.0377053	0.0008459	8.267E-07	3.19E-05	3.157E-08
0.055	0.049789	0.995770	0.539	0.000514	0.029645	2.851E-05	0.0387053	0.0008075	7.892E-07	3.13E-05	3.093E-08
0.056	0.049814	0.996282	0.489	0.000466	0.027384	2.632E-05	0.0397053	0.0007709	7.525E-07	3.06E-05	3.024E-08
0.057	0.049837	0.996748	0.443	0.000422	0.025251	2.425E-05	0.0407053	0.000734	7.157E-07	2.99E-05	2.948E-08
0.058	0.049858	0.997168	0.401	0.000382	0.023258	2.234E-05	0.0417053	0.0006975	6.797E-07	2.91E-05	2.868E-08
0.059	0.049878	0.997550	0.363	0.000345	0.021417	2.052E-05	0.0427053	0.000662	6.433E-07	2.83E-05	2.779E-08
0.060	0.049895	0.997894	0.327	0.000311	0.019620	1.884E-05	0.0437053	0.0006246	6.081E-07	2.73E-05	2.687E-08
0.061	0.049910	0.998204	0.296	0.000282	0.018056	1.734E-05	0.0447053	0.0005916	5.757E-07	2.64E-05	2.602E-08
0.062	0.049924	0.998486	0.268	0.000255	0.016616	1.596E-05	0.0457053	0.0005598	5.45E-07	2.56E-05	2.517E-08
0.063	0.049937	0.998740	0.243	0.000232	0.015309	1.473E-05	0.0467053	0.0005301	5.165E-07	2.48E-05	2.438E-08
0.064	0.049949	0.998972	0.221	0.000211	0.014144	1.36E-05	0.0477053	0.000503	4.899E-07	2.4E-05	2.361E-08
0.065	0.049959	0.999182	0.201	0.000192	0.013065	1.26E-05	0.0487053	0.0004768	4.657E-07	2.32E-05	2.291E-08
0.066	0.049969	0.999374	0.184	0.000175	0.012144	1.167E-05	0.0497053	0.0004546	4.42E-07	2.26E-05	2.218E-08
0.067	0.049978	0.999550	0.167	0.000159	0.011189	1.073E-05	0.0507053	0.0004294	4.165E-07	2.18E-05	2.132E-08
0.068	0.049985	0.999708	0.151	0.000144	0.010268	9.86E-06	0.0517053	0.0004037	3.921E-07	2.09E-05	2.047E-08
0.069	0.049993	0.999852	0.137	0.000105	0.009453	7.316E-06	0.0527053	0.0003806	2.97E-07	2.01E-05	1.576E-08
0.070	0.049999	0.999982	0.074	0.000037	0.005180	2.59E-06	0.0537053	0.0002134	1.067E-06	1.15E-05	5.731E-09
0.071	0.050000	1.000000	0.000	0.000000	0.000000	0	0.0547053	0	0	0	0

area under		mean res. time		variance		skewness	
E curve=	0.999991	t_m (s) =	0.0162947	σ² (s²)=	6.077E-05	s³=	1.122E-06
				standard deviation			
				σ (s)=	0.0077954		

B-2. Residence Time Distribution Information for the Kronos reactor.

reactor simulation data					mean time calc		standard deviation calc			skewness calc	
t	m(t)	F(t)	E(t) (s⁻¹)	intergrate	t*E(t)	intergrate	t-t_m	(t-t_m)²*E(t)	intergrate	(t-t_m)³*E(t)	intergrate
Time (s)	Tracer exit (kg/s)	Tracer exit/Tracer input	RTD fuction	E(t)		t*E(t)			(t-t_m)²*E(t)		(t-t_m)³*E(t)
0	0.000000	0.000000	0	4.39E-08	0	2.194E-09	-0.142682	0	3.769E-10	0	-3.49E-11
0.05	0.000000	0.000000	1.7552E-06	3.84E-06	8.8E-08	2.301E-07	-0.092682	1.51E-08	2.624E-08	-1.4E-09	-2.17E-09
0.06	0.000000	0.000000	0.00076545	0.000122	4.6E-05	8.515E-06	-0.082682	5.23E-06	6.514E-07	-4.33E-07	-4.76E-08
0.07	0.000012	0.000015	0.02367133	0.000985	0.00166	7.764E-05	-0.072682	0.000125	4.031E-06	-9.09E-06	-2.59E-07
0.08	0.000369	0.000474	0.17338349	0.002857	0.01387	0.0002406	-0.062682	0.000681	9.765E-06	-4.27E-05	-5.72E-07
0.085	0.002037	0.002616	0.96924932	0.008251	0.08239	0.0007305	-0.057682	0.003225	2.424E-05	-0.000186	-1.32E-06
0.09	0.007915	0.010166	2.33109346	0.015544	0.2098	0.0014475	-0.052682	0.00647	3.827E-05	-0.000341	-1.91E-06
0.095	0.020187	0.025927	3.88652701	0.022623	0.36922	0.0022138	-0.047682	0.008836	4.56E-05	-0.000421	-2.06E-06
0.1	0.038177	0.049031	5.16284643	0.029411	0.51628	0.0030236	-0.042682	0.009405	4.695E-05	-0.000401	-1.89E-06
0.105	0.060386	0.077555	6.60162827	0.040222	0.69317	0.0043419	-0.037682	0.009374	4.877E-05	-0.000353	-1.71E-06
0.11	0.089578	0.115048	9.48733459	0.059391	1.04361	0.0067114	-0.032682	0.010134	5.267E-05	-0.000331	-1.58E-06
0.115	0.134256	0.172429	14.2691464	0.084256	1.64095	0.0099324	-0.027682	0.010934	5.233E-05	-0.000303	-1.32E-06
0.12	0.200680	0.257739	19.4333029	0.105036	2.332	0.0128866	-0.022682	0.009998	4.265E-05	-0.000227	-8.79E-07
0.125	0.285567	0.366762	22.5810636	0.112699	2.82263	0.0143685	-0.017682	0.00706	2.67E-05	-0.000125	-4.27E-07
0.13	0.376500	0.483550	22.4983528	0.106202	2.92479	0.0140561	-0.012682	0.003619	1.199E-05	-4.59E-05	-1.37E-07
0.135	0.460743	0.591745	19.9826102	0.091196	2.69765	0.0125177	-0.007682	0.001179	3.245E-06	-9.06E-06	-2.34E-08
0.14	0.532088	0.683376	16.4959152	0.073546	2.30943	0.010458	-0.002682	0.000119	4.702E-07	-3.18E-07	-3.93E-10
0.145	0.589183	0.756705	12.9226565	0.056525	1.87379	0.0083172	0.0023179	6.94E-05	1.471E-06	1.61E-07	9.893E-09
0.15	0.632706	0.812602	9.68730454	0.041791	1.4531	0.0063565	0.0073179	0.000519	3.963E-06	3.8E-06	4.233E-08
0.155	0.664610	0.853578	7.02900142	0.030105	1.0895	0.0047289	0.0123179	0.001067	6.425E-06	1.31E-05	9.793E-08
0.16	0.687435	0.882892	5.01299098	0.021448	0.80208	0.0034763	0.0173179	0.001503	8.199E-06	2.6E-05	1.642E-07
0.165	0.703642	0.903707	3.56632337	0.01529	0.58844	0.0025548	0.0223179	0.001776	9.198E-06	3.96E-05	2.291E-07
0.17	0.715203	0.918556	2.54977736	0.010951	0.43346	0.0018845	0.0273179	0.001903	9.537E-06	5.2E-05	2.844E-07
0.175	0.723495	0.929205	1.83042497	0.007875	0.32032	0.0013947	0.0323179	0.001912	9.374E-06	6.18E-05	3.259E-07
0.18	0.729455	0.936860	1.31964753	0.0057	0.23754	0.001038	0.0373179	0.001838	8.894E-06	6.86E-05	3.534E-07
0.185	0.733770	0.942402	0.96029242	0.004173	0.17765	0.0007809	0.0423179	0.00172	8.268E-06	7.28E-05	3.697E-07
0.19	0.736932	0.946463	0.70894933	0.003105	0.1347	0.0005966	0.0473179	0.001587	7.616E-06	7.51E-05	3.786E-07
0.195	0.739290	0.949491	0.53312476	0.002254	0.10396	0.0004441	0.0523179	0.001459	6.673E-06	7.63E-05	3.643E-07
0.2	0.741083	0.951794	0.36834541	0.003186	0.07367	0.0006507	0.0573179	0.00121	1.214E-05	6.94E-05	7.569E-07
0.21	0.743592	0.955016	0.26887417	0.002288	0.05646	0.0004899	0.0673179	0.001218	1.173E-05	8.2E-05	8.463E-07
0.22	0.745270	0.957171	0.18873207	0.001692	0.04152	0.0003797	0.0773179	0.001128	1.135E-05	8.72E-05	9.342E-07
0.23	0.746531	0.958791	0.14962427	0.001416	0.03441	0.0003323	0.0873179	0.001141	1.203E-05	9.96E-05	1.113E-06
0.24	0.747600	0.960164	0.13350595	0.001321	0.03204	0.0003235	0.0973179	0.001264	1.384E-05	0.000123	1.422E-06
0.25	0.748610	0.961461	0.13061621	0.001324	0.03265	0.0003377	0.1073179	0.001504	1.676E-05	0.000161	1.891E-06
0.26	0.749634	0.962776	0.13421233	0.001359	0.0349	0.0003603	0.1173179	0.001847	2.04E-05	0.000217	2.504E-06
0.27	0.750700	0.964145	0.13768001	0.001388	0.03717	0.0003818	0.1273179	0.002232	2.435E-05	0.000284	3.232E-06
0.28	0.751778	0.965530	0.13992759	0.001409	0.03918	0.0004017	0.1373179	0.002639	2.859E-05	0.000362	4.08E-06
0.29	0.752879	0.966944	0.1419183	0.001422	0.04116	0.0004196	0.1473179	0.00308	3.304E-05	0.000454	5.044E-06
0.3	0.753988	0.968368	0.14256046	0.001424	0.04277	0.0004344	0.1573179	0.003528	3.756E-05	0.000555	6.108E-06
0.31	0.755099	0.969795	0.1423036	0.001419	0.04411	0.000447	0.1673179	0.003984	4.217E-05	0.000667	7.278E-06
0.32	0.756204	0.971214	0.141533	0.001409	0.04529	0.000458	0.1773179	0.00445	4.687E-05	0.000789	8.556E-06
0.33	0.757303	0.972626	0.14031289	0.001391	0.0463	0.0004659	0.1873179	0.004923	5.146E-05	0.000922	9.907E-06
0.34	0.758389	0.974021	0.13787266	0.001361	0.04688	0.0004696	0.1973179	0.005368	5.572E-05	0.001059	1.128E-05
0.35	0.759450	0.975383	0.13440498	0.001324	0.04704	0.0004699	0.2073179	0.005777	5.967E-05	0.001198	1.268E-05
0.36	0.760482	0.976709	0.13035934	0.001282	0.04693	0.0004679	0.2173179	0.006156	6.335E-05	0.001338	1.409E-05
0.37	0.761480	0.977990	0.12605684	0.001239	0.04664	0.0004645	0.2273179	0.006554	6.685E-05	0.001441	1.554E-05
0.38	0.762445	0.979230	0.12175434	0.001196	0.04627	0.0004604	0.2373179	0.006857	7.021E-05	0.001627	1.702E-05
0.39	0.763376	0.980426	0.11745184	0.001162	0.04581	0.0004588	0.2473179	0.007184	7.395E-05	0.001777	1.867E-05
0.4	0.764274	0.981579	0.11488318	0.001116	0.04595	0.0004517	0.2573179	0.007607	7.672E-05	0.001957	2.013E-05
0.41	0.765165	0.982723	0.10826889	0.00105	0.04439	0.0004357	0.2673179	0.007737	7.782E-05	0.002068	2.119E-05
0.42	0.765960	0.983744	0.10178303	0.001005	0.04275	0.0004272	0.2773179	0.007828	8.012E-05	0.002171	2.263E-05
0.43	0.766750	0.984759	0.09927859	0.000972	0.04269	0.0004227	0.2873179	0.008196	8.301E-05	0.002355	2.427E-05
0.44	0.767506	0.985730	0.09510453	0.000940	0.04185	0.0004143	0.2973179	0.008407	8.507E-05	0.0025	2.572E-05
0.45	0.768231	0.986661	0.09112311	0.000892	0.04101	0.0004057	0.3073179	0.008606	8.697E-05	0.002645	2.717E-05
0.46	0.768925	0.987552	0.08727012	0.000855	0.04014	0.0003977	0.3173179	0.008787	8.883E-05	0.002788	2.864E-05
0.47	0.769590	0.988406	0.08380243	0.000821	0.03939	0.0003897	0.3273179	0.008978	9.06E-05	0.002939	3.011E-05
0.48	0.770230	0.989228	0.08033475	0.000787	0.03856	0.0003814	0.3373179	0.009141	9.214E-05	0.003083	3.155E-05
0.49	0.770841	0.990013	0.07699549	0.000755	0.03773	0.0003737	0.3473179	0.009288	9.371E-05	0.003226	3.302E-05
0.5	0.771429	0.990768	0.07404154	0.000726	0.03702	0.0003665	0.3573179	0.009453	9.527E-05	0.003378	3.452E-05
0.51	0.771994	0.991494	0.0711518	0.000699	0.03629	0.0003594	0.3673179	0.0096	9.673E-05	0.003526	3.602E-05
0.52	0.772537	0.992191	0.06845471	0.000672	0.0356	0.0003526	0.3773179	0.009746	9.815E-05	0.003677	3.753E-05
0.53	0.773060	0.992863	0.06588605	0.000646	0.03492	0.0003456	0.3873179	0.009884	9.94E-05	0.003828	3.9E-05
0.54	0.773563	0.993509	0.06331739	0.000621	0.03419	0.0003384	0.3973179	0.009995	0.0001005	0.003971	4.043E-05
0.55	0.774046	0.994129	0.06087717	0.000597	0.03348	0.0003312	0.4073179	0.0101	0.0001014	0.004114	4.183E-05
0.56	0.774511	0.994727	0.05850116	0.000573	0.03276	0.0003239	0.4173179	0.010188	0.0001022	0.004252	4.318E-05
0.57	0.774957	0.995299	0.05618937	0.000551	0.03203	0.0003169	0.4273179	0.01026	0.000103	0.004384	4.453E-05
0.58	0.775386	0.995850	0.05407023	0.000531	0.03136	0.0003104	0.4373179	0.010341	0.0001038	0.004522	4.592E-05
0.59	0.775799	0.996381	0.05207952	0.000511	0.03073	0.0003043	0.4473179	0.010421	0.0001046	0.004661	4.732E-05
0.6	0.776197	0.996892	0.05021724	0.000493	0.03013	0.0002983	0.4573179	0.010502	0.0001054	0.004803	4.872E-05
0.61	0.776581	0.997385	0.04841918	0.000476	0.02954	0.0002924	0.4673179	0.010574	0.0001061	0.004941	5.009E-05
0.62	0.776951	0.997860	0.04668534	0.000459	0.02894	0.0002865	0.4773179	0.010636	0.0001066	0.005077	5.143E-05
0.63	0.777308	0.998319	0.04501571	0.000442	0.02836	0.0002807	0.4873179	0.01069	0.0001071	0.00521	5.274E-05
0.64	0.777652	0.998761	0.0434103	0.000427	0.02778	0.0002754	0.4973179	0.010736	0.0001077	0.005339	5.412E-05
0.65	0.777984	0.999187	0.04199754	0.000413	0.0273	0.0002706	0.5073179	0.010809	0.0001084	0.005484	5.556E-05
0.66	0.778306	0.999601	0.040649	0.000303	0.02683	0.000201	0.5173179	0.010878	8.216E-05	0.005628	4.278E-05
0.67	0.778617	1.000000	0.01997131	9.99E-05	0.01338	6.69E-05	0.5273179	0.005553	2.777E-05	0.002928	1.464E-05
0.68	0.778617	1.000000	0	0	0	0	0.5373179	0	0	0	0

area under E curve= 1

mean res. time t_m (s) = 0.1426821

variance σ²(s²)= 0.0038514

standard deviation σ(s)= 0.0620597

skewness s³= 0.0760808

B-3. Residence Time Distribution Information for the Simplified Kerr-McGee reactor.

reactor simulation data					mean time calc		standard deviation calc			skewness calc	
t	m(t)	F(t)	E(t) (s⁻¹)	intergrate	t*E(t)	intergrate	t-tm	(t-tm)²*E(t)	intergrate	(t-tm)³*E(t)	intergrate
Time (s)	Tracer exit (kg/s)	Tracer exit/Tracer input	RTD fuction	E(t)		t*E(t)			(t-tm)²*E(t)		(t-tm)³*E(t)
0	0.000000	0.000000	0	8.03E-12	0	5.422E-14	-0.216316	0	3.528E-13	0	-7.39E-14
0.00675	0.000000	0.000000	2.3799E-09	8.11E-10	1.6E-11	1.09E-11	-0.209566	1.05E-10	3.339E-11	-2.19E-11	-6.77E-12
0.03375	0.000001	0.000000	0.0005584	1.43E-05	1.9E-05	5.652E-07	-0.182566	1.86E-05	4.457E-07	-3.4E-06	-7.88E-08
0.0405	0.000013	0.000000	0.00366987	7.08E-05	0.00015	3.26E-06	-0.175816	0.000113	2.051E-06	-1.99E-05	-3.49E-07
0.06075	0.001646	0.000987	0.2228718	0.002609	0.01354	0.000171	-0.155566	0.005394	5.933E-05	-0.000839	-8.95E-06
0.0675	0.005422	0.003250	0.55022237	0.005453	0.03714	0.0003923	-0.148816	0.012185	0.0001137	-0.001813	-1.64E-05
0.08775	0.052465	0.031448	2.37034728	0.018049	0.208	0.0016517	-0.128566	0.03918	0.0002814	-0.005037	-3.52E-05
0.0945	0.082801	0.049632	2.97757966	0.021651	0.28138	0.0021243	-0.121816	0.044185	0.0003027	-0.005382	-3.58E-05
0.10125	0.119527	0.071646	3.43748175	0.024145	0.34805	0.0025293	-0.115066	0.045513	0.0003008	-0.005237	-3.36E-05
0.1215	0.247891	0.148588	3.98234008	0.026889	0.48385	0.0033578	-0.094816	0.035801	0.0002251	-0.003395	-2.06E-05
0.12825	0.292923	0.175581	3.98473772	0.026896	0.51104	0.0035401	-0.088066	0.030904	0.0001932	-0.002722	-1.64E-05
0.135	0.337636	0.202382	3.98433811	0.026984	0.53789	0.0037342	-0.081316	0.026346	0.0001642	-0.002142	-1.28E-05
0.14175	0.382659	0.229369	4.01088971	0.027222	0.56854	0.0039511	-0.074566	0.022301	0.0001382	-0.001663	-9.88E-06
0.1485	0.427970	0.256529	4.05489077	0.027695	0.60215	0.0042072	-0.067816	0.018648	0.0001152	-0.001265	-7.46E-06
0.15525	0.473984	0.284110	4.15092941	0.028424	0.64443	0.0045101	-0.061066	0.015479	9.477E-05	-0.000945	-5.5E-06
0.162	0.521458	0.312567	4.2709	0.029282	0.69189	0.004844	-0.054316	0.0126	7.616E-05	-0.000684	-3.91E-06
0.16875	0.570174	0.341767	4.40516762	0.03019	0.74337	0.005198	-0.047566	0.009967	5.916E-05	-0.000474	-2.64E-06
0.1755	0.620672	0.372036	4.54001244	0.031017	0.79677	0.0055493	-0.040816	0.007563	4.374E-05	-0.000309	-1.66E-06
0.18225	0.672425	0.403058	4.65008169	0.031717	0.84748	0.0058885	-0.034066	0.005396	3.017E-05	-0.000184	-9.47E-07
0.189	0.725402	0.434812	4.74749675	0.032366	0.89728	0.0062274	-0.027316	0.003542	1.887E-05	-9.68E-05	-4.69E-07
0.20925	0.889864	0.533392	4.92860706	0.033263	1.03131	0.0070724	-0.007066	0.000246	8.321E-07	-1.74E-06	-5.87E-09
0.2295	1.055080	0.632424	4.68737825	0.030631	1.07575	0.0071299	0.0131841	0.000815	8.635E-06	1.07E-05	1.536E-07
0.23625	1.106400	0.663186	4.38856177	0.028505	1.0368	0.0068267	0.0199341	0.001744	1.564E-05	3.48E-05	3.775E-07
0.243	1.153920	0.691670	4.0573328	0.026437	0.98593	0.0065102	0.0266841	0.002889	2.4E-05	7.71E-05	7.365E-07
0.26325	1.277430	0.765703	3.28120917	0.021186	0.86378	0.0056455	0.0469341	0.007228	5.354E-05	0.000339	2.709E-06
0.27	1.312860	0.786940	2.9961569	0.019171	0.80896	0.0052372	0.0536841	0.008635	6.223E-05	0.000464	3.564E-06
0.27675	1.344910	0.806151	2.68402022	0.017019	0.7428	0.0047637	0.0604341	0.009803	6.901E-05	0.000592	4.413E-06
0.2835	1.373310	0.823174	2.35856335	0.014867	0.66865	0.0042614	0.0671841	0.010646	7.368E-05	0.000715	5.205E-06
0.29025	1.398030	0.837992	2.04642667	0.012875	0.59398	0.0037773	0.0739341	0.011186	7.661E-05	0.000827	5.926E-06
0.297	1.419400	0.850801	1.7684785	0.011146	0.52524	0.0033453	0.0806841	0.011513	7.844E-05	0.000929	6.596E-06
0.30375	1.437860	0.861866	1.53404299	0.009715	0.46597	0.0029815	0.0874341	0.011727	7.983E-05	0.001025	7.252E-06
0.3105	1.453950	0.871511	1.34445215	0.00857	0.41745	0.0026882	0.0941841	0.011926	8.133E-05	0.001123	7.938E-06
0.31725	1.468140	0.880016	1.19482191	0.007678	0.37906	0.0024606	0.1009341	0.012172	8.336E-05	0.001229	8.699E-06
0.324	1.480860	0.887641	1.08026819	0.006994	0.35001	0.0022885	0.1076841	0.012527	8.612E-05	0.001349	9.569E-06
0.33075	1.492470	0.894600	0.99191086	0.006454	0.32807	0.0021557	0.1144341	0.012989	8.946E-05	0.001486	1.055E-05
0.3375	1.503200	0.901032	0.92042579	0.006009	0.31064	0.0020477	0.1211841	0.013517	9.313E-05	0.001638	1.161E-05
0.34425	1.513200	0.907026	0.86004089	0.005627	0.29607	0.0019555	0.1279341	0.014076	9.693E-05	0.001801	1.273E-05
0.351	1.522570	0.912642	0.8072041	0.005285	0.28333	0.0018724	0.1346841	0.014643	0.0001006	0.001972	1.39E-05
0.35775	1.531380	0.917923	0.75880737	0.004974	0.27146	0.0017956	0.1414341	0.015179	0.0001042	0.002147	1.51E-05
0.3645	1.539660	0.922886	0.71485071	0.004687	0.26056	0.0017239	0.1481841	0.015697	0.0001076	0.002326	1.631E-05
0.37125	1.547480	0.927573	0.6740021	0.004416	0.25022	0.0016539	0.1549341	0.016179	0.0001106	0.002507	1.751E-05
0.378	1.554840	0.931985	0.63448551	0.004158	0.23984	0.0015855	0.1616841	0.016587	0.0001132	0.002682	1.869E-05
0.38475	1.561770	0.936139	0.59763298	0.003917	0.22994	0.0015199	0.1684341	0.016955	0.0001155	0.002856	1.985E-05
0.3915	1.568300	0.940053	0.56300044	0.003691	0.22041	0.0014571	0.1751841	0.017278	0.0001176	0.003027	2.1E-05
0.39825	1.574450	0.943739	0.53058795	0.003478	0.21131	0.0013965	0.1819341	0.017562	0.0001193	0.003195	2.212E-05
0.405	1.580250	0.947216	0.49995149	0.003277	0.20248	0.001338	0.1886841	0.017799	0.0001208	0.003358	2.32E-05
0.41175	1.585710	0.950489	0.47109106	0.003088	0.19397	0.0012818	0.1954341	0.017993	0.000122	0.003516	2.425E-05
0.4185	1.590860	0.953576	0.44400665	0.002909	0.18582	0.0012268	0.2021841	0.01815	0.0001228	0.00367	2.525E-05
0.42525	1.595710	0.956483	0.41781026	0.002738	0.17767	0.0011732	0.2089341	0.018239	0.0001233	0.003811	2.618E-05
0.432	1.600270	0.959216	0.3933899	0.002579	0.16994	0.0011226	0.2156841	0.0183	0.0001237	0.003947	2.709E-05
0.43875	1.604570	0.961794	0.37074556	0.002428	0.16266	0.0010731	0.2224341	0.018343	0.0001237	0.00408	2.793E-05
0.4455	1.608620	0.964221	0.34854522	0.002284	0.15528	0.0010249	0.2291841	0.018307	0.0001234	0.004196	2.87E-05
0.45225	1.612420	0.966499	0.32812092	0.002153	0.14839	0.0009809	0.2359341	0.018265	0.0001232	0.004309	2.949E-05
0.459	1.616010	0.968651	0.30991664	0.00203	0.14225	0.0009386	0.2426841	0.018253	0.0001229	0.00443	3.023E-05
0.46575	1.619400	0.970683	0.29171237	0.001912	0.13587	0.0008968	0.2494341	0.01815	0.0001221	0.004527	3.087E-05
0.4725	1.622580	0.972589	0.27484012	0.001804	0.12986	0.0008584	0.2561841	0.018038	0.0001215	0.004621	3.153E-05
0.47925	1.625590	0.974393	0.25974389	0.001702	0.12448	0.0008214	0.2629341	0.017957	0.0001207	0.004722	3.213E-05
0.486	1.628430	0.976096	0.24464767	0.001603	0.1189	0.0007845	0.2696841	0.017793	0.0001195	0.004799	3.262E-05
0.49275	1.631100	0.977696	0.23043945	0.001512	0.11355	0.00075	0.2764341	0.017609	0.0001183	0.004868	3.31E-05
0.4995	1.633620	0.979207	0.21756326	0.001427	0.10867	0.0007173	0.2831841	0.017447	0.0001171	0.004941	3.355E-05
0.5265	1.642340	0.984433	0.17138657	0.001122	0.09024	0.0005946	0.3101841	0.01649	0.0001103	0.005115	3.458E-05
0.53325	1.644210	0.985554	0.16117442	0.001056	0.08595	0.0005668	0.3169341	0.01619	0.0001083	0.005131	3.47E-05
0.55425	1.649360	0.988641	0.12964994	0.000862	0.07186	0.0004804	0.3379341	0.014806	0.0001004	0.005003	3.425E-05
0.561	1.650820	0.989516	0.12565388	0.000824	0.07049	0.0004651	0.3446841	0.014929	9.98E-05	0.005146	3.473E-05
0.56775	1.652190	0.990338	0.11854978	0.000776	0.06731	0.0004432	0.3514341	0.014642	9.767E-05	0.005146	3.465E-05
0.59475	1.656940	0.993185	0.0936854	0.000614	0.05572	0.0003674	0.3784341	0.013417	8.953E-05	0.005077	3.418E-05
0.6015	1.657960	0.993796	0.08835732	0.00058	0.05315	0.0003507	0.3851841	0.013109	8.752E-05	0.005049	3.4E-05
0.6285	1.661500	0.995918	0.06926504	0.000454	0.04353	0.0002869	0.4121841	0.011768	7.838E-05	0.004851	3.257E-05
0.63525	1.662260	0.996374	0.06526898	0.000429	0.04146	0.0002737	0.4189341	0.011455	7.641E-05	0.004799	3.226E-05
0.642	1.662970	0.996799	0.06171692	0.000406	0.03962	0.0002621	0.4256841	0.011184	7.473E-05	0.004761	3.206E-05
0.669	1.665480	0.998304	0.04972875	0.000327	0.03327	0.0002196	0.4526841	0.010191	6.792E-05	0.004613	3.097E-05
0.67575	1.666020	0.998627	0.04706471	0.00031	0.0318	0.0002106	0.4594341	0.009934	6.642E-05	0.004564	3.074E-05
0.6825	1.666540	0.998939	0.04484467	0.000295	0.03061	0.0002025	0.4661841	0.009746	6.507E-05	0.004543	3.055E-05
0.7095	1.668310	1.000000	0.01598424	7.99E-07	0.01134	5.67E-07	0.4931841	0.003888	1.944E-07	0.001917	9.587E-08
0.7096	1.668310	1.000000	0	0	0	0	0.4932841	0	0	0	0

area under E curve= 0.999903
mean res. time tₘ (s) = 0.2163159
variance σ⁴ (s⁴)= 0.0096816
skewness s³= 0.0433046
standard deviation σ (s)= 0.0983953

71

APPENDIX C

ADDITIONAL CFX RESULTS
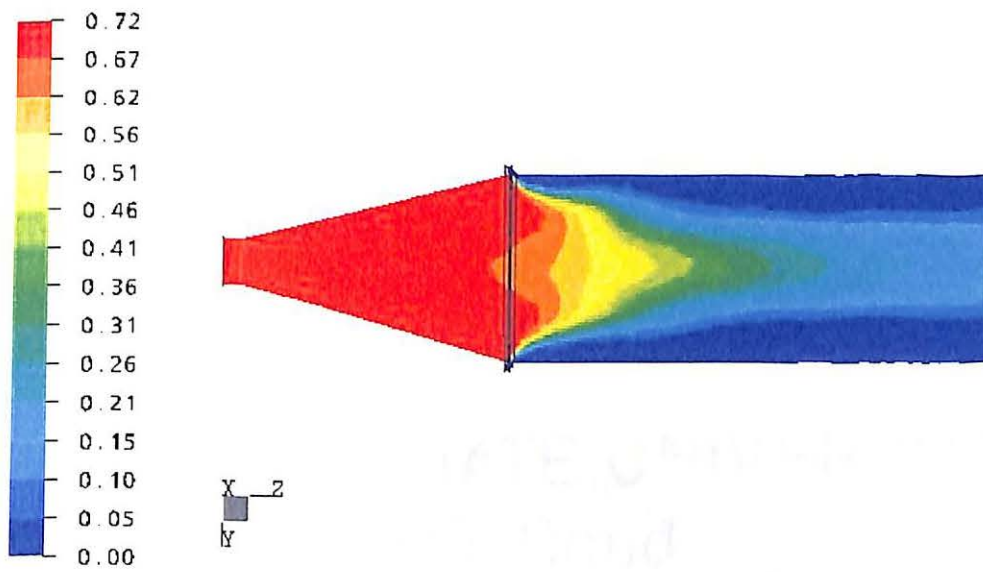
Montecatini Edison Reactor

FIGURE C-1. O_2 molar fraction contours for the Montecatini Edison reactor.
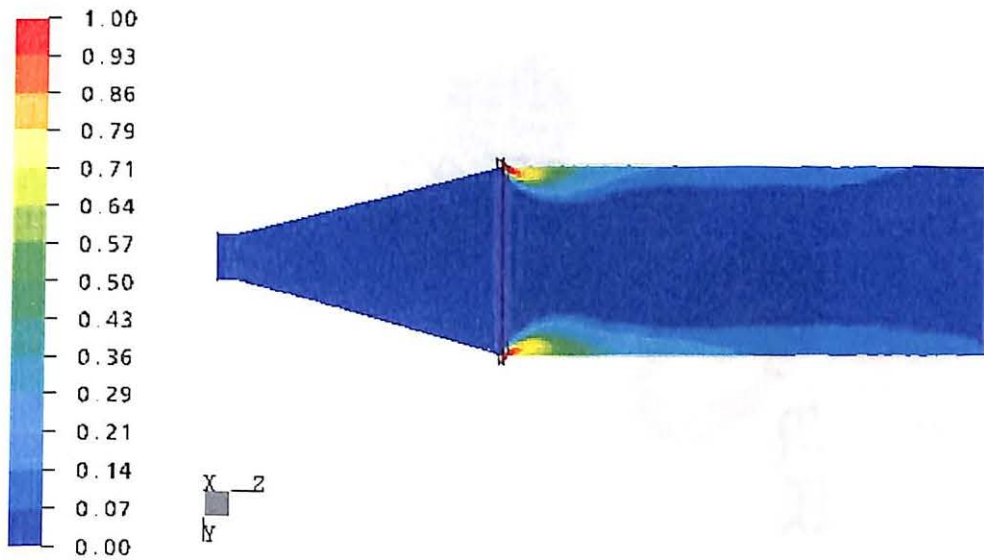
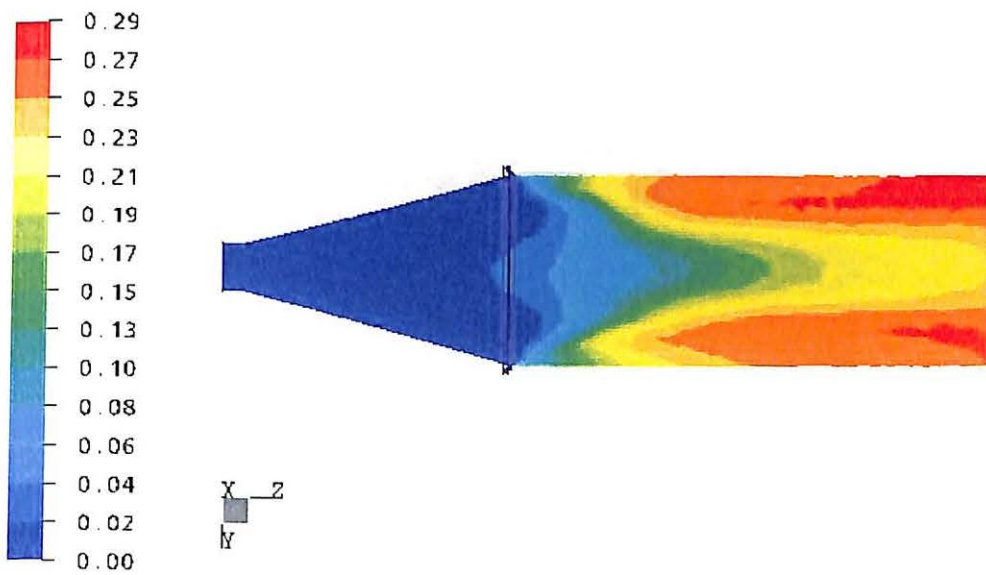**FIGURE C-2.** $TiCl_4$ molar fraction contours for the Montecatini Edison reactor.

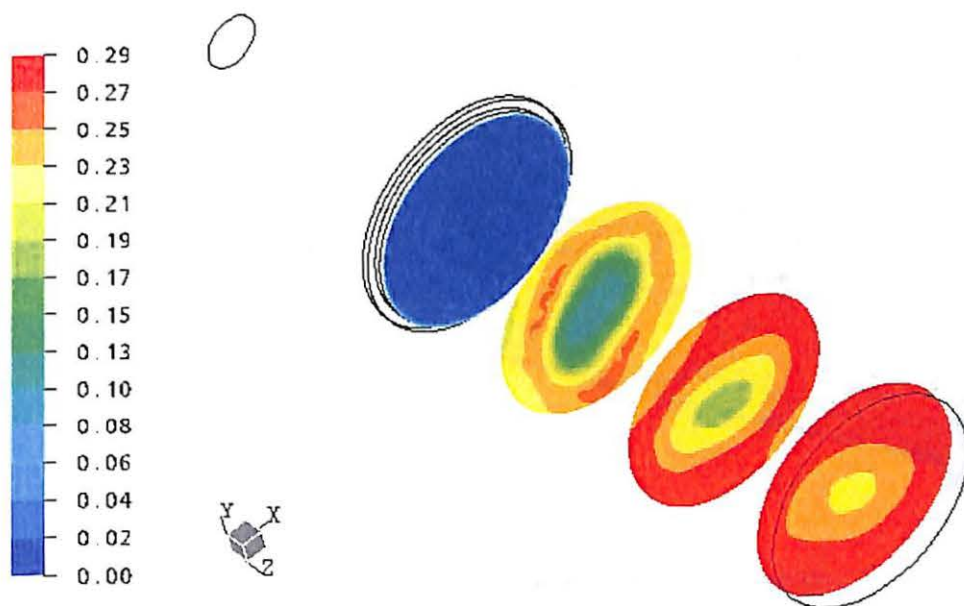**FIGURE C-3.** TiO_2 molar fraction contours for the Montecatini Edison reactor.

73

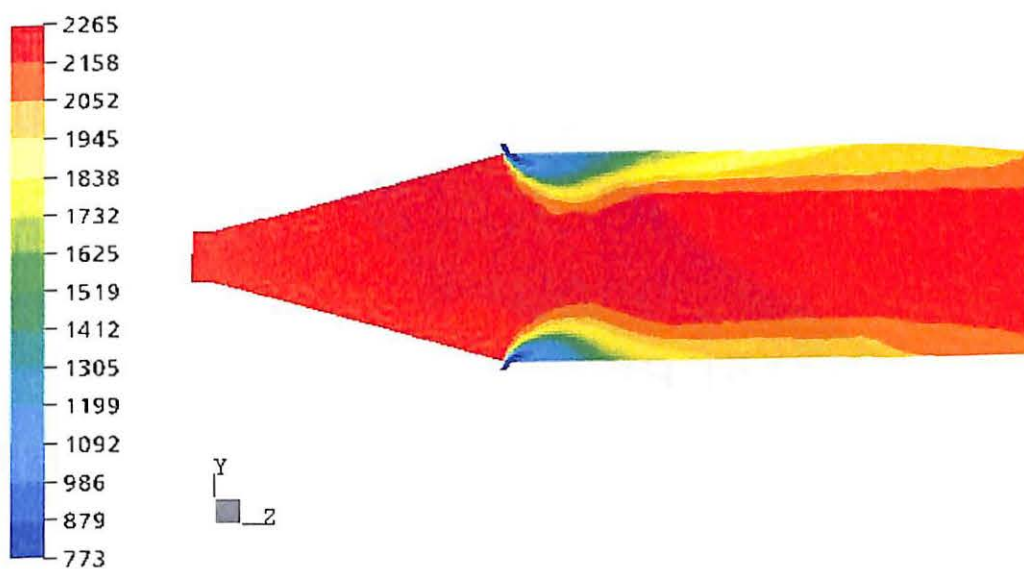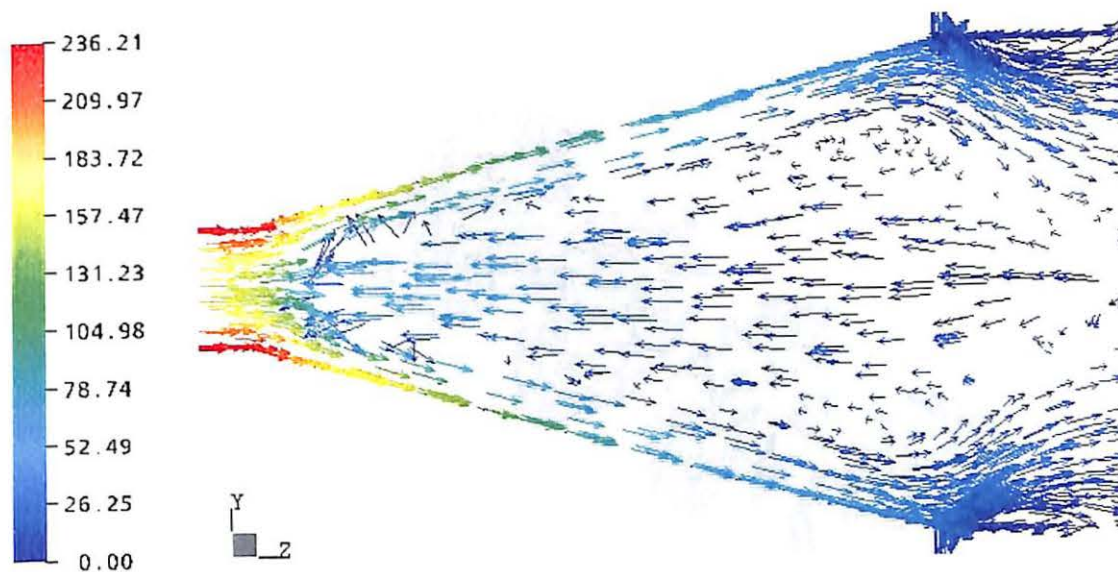**FIGURE C-4.** TiO_2 molar fraction contours for the Montecatini Edison reactor.

FIGURE C-5. Temperature contours for the Montecatini Edison reactor (K).

FIGURE C-6. Velocity vectors in preheat zone of Montecatini Edison reactor showing recirculation (m/s).
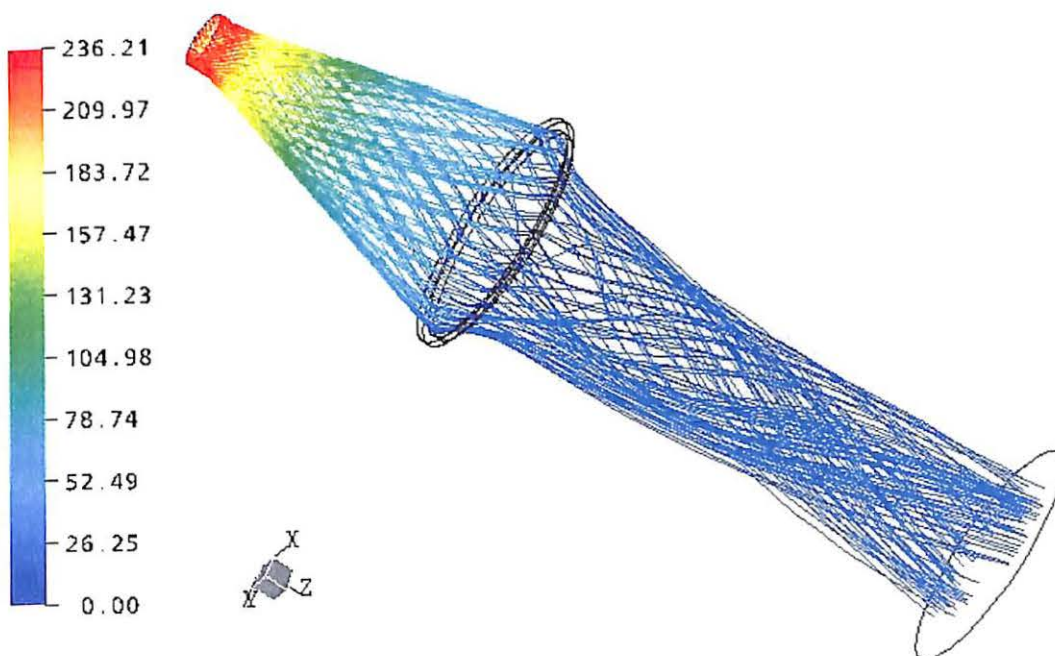
FIGURE C-7. Streamlines showing the swirling motion of the O_2 inlet gas and channeling occurring at the $TiCl_4$ inlet (m/s).
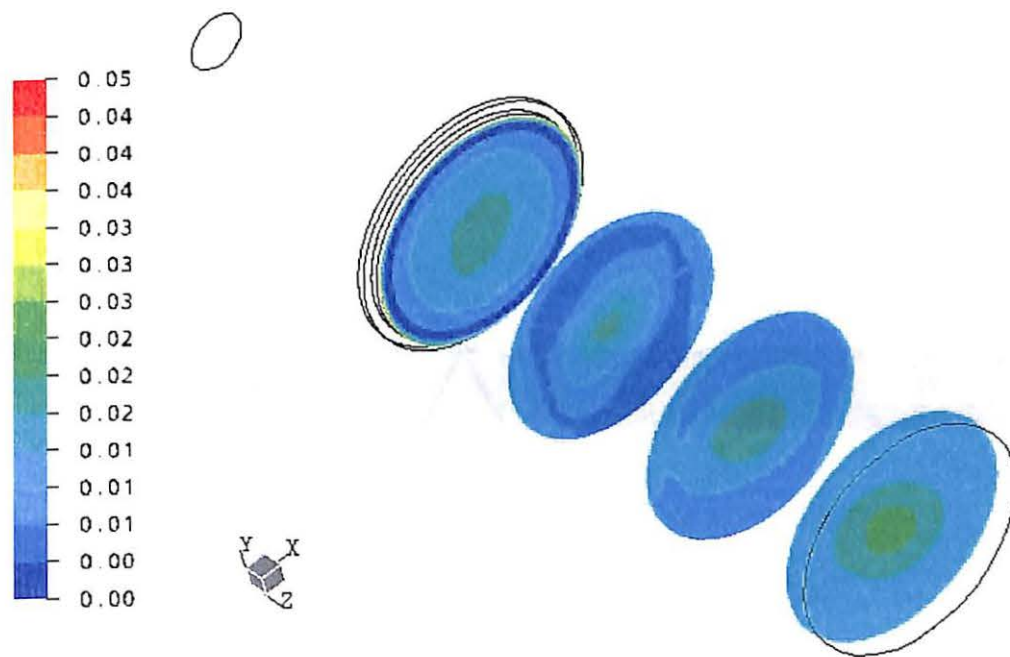
FIGURE C-8. Fluid age contours for the Montecatini Edison reactor (s).
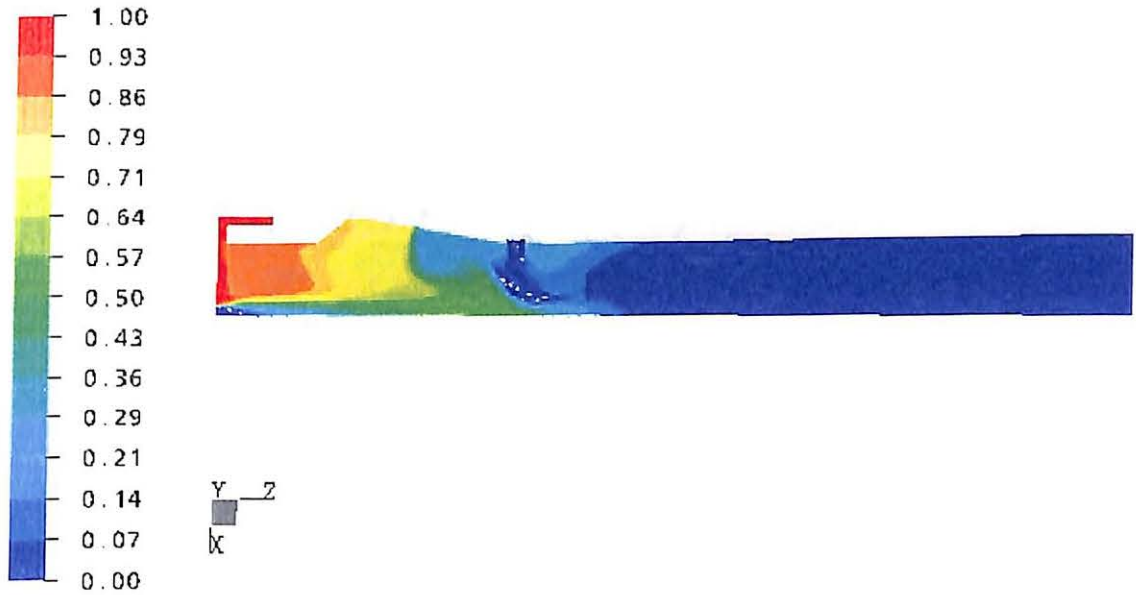
FIGURE C-9. O_2 molar fraction contours for the Kronos reactor on a symmetry plane.
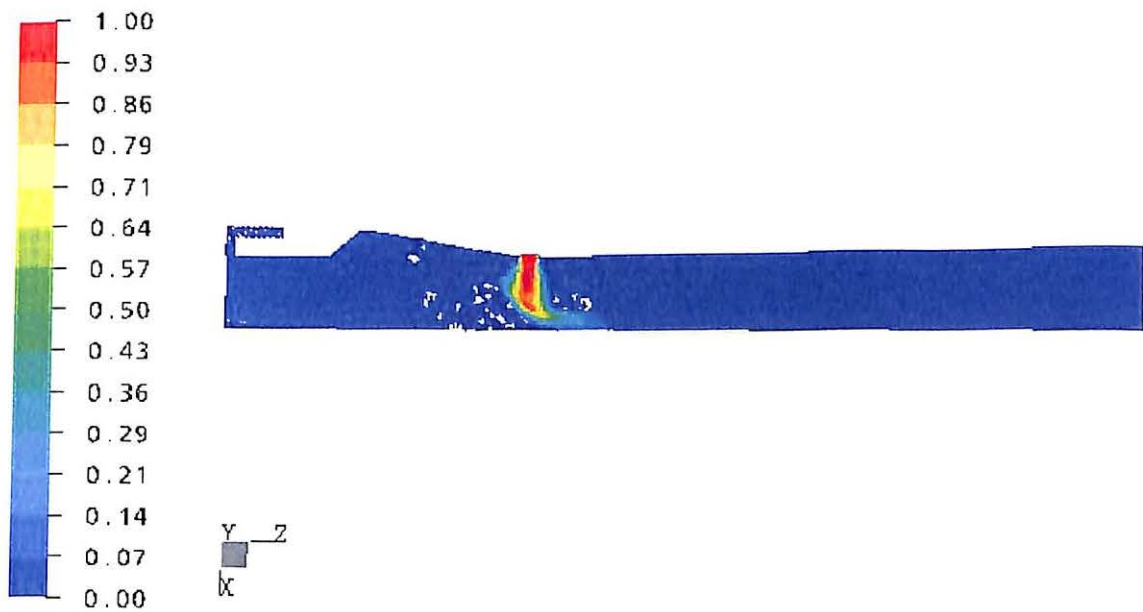
FIGURE C-10. $TiCl_4$ molar fraction contours for the Kronos reactor on a symmetry plane.
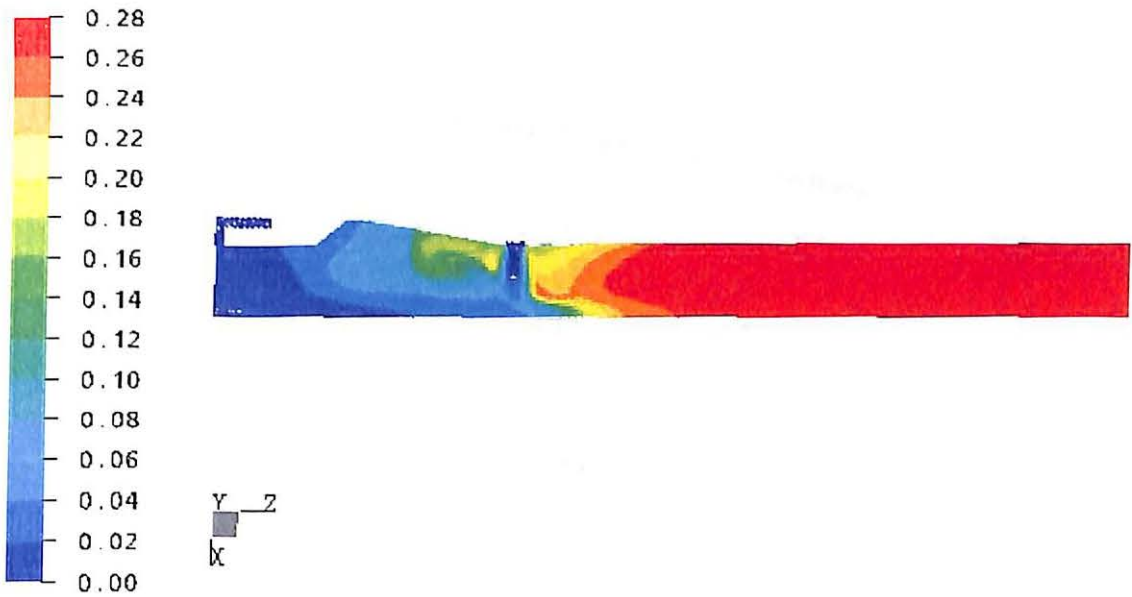
FIGURE C-11. TiO$_2$ molar fraction contours for the Kronos reactor on a symmetry plane.
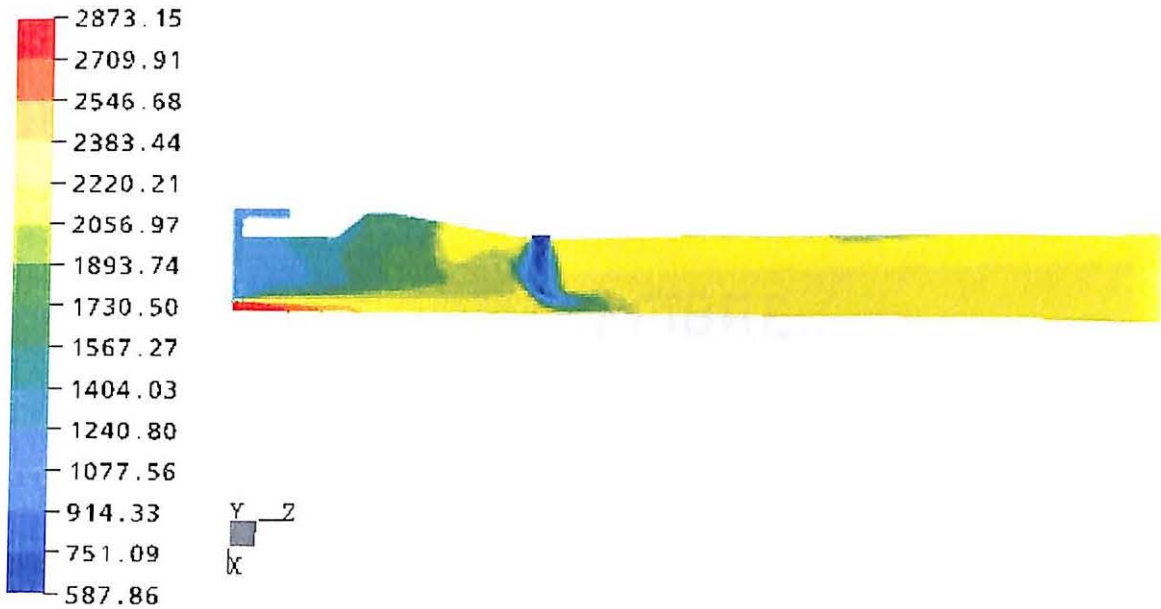
FIGURE C-12. Temperature contours for the Kronos reactor on a symmetry plane (K).
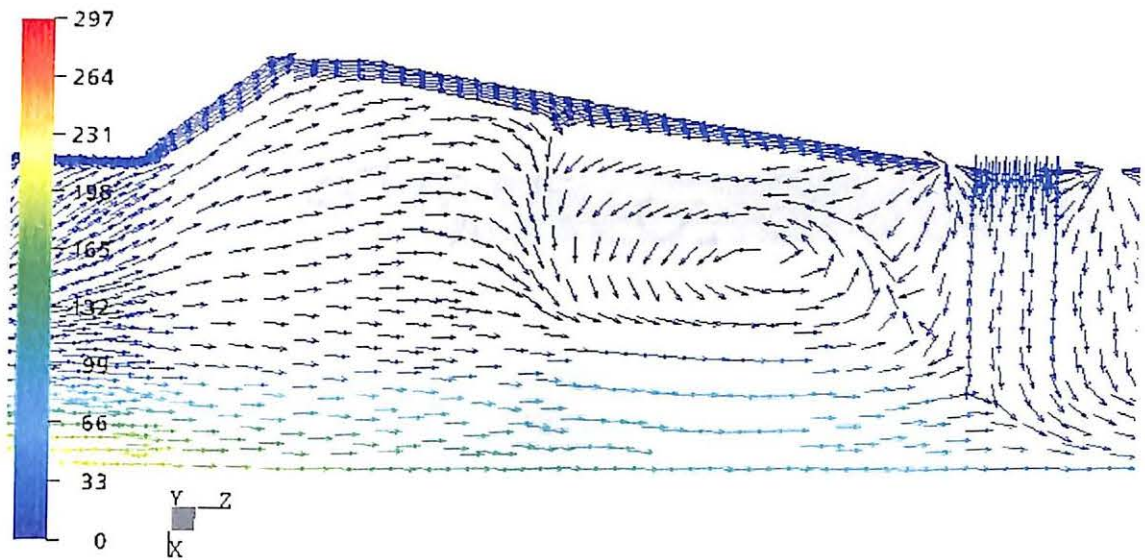
FIGURE C-13. Velocity vectors for the Kronos reactor in preheating zone on symmetry plane (m/s).
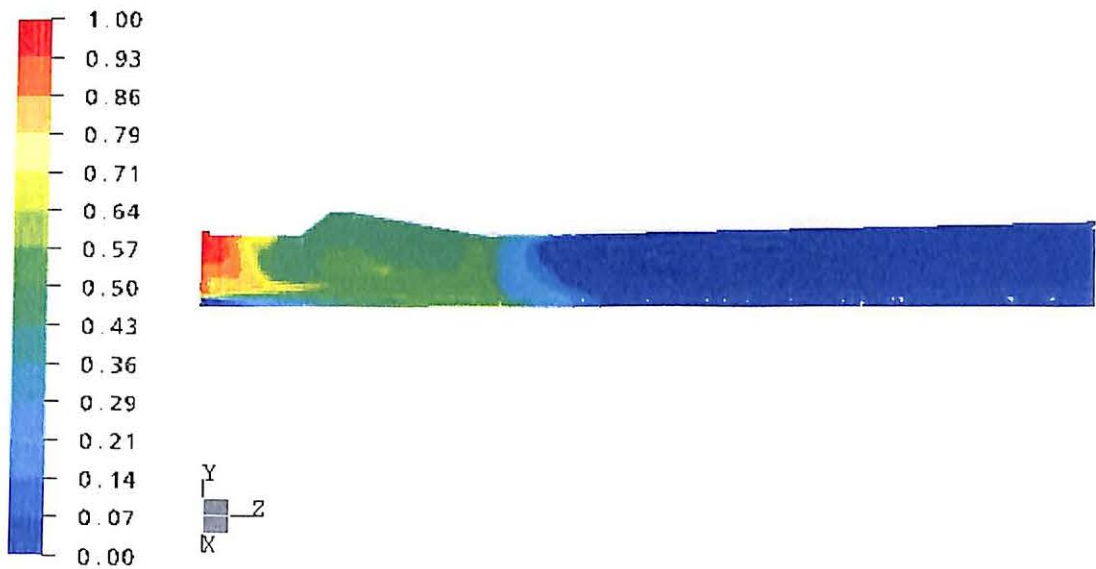
FIGURE C-14. O_2 molar fraction contours for the Kronos reactor half-way between $TiCl_4$ inlets.
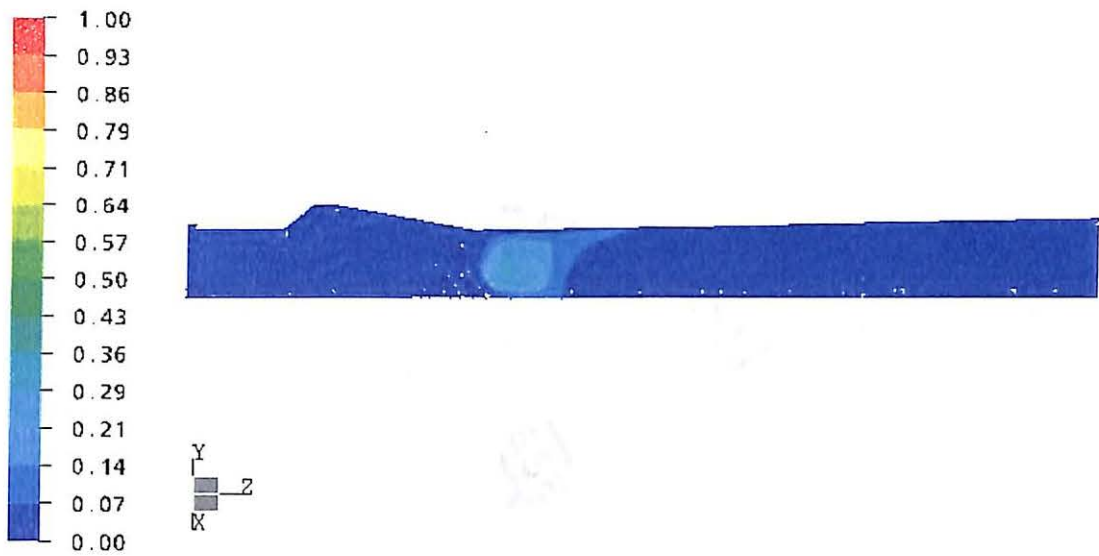
FIGURE C-15. TiCl$_4$ molar fraction contours for the Kronos reactor half-way between TiCl$_4$ inlets.
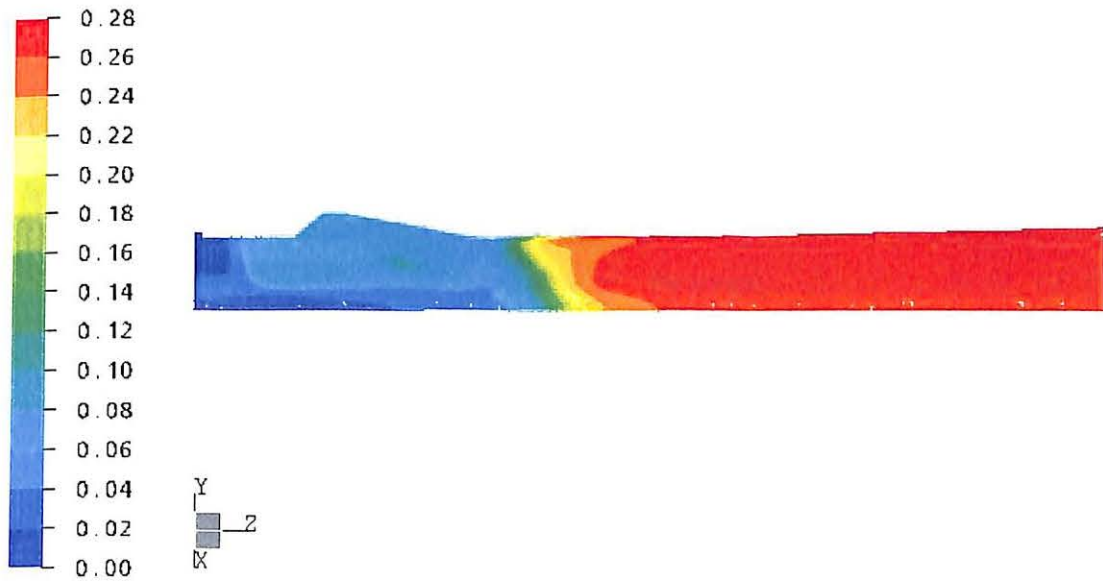
FIGURE C-16. TiO$_2$ molar fraction contours for the Kronos reactor half-way between TiCl$_4$ inlets.
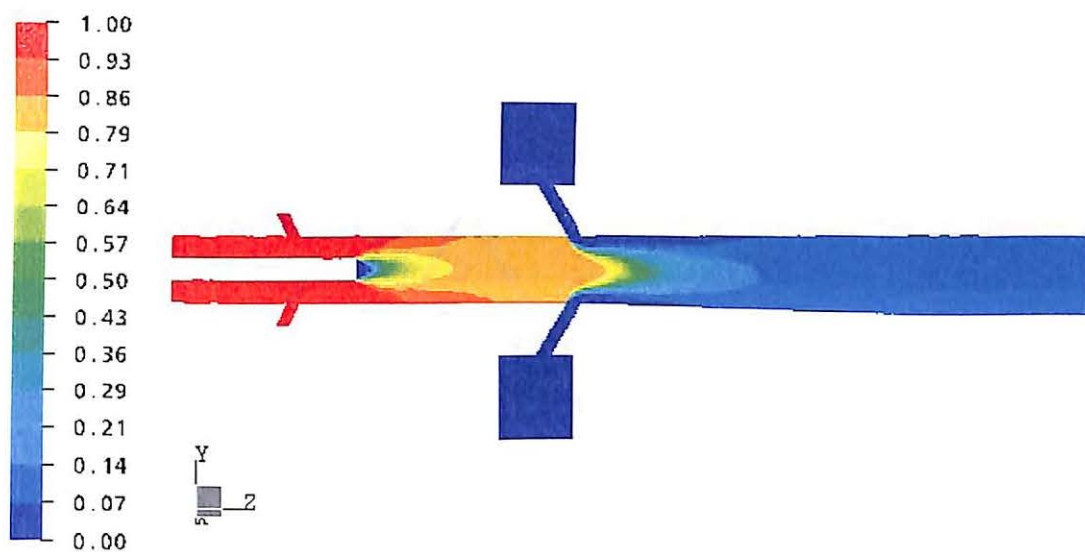
FIGURE C-17. O_2 molar fraction contours for the Simplified Kerr-McGee reactor.
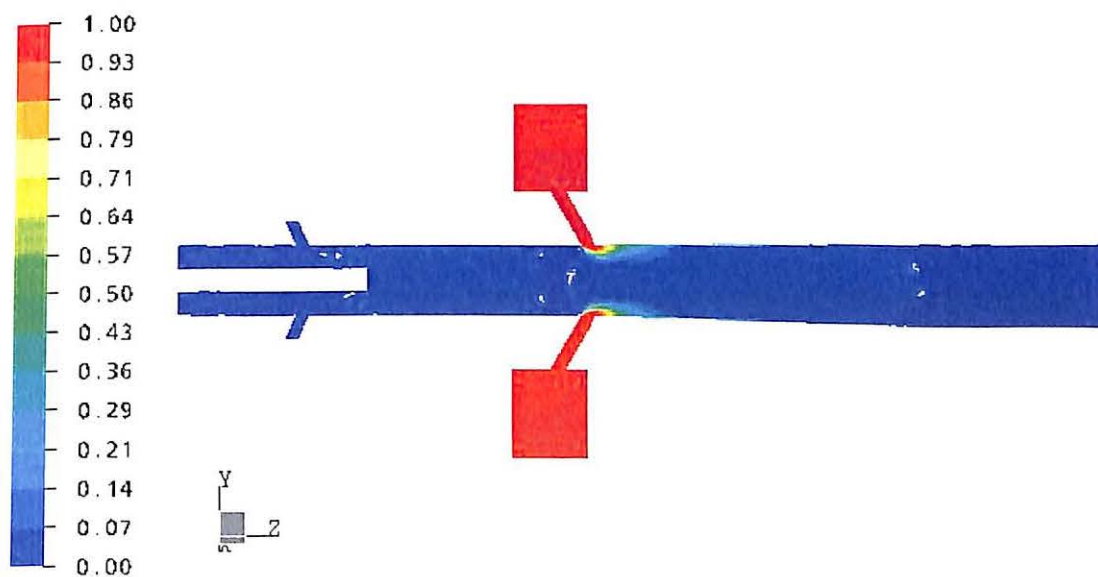
FIGURE C-18. $TiCl_2$ molar fraction contours for the Simplified Kerr-McGee reactor.
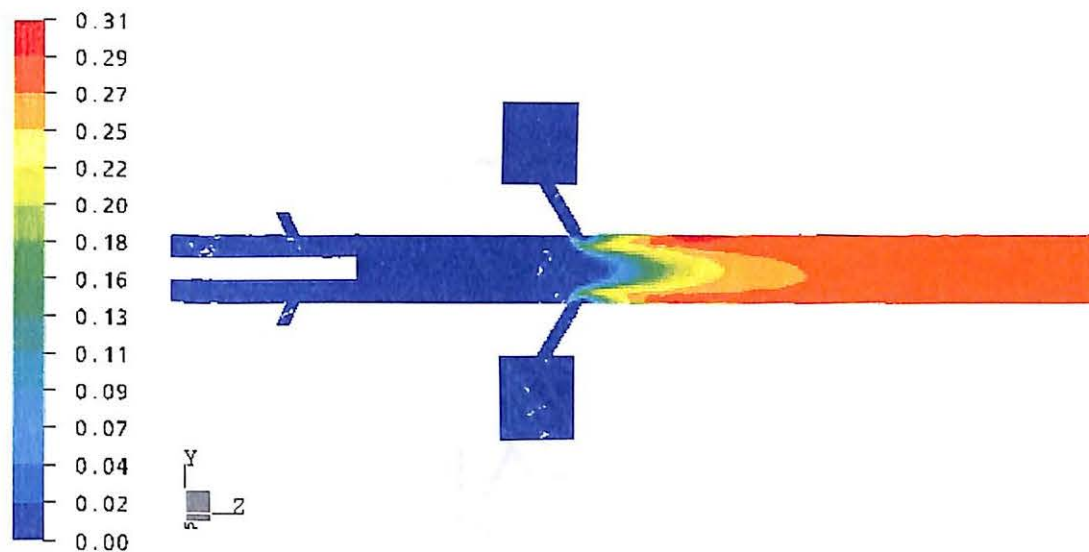
FIGURE C-19. TiO_2 molar fraction contours for the Simplified Kerr-McGee reactor.
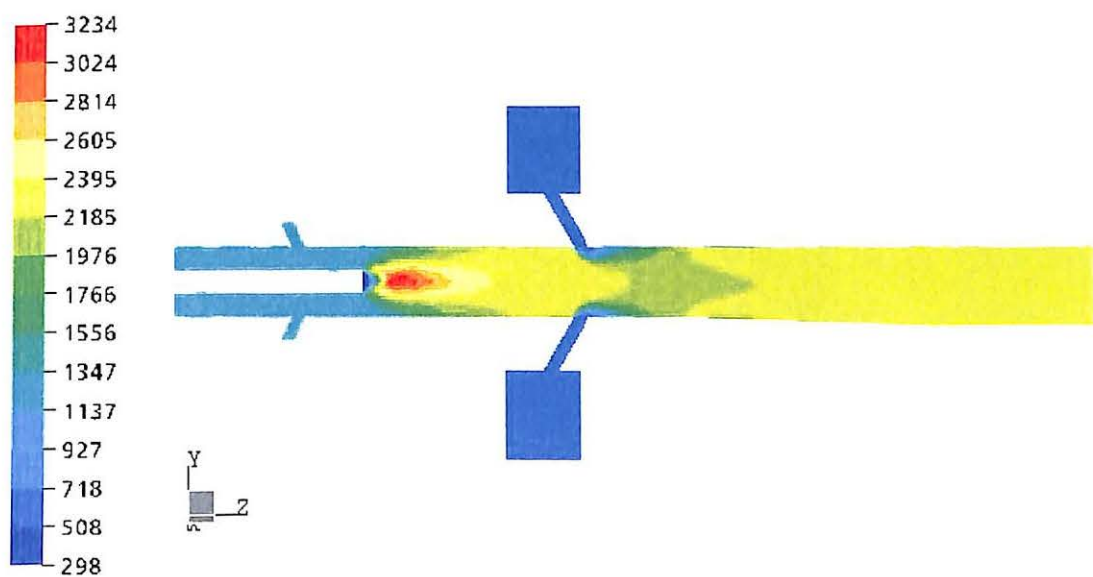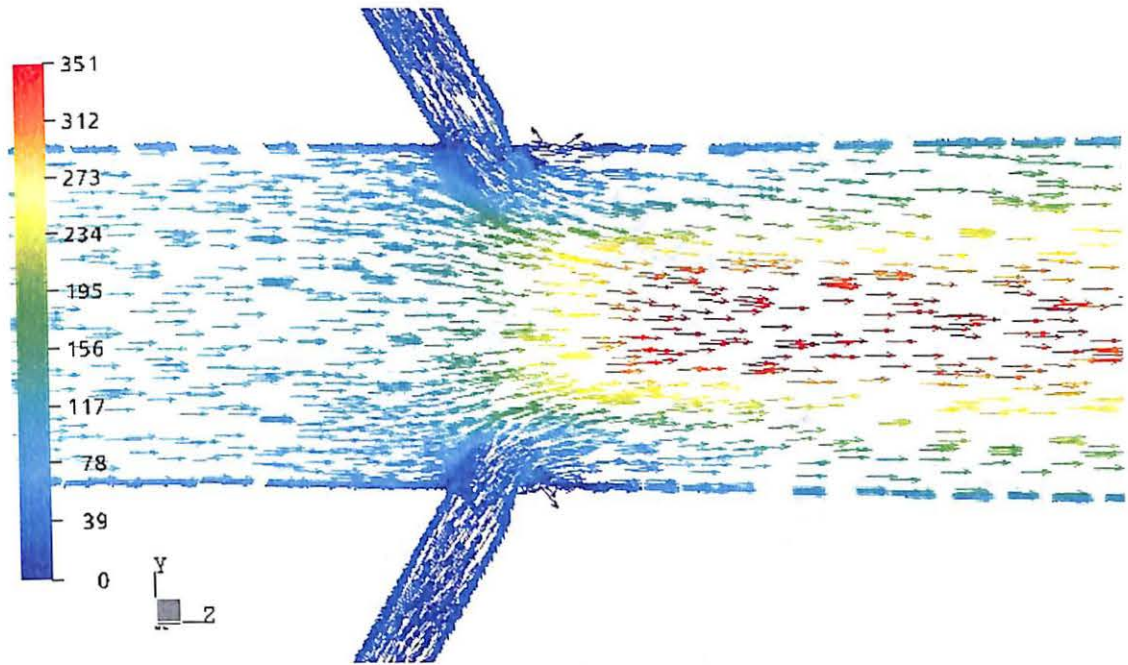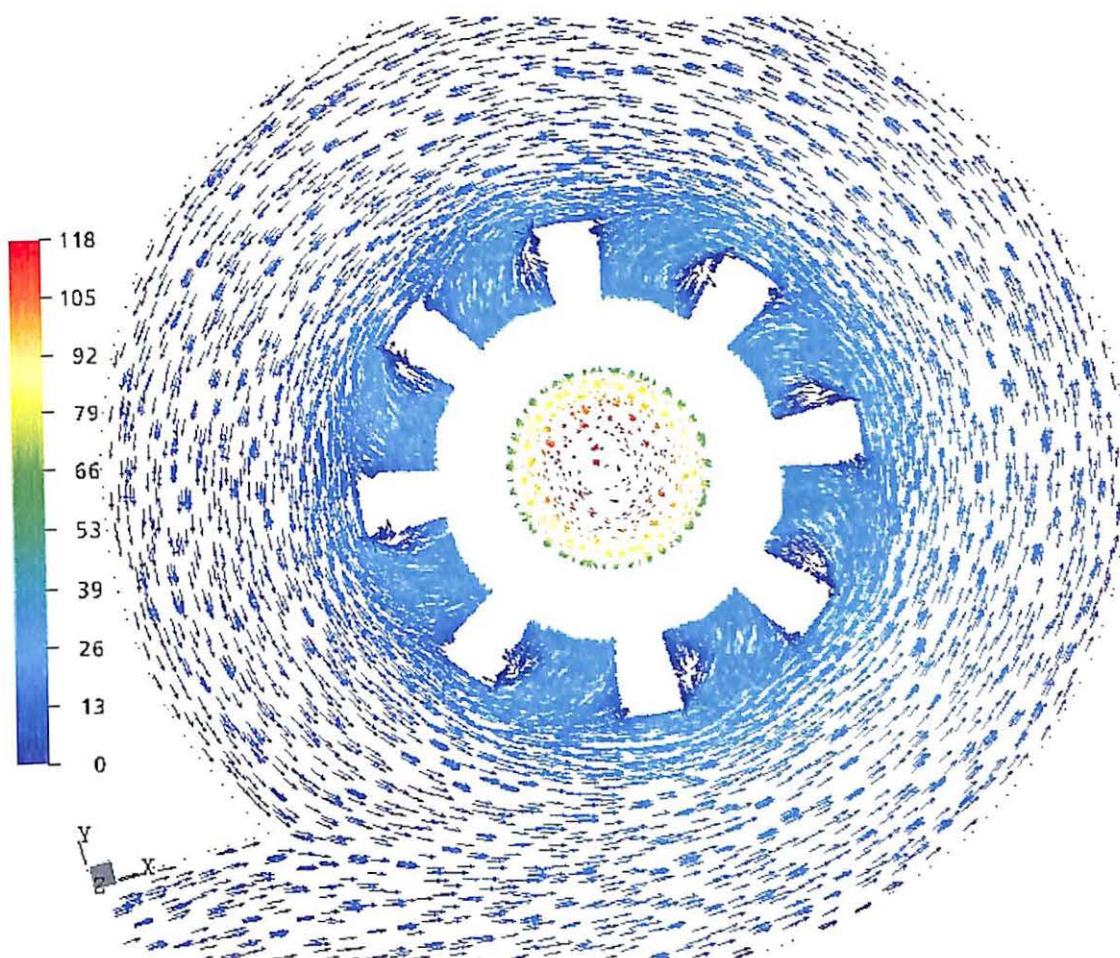

FIGURE C-20. Temperature contours for the Simplified Kerr-McGee reactor.

FIGURE C-21. Velocity vectors for the Simplified Kerr-McGee reactor near TiCl$_4$ inlet to reaction chamber (m/s).

FIGURE C-22. Velocity vectors for the Simplified Kerr-McGee reactor in the TiCl$_4$ distribution spool (m/s).

VITA $\textcircled{1}$

Jason A. Carlisle

Candidate for the Degree of

Master of Science

Thesis: QUANTIFYING MIXING INSIDE TITANIUM DIOXIDE REACTOR
THROUGH COMPUTATIONAL FLUID DYANMICS

Major Field: Chemical Engineering

Biographical:

  Education: Received Bachelor of Science degree in Chemical Engineering from
  Oklahoma State University in Stillwater, Oklahoma in May 2001. Completed the
  requirements for the Masters of Science degree with a major in Chemical
  Engineering at Oklahoma State University in July 2004.

  Experience: Employed as a teaching assistant at Oklahoma State University
  School of Chemical Engineering, August 2001 to May 2002. Employed as a
  research assistant from August 2002 to December 2003.